جامعة زيان عاشور بالجلفة
Ziane Achour University of Djelfa

كلية العلوم والتكنولوجيا
Faculty of Science and Technology

Department: Civil engineering

Order N° : . …. / 2023

Defense authorization N° ………….∕2023

DOCTORAL THESIS

3rd Cycle Doctoral (D-LMD)

Presented by

Maroua Layachi

With a view to obtaining the doctoral diploma in 3rd Cycle Doctoral (D-LMD)

Branch: Civil engineering

Specialty: Materials in civil engineering

Topic

Characterization and modeling of the damage and failure of composite plates containing geometric sigularities

Supported, on 30 /09 / 2023, before the jury composed of:

Last and first name	Grade	Institution of affiliation	Designation
Mr Douara Taha-Hocine	MCA	University of Djelfa	President
Mr Ghrieb Abderrahamane	MCA	University of Djelfa	supervisor
Mr Khechai Abdelhak	MCB	University of Biskra	Co-supervisor
Mr Guettala Salim	Professor	University of Djelfa	Examiner
Mr Tati Abdelouahab	Professor	University of Biskra	Examiner
Mr Belarbi Mohamed-Ouejdi	MCA	University of Djelfa	Examiner

Djelfa University, FST - 2023

DEDICATION

To my dear parents, to all my family

Maroua LAYACHI

ACKNOWLEDGMENTS

'Life will destory you many times, sometimes you will fail and grieve, but do not give up and never lose hope '

'In order to succeed, we must first believe that we can'

Abstract

In general, the creation of laminated composite plates requires a thorough understanding of failure mechanisms and accurate modeling. This work focuses on two main objectives. The first primary objective is to analyze the failure behavior of laminated plates and beams under various static and hygrothermal loads with different boundary conditions, utilizing analytical and numerical methods through finite element analysis. The First Ply Failure (FPF) analysis is performed using a refined rectangular plate element formulated based on the Classical Lamination Theory (CLT) to calculate the in-plane stresses. To achieve this goal, several failure criteria, including Tsai-Wu, Tsai-Hill, Hashin, and Maximum Stress criteria, are used to predict failure mechanisms. These criteria are implemented within the finite element code to predict the different failure damages and responses of laminated plates and beams from the initial loading to the final failure, in order to comprehend the effect of different types of loads on the FPF load. Sometimes, designers need to make holes in different shapes in the laminate to meet the design requirements and for practical reasons. Cutouts alter the behavior of materials and create undesirable stress concentrations around these holes. For this reason, the second objective of this work is to determine the stress concentration factor and stress resultant in an infinite plate with an unsymmetrical stacking sequence of laminated plates that include a circular hole of various sizes under arbitrary axial, biaxial, and shear loading at infinity. This is done using a general analytical solution that extends the Greszczuk's method by introducing different arbitrarily oriented in-plane loads. In the current solution, the formulations of the effective moduli of unsymmetrical composite laminated plates are presented. The accuracy of this analytical solution is assessed by contrasting its findings with the results of finite element models and analytical results obtained using the complex variable approach, revealing a high level of agreement between these results. This demonstrates the validity and accuracy of the present analytical solution. The Tsai-Wu failure criterion is also used to calculate the FPF and show the effect of the presence of the circular hole on the FPF loads.

Keywords: Laminated composite , Failure load, Finite element, First ply failure FPF, Stress concentration, Hole, Cutout, unsymmetrical composite laminated.

الملخص

بشكل عام ، يتطلب إنشاء الألواح المركبة المصفحة فهماً شاملاً لآليات الفشل والنمذجة الدقيقة .يركز هذا العمل على هدفين رئيسيين .الهدف الأساسي الأول هو تحليل سلوك فشل الألواح والروافد المصفحة تحت أحمال ساكنة ورطوبة حرارية مختلفة مع شروط حدية مختلفة ، وذلك باستخدام الطرق التحليلية والرقمية من خلال تحليل العناصر المحدودة .تم إجراء تحليل فشل الطبقة الاولئ باستخدام عنصر لوحة مستطيل مصقول تم صياغته بناءً على نظرية التصفيح الكلاسيكية (CLT) لحساب الضغوط داخل المستوى .لتحقيق هذا الهدف ، تم استخدام العديد من معايير الفشل ، بما في ذلك معايير تسايو وتساي هيل و هاشين ،و اقصئ اجهاد ، للتنبؤ بآليات الفشل .تم تنفيذ هذه المعايير ضمن خوارزمية العنصر المحدد للتنبؤ بأضرار الفشل المختلفة واستجابات الصفائح الرقائقية من التحميل الأولي إلى الفشل النهائي ، من أجل فهم تأثير أنواع مختلفة من الأحمال على حمل فشل الطبقة الأولى .في بعض الأحيان ، يحتاج المصممون إلى عمل ثقوب بأشكال مختلفة في الصفيحة لتلبية متطلبات التصميم ولأسباب عملية .تغير الفتحات سلوك المواد وتخلق تركيزات إجهاد غير مرغوب فيها حول هذه الثقوب .لهذا السبب ، الهدف الثاني من هذا العمل هو تحديد عامل تركيز الضغط والضغط الناتج في لوحة لا نهائية مع تسلسل تكديس غير متماثل من الصفائح المصفحة التي تتضمن ثقب دائري بأحجام مختلفة تحت محوري تعسفي ، ثنائي المحور ، و تحميل القص عند اللانهاية .تم ذلك باستخدام حل تحليلي عام يوسع طريقة Greszczuk من خلال إدخال أحمال مختلفة بشكل تعسفي داخل الصفيحة .في الحل الحالي ، تم تقديم تركيبات المعادلات الفعالة للألواح الرقائقية المركبة الغير المتماثلة .تم تقييم دقة هذا الحل التحليلي من خلال مقارنة نتائجه مع نتائج نماذج العناصر المحدودة والنتائج التحليلية التي تم الحصول عليها باستخدام النهج المتغير المعقد ، مما يكشف عن مستوى عالٍ من التوافق بين هذه النتائج .هذا يوضح صحة ودقة الحل التحليلي الحالي .يُستخدم معيار فشل تسايو أيضًا لحساب حمل فشل الطبقة الأولى (FPF) وإظهار تأثير وجود الفتحة الدائرية على أحمالFPF

الكلمات الرئيسية: مركب مصفح ، تحميل فشل ، العناصر المنتهية ، فشل الطبقة الأولى FPF ، تركيز الإجهاد ، ثقب ، مركب غير متماثل.

LIST OF FIGURES

LIST OF TABLES

Content Table

Frequently Used Symbols

Symbol	Explanation
(X,Y,Z)	Global coordinate system
$(1,2,3)$	Local coordinate system
E_1	Young's modulus in 1-direction
E_2	Young's modulus in 2-direction
G_{12}	Shear modulus in 12 plane
G_{23}	Shear modulus in 13 plane
v_{12}	Poisson's ratio in 12 plane
θ	Fiber orientation angle
σ	Applied stress
S	Applied shear stress
t	Thickness
U_j	Laminate invariants
Q_{ij}	Reduced stiffness matrix
$[A]$	Extensional rigidity matrix
$[B]$	Coupling rigidity matrix
$[D]$	Bending rigidity matrix
K_T^{∞}	Stress concentration factor in infinite plate
W	Plate width
L	Plate length
K_T	Stress concentration factor in infinite plate

σ_f	Failure load (strength)
X_t	longitudinal strengths in tension
X_c	longitudinal strengths in compression
Y_t	the transverse strengths in tension
Y_c	the transverse strengths in compression
S	the in-plane shear strength.
$\bar{Q}_{ij}$	Stiffness coefficients of a layer in the global coordinate system
α	Circumferential angle
$\sigma\alpha$	Circumferential stress
D	Circular cutout of diameter
E_x	Young's modulus in x-direction
E_y	Young's modulus in y-direction
G_{xy}	Shear modulus in xy plane
v_{xy}	Poisson's ratio in xy plane
α_2, α_1	thermal expansion coefficients
β_2, β_1	moisture expansion coefficients
ΔT	The temperature rise
ΔC	moisture rise
β	Load orientation
ς	Circular hole diameter to width ratio

Chapter 1

GENERAL INTRODUCTION

Chapter 1

General Introduction

1.1 Research background

The development of modern technologies requires the use of materials with high mechanical properties suited for their intended purpose. Nowadays, composite materials have become essential and are gradually becoming an alternative to conventional materials, thanks to the advantages they present. High-performance composite materials are used to manufacture aircraft, marine vehicles, and various structures. Due to their properties such as high specific strength, stiffness, and lightweight, the application of these composite materials has now gone beyond the bounds of aircraft design and has reached the realm of civil engineering.

Laminates are one of the most sought-after composite materials and are commonly used in structural elements. They're formed by stacking several layers, with each layer having a different orientation, resulting in varying mechanical characteristics depending on the directions considered. When the layers of a laminate are identical on both sides of the mid-plane, it's considered symmetric, and designers often prefer them due to their ease of construction and analysis. In contrast, designers often avoid unsymmetrical laminates due to the difficulty of analyzing their behavior. These plates exhibit a distinct structural behavior that not found in the classical materials. However, the behavior of these unsymmetrical plates has to be understood. As composite technology advances, the use of unsymmetrical laminates to satisfy design requirements effectively and affordably has become more common. However, plates or beams made of composite materials are subjected to various influences, such as mechanical load (static and dynamic loads), which can weak them and lead to structural failure.

In addition, composite laminates are exposed to a range of thermal and moisture conditions during production and preservation, and are also used in a variety of environments, including high and low temperatures, humidity, solar radiation, and erosion hazards (rain, hail, dust, and sand)[1, 2]. Temperature and humidity are the most important environmental factors.which

induce stress and strains. Where the stiffness and strength of composites are affected by variations in moisture and temperature [3], which generates complex strain and stress in laminated composite plates because material characteristics might fluctuate significantly between layers. The elastic modulus and strength of composite laminates will decrease as temperature and moisture concentrations rise. As a result of the change in the environment, hygrothermal internal tensions are formed. These stresses often cause significant deformation and may possibly lead to the structure's failure.

Sometimes designers need to make holes in different shapes in the laminate in order to meet the design requirements and for various practical reasons. For example, in civil engineering, holes are used as doors, windows, and others. And in many cases, holes are used to reduce weight. These structures with openings are subjected to different types of loading, which leads to the creation of stress concentrations around the opening [4, 5] and sometimes leads to cracks and failure of the structures. Therefore, the study of the stress on infinite plates with perforations or openings subjected to various types of loading is an interesting field of analysis for many researchers.

To predict the failure strength of notched composite laminates accurately, it is important to have a simple and correct method to determine the stress distribution. This is because the mechanical behavior of notched composite laminates is more complex than unnotched ones due to their unique features such as heterogeneity, anisotropy, and stress gradients.

Therefore, the most significant criterion for the safety design of laminated composite structures is failure. Failure analysis of laminated composite materials is far more complicated than that of isotropic materials. In general, the creation of laminated composite plates requires a thorough understanding of the damage and failure modes, as well as accurate modeling. To date, many failure criteria have been proposed to predict the behavior of composite structures.

Analyzing the failure of a laminate is more challenging compared to a single layer as it involves accurately predicting the strength of each layer. This requires assessing the local stress levels of each layer and applying appropriate failure criteria. If a single layer fails, it doesn't necessarily imply that the entire laminate will fail, but it does indicate the start of the failure process. The load at which the first layer fails is referred to as the First Ply Failure (FPF) load.

1.2 Motivation

To fully leverage the advantages of composite materials, it is imperative to understand their complex behavior, especially when exposed to different types of loading, as this can lead to their weakening. Additionally, structures are not only subjected to loads or forces but also environmental factors such as temperature and humidity, which can weaken their strength and cause failure. Therefore, these factors must be taken into account when calculating the strength of failure, whether in non-perforated or perforated plates. Perforation is also considered a major cause of failure, as the presence of cutouts leads to the weakening of plates due to local stress concentration. The area around these holes is often where cracks initiate and can also be the source of a sudden rupture. Designers are concerned about stress concentration and stress distribution around openings, which must be defined in order to forecast the failure load. Hence, this work focuses on extending Greszczuk's analytical solution to calculate stress distribution in an infinite plate with an unsymmetrical stacking sequence containing circular holes subjected to arbitrary in-plane loadings. Designers often avoid unsymmetrical laminates due to the difficulty of analyzing their behavior. However, it is important to understand the behavior of these unsymmetrical plates as composite technology advances and the use of unsymmetrical laminates to satisfy design requirements effectively and affordably becomes more common. Since the application of unsymmetrical laminates to structures differs from that of regular ones, stress concentration problems for such laminates must be addressed. The finite element method is a versatile and powerful mathematical tool to handle such complex problems. Understanding the influence of different parameters on stress concentration and failure load is critical to making the most of composites. Therefore, the most significant criterion for the safe design of laminated composite structures is failure. The drawbacks of existing methods to find stresses and strengths and to ensure the integrity of laminated composite plates motivated us to analyze and determine stress analysis and failure loads.

1.3 Objective of the present study

The primary objective of this study is to analyze the failure behavior of laminated plates and beams under various static and hygrothermal loads with differing boundary conditions, utilizing analytical and numerical methods through finite element analysis. To comprehend the effect of different types of loads on the first-ply failure load, we will employ one of the available failure criteria in the literature. Additionally, we will determine the stress concentration factor and stress resultant in an infinite plate with an unsymmetrical stacking sequence containing a circular hole of varying sizes under arbitrary axial, biaxial, and shear loading at infinity using a general analytical solution. Furthermore, we will present the formulations of the effective moduli of unsymmetrical composite laminated plates. The main objectives of this work can be summarized by the following points:

- ✓ The first ply failure load (FPF) and damage location of a composite plate and beam subjected to bending loads using different failure criterions .
- ✓ To study the effects of several parameters, such as fiber orientations, stacking sequences, and boundary conditions, are considered to determine and understand their effects on the strength of laminated beams.
- ✓ analyze the effects of hygrothermal conditions (temperature and moisture) on the failure load and mechanism of laminated composite beams using various failure criteria. Several parameters were investigated.
- ✓ The present thesis work also focuses on extending the previous analytical solution of Greszczuk to calculating the stress distribution (SCF) and stress resultant around a circular hole in an infinite plate with an unsymmetrical stacking sequence under arbitrary axial, biaxial, and shear loading at infinity.
- ✓ The effects of several parameters were studied, such as the stacking sequence of different materials, fiber orientation, load orientation angle, size of the hole, and type of load, on stress concentration and failure load.

1.4 Plan of the thesis

The thesis is divided into six main chapters, each of which covers a specific aspect of the research conducted to achieve the stated aims and objectives.

- ❖ In the first chapter, a broad introduction to the thesis is given, along with its objectives. The study's context, the problems being addressed, and the objectives of the work were all specified.

- ❖ Chapter 2 provides an overview of the literature, encompassing general information on composite materials as well as specific details on laminated plates and a summary of various approaches and theories. Additionally, it presents a systematic review of existing literature, including previous models for predicting the strength of laminated plates, and previous solutions for isotropic and anisotropic plates with perforations under in-plane loading.

- ❖ Chapter 3 presents the mathematical formulations of the finite element method and the failure load prediction using different failure criteria. In addition, it includes the formulation of stress concentration around circular holes in unsymmetric laminated plates using a general analytical solution. Moreover, the chapter covers the formulations of the effective moduli of unsymmetrical composite laminated plates. To account for the behavior of real structures where the plates are not infinite, we use and present the finite-width correction factor given by Tan.

- ❖ Chapter four presents and analyzes the results obtained for the non-perforated plates and beams subjected to static and hygrothermal loads. The first section of this chapter covers the validation of the numerical element used in the study. The results are compared with analytical results and those found in the literature. In the second section, we conduct a parametric study, including the failure study of laminated plates and beams subjected to static bending, in-plane loading, and hygrothermal environmental conditions. Different failure criteria are used in this study.

❖ Chapter 5 presents the results and discussion for perforated laminated plates. This chapter investigated the distribution of stress concentration around circular holes in unsymmetrical laminated plates with perforations. The first validates an extended analytical solution by calculating the stress distribution and stress resultants in an infinite plate with an unsymmetrical stacking sequence under arbitrary axial, biaxial, and shear loading at infinity, while several parameters such as fiber orientation, stacking sequence, bondary conditions, load orientation, and hole size are considered.

❖ Chapter 6 summarizes the main findings and conclusions of the present research while also discussing the contributions and suggestions for future study.

Chapter 2

GENERALITY AND

LITERATURE REVIEW

Chapter 2

Generality and Literature Review

2.1 Introduction :

For thousands of years, humans have used composite materials in a variety of applications. Composites have been utilized since 1500 B.C., when early Egyptians and Mesopotamian immigrants employed a combination of mud and straw to make sturdy and lasting structures. A brick block's composition of mud and straw provides it with high resilience to squeezing, ripping, and bending. Straw was still utilized to strengthen ancient composite artifacts such as ceramics and boats [6, 7]. And this was the beginning, using simple and available natural materials.

After several years, plastic scientists developed. At that time, the only source of adhesives were natural resins taken from animals and plants. Plastics such as polystyrene, polyester, and phenolic were developed in the early twentieth century. These novel synthetic materials have overcome natural resins. However, for some structural applications, polymers by themselves might not offer sufficient strength. Therefore, reinforcement is required to provide strength and stiffness. For this reason, Owens Corning created the first glass fiber in 1935 [8] When fiberglass was mixed with a plastic polymer, the result was a lightweight and rigid structure. This was the industry's first start with fiber-reinforced polymers (FRP).

Composite materials were used and developed as a result of the needs of the wars "World War 1 and 2," such as aircraft and military vehicles, due to their strength and lightweight. After the end of World War II, the demand for military equipment began to decline. For this reason, many researchers tried to introduce composite materials in different industries and markets, including boats; the first composite commercial boat was made in 1946. In 1947, an entire vehicle body was manufactured from composite and was tested. Furthermore, composite materials entered the marine industry, with the marine industry becoming the largest user of composite materials in the 1960s. Composites were first employed in infrastructure applications in Asia and Europe in the late 1970s and early 1980s.

Composite materials also made their way into civil engineering, where the first pedestrian bridge was built in Scotland in the 1990s and the first bridge deck for vehicles was built in Russell, Kansas.

Nowadays, the industry with composite materials is constantly and significantly developing, as it has entered almost all fields. Composites are employed in a wide range of industries, including aircraft, architecture, automotive, energy, infrastructure, marine, military, sports, and recreation.

This chapter begins by presenting a general overview of composite materials, covering their definition, classification, and components. Subsequently, it delves into the mechanical behavior of laminated composite plates using various theories. The chapter also presents a compilation of exclusive research papers that review the failure strength and stress concentration of composite materials.
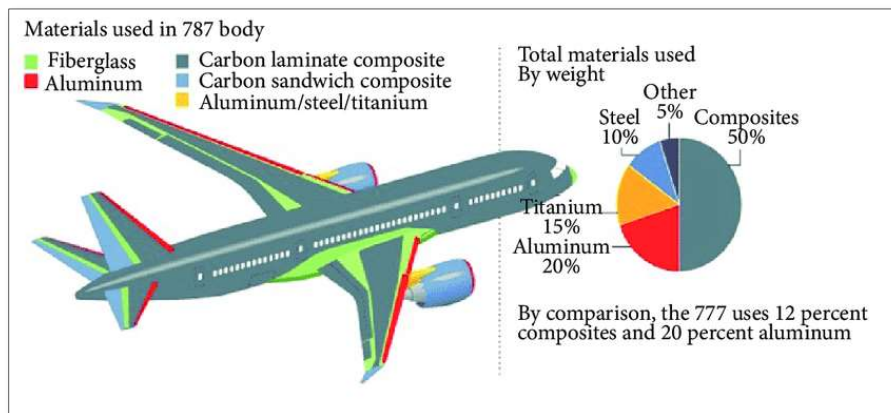
Fig 2. 1: The amount of composite material used in the aircraft industry

Fig 2. 2: The use of composite materials in engineering Mighty Buildings, Oakland, California

Fig 2. 3: AIT Bridges uses a braided fiber-reinforced polymer (FRP) tube filled with concrete
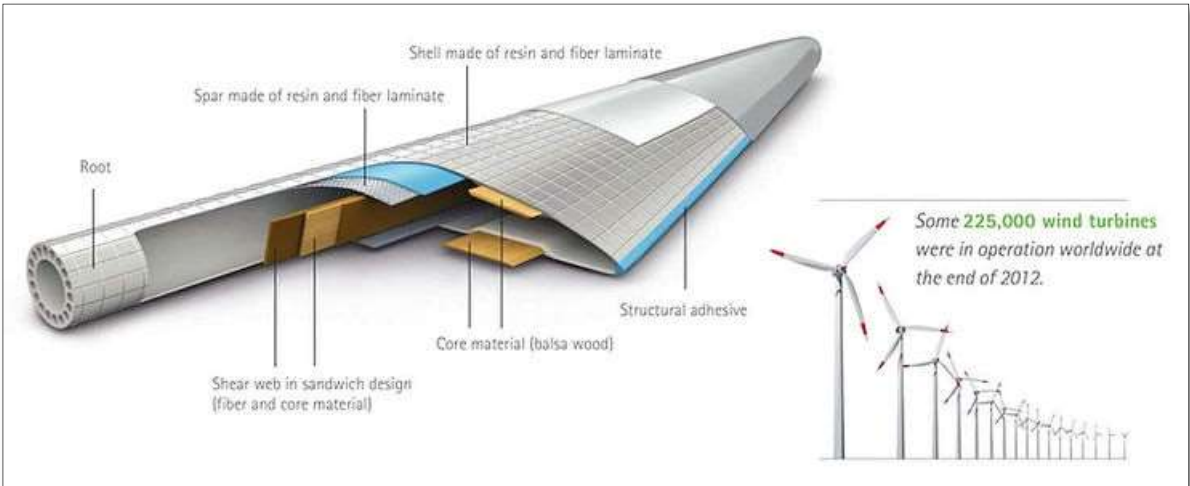
Fig 2. 4: the usage of composite materials in wind turbines. Nolet, 2011

2.2 Generality of composite materials :

2.2.1 Composite materials

A composite material is defined as a material system that consists of a mixture or combination of two or more distinctly different materials. It can also be defined as two or more chemically different constituents combined macroscopically to yield a useful material [9], A composite material consists of the assembly of two materials of different natures that complement each other and make it possible to obtain a material whose overall performance is greater than that of the components taken separately. In addition, composite material consists, in the most general case, of one or more discontinuous phases distributed in a continuous phase. The discontinuous phase is usually harder, with mechanical properties superior to those of the continuous phase. The continuous phase is called the matrix. The discontinuous phase is called the reinforcement phase. [10]
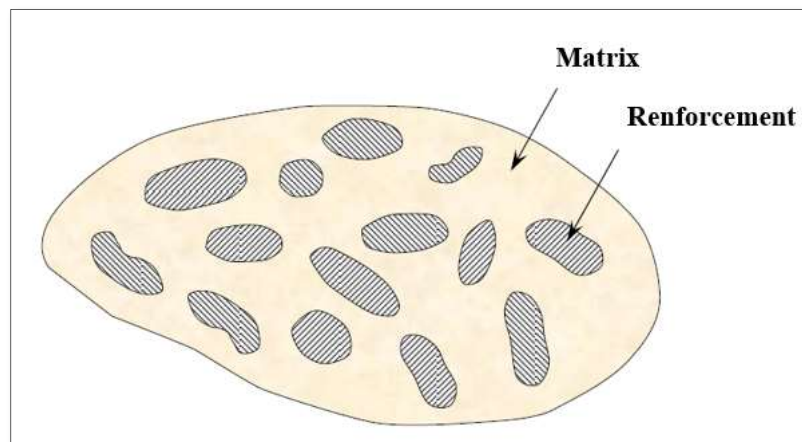
Fig 2. 5: Composite material

2.2.2 Constituent elements of a composite material :

2.2.2.1 Matrix:

In a large number of cases, the matrix constituting the composite material is a polymeric resin, which has three main functions: the distribution of the mechanical load on all the reinforcements, the cohesion of the fibers for better homogenization of the whole, and the protection of the reinforcements from the external environment (thermal or mechanical shocks) [11]. The most widely used polymeric resins in composite materials are thermosetting resins and thermoplastic resins.

The most widely used matrices are as follows (Fig 2.6):
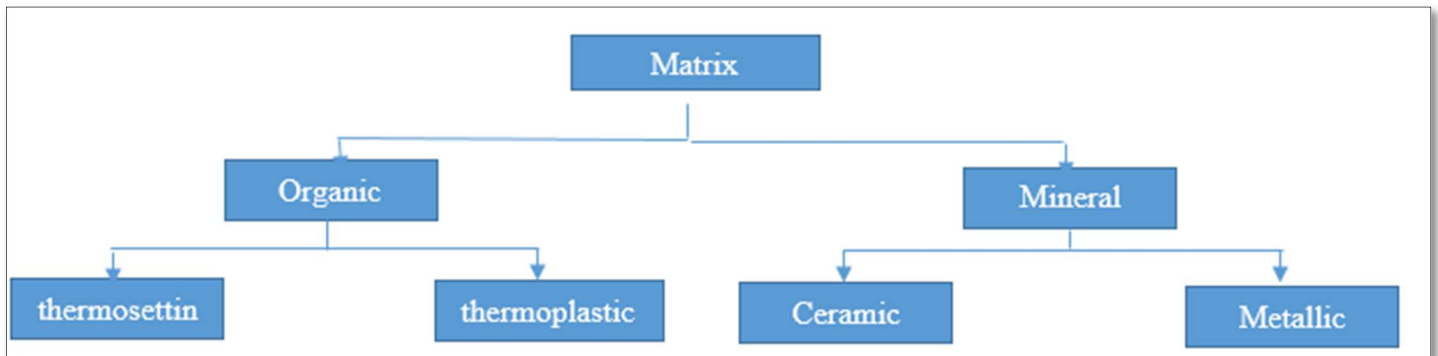
Fig 2. 6: Classification of Matrix

2.2.2.1.a Thermosetting resins:

A thermosetting resin is a polymer, often called a thermoset are usually formed from low viscosity liquids composed of long and independent molecules. Traditionally, thermoset polymers are used in fiber reinforced composites. They are an important source of properties, excellent mechanical characteristics, and better handling properties compared to thermoplastic resin.[12] The most important thermoset resins for the use in composites are: Phenolics, Epoxies, and Unsaturated polyesters . However, the two main resins used are polyesters (70%), and epoxies (25%) [13].

 Epoxy resins are generally used for high-performance applications because their shrinkage is significantly lower than that of polyesters, they have good adhesion, good mechanical and chemical resistance [13], and they Performs well at high temperatures. As for polyester resins, they are still the most widely used matrix materials. They are cheap, easy to work with liquid resin at room temperature, and have attractive mechanical, chemical, and electrical properties [12]. Phenolic resins with high performance properties such as high temperature.

The most efficient materials have high mechanical characteristics and a low density. These characteristics are presented in Table 2.1.

Table 2. 1: Characteristics of thermosetting resins [14]

resin	$T_f(C°)$	$\rho(\frac{Kg}{m^3})$	$\varepsilon_t^R(\%)$	$\sigma_t^R(MPa)$	$\sigma_C^R(MPa)$	E(Gpa)
polyesters	60 à 100	1140	2 à 5	50 à85	90 à 200	2,8 à 3,6
Phenolics	120	1200	2,5	40	250	3 à 5
Epoxies	290	1100 à 1500	2 à 5	60 à80	250	3 à 5

2.2.2.1.b Thermoplastic resins:

Thermoplastic polymers have unique advantages. The most important advantage is that it reduces manufacturing costs and has high impact strength and fracture resistance. These attractive mechanical properties produce very good damage-tolerant behavior in composite materials [15]. The most important thermoplastic resins are: Polyvinyl chloride (PVC), Polyethylene, Polypropylene, Polystyrene, Polycarbonate, and Polyamide.

Table 2.2: Characteristics of thermoplastic resins [14]

resin	$T_f(C°)$	$\rho(\dfrac{Kg}{m^3})$	$\varepsilon_t^R(\%)$	$\sigma_t^R(MPa)$	$\sigma_C^R(MPa)$	E(Gpa)
polyamide	65 à 100	1140	-	60 à85	-	1,2 à 2,5
Polypropylene	900	1200	-	20 à35	-	1,1 à 1,4

2.2.2.2 Reinforcement :

Fibers are the most important constituent of a fiber-reinforced composite material. The purpose of the reinforcement is to support most of the mechanical effort applied to the composite material thanks to its high mechanical characteristics (young modules, mechanical strength, etc.). [11] and greatly impedes crack propagation. It can be found in the form of fibers, particles, or whiskers.

The most widely used reinforcements are as follows (Fig 2.7):
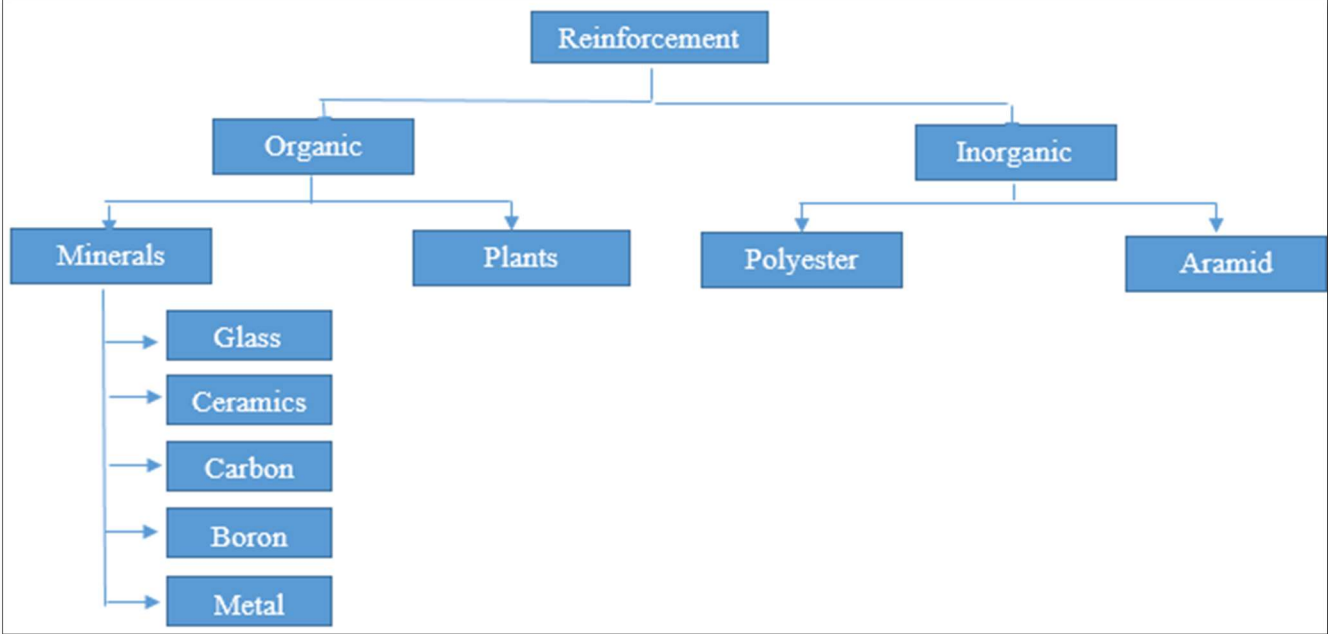
Fig 2. 7: Classification of Renforcement

Fig 2. 8: type of fibers (a: glass , b: carbon , c: Aramid , d: steel)

2.2.2.2.a. Glass Fibers :

Glass fiber is generally obtained from silica (SiO2) and additives. It has an excellent cost-performance ratio, placing it at the forefront of the current reinforcement materials used in composite structures. There are different varieties of glass fiber:

➢ E Glass : much more common, it has good dielectric properties, low costs, and high strength . E-glass fiber products have excellent flexibility and are particularly resistant to abrasion and vibration.

➢ D Glass : excellent electrical properties but low mechanical properties.

➢ C Glass : high chemical corrosion resistance

➢ R Glass and S Glass : They are suitable for high-performance applications due to their higher tensile strength and modulus of elasticity than other glass fibers and their high strength heat resistance.

Table 2. 2: Mechanical characteristics of glass types E, A, R, S and D [11]

	E-Glass	A-Glass	R or S-Glass	D-Glass
Density ($\frac{Kg}{m^3}$)	2540	2460	2550	2160
Young's modulus (Mpa)	72000	71000	86000	55000
Failure strangth (Mpa)	3500	3100	4500	2500
Elongation at break (%)	4,4	-	5,2	-

2.2.2.2.b Carbon Fibers :

Carbon fibers have very good mechanical characteristics (density is low generally less than 2000 kg/m3), carbon fibers have excellent temperature resistance in a non-oxidizing atmosphere. In fact, their mechanical characteristics are maintained up to approximately 1,500°C [10] . This property has led to the development of carbon fiber / carbon matrix composites, with high thermal resistance. However, their use is limited because the manufacturing cost remains high [15]. Some examples of conventionally encountered carbon fibers : HM, HR.

High modulus fibers (HM): for a combustion temperature of 1800 to 2000 °C.

High resistance fibers (HR): for combustion from 1000 to 1500 °C. [16]

2.2.3 Structural of composite materials :

Composite materials typically consist of two or more constituent materials that are combined to create a material with the desired properties. the properties of which depend not only on the properties of composite materials of the constituent materials but also on the geometrical design of the various structural elements. and orientation within the composite structure.

Composite laminates and sandwich panels are two of the most common structural composites.

2.2.3.1 Laminate composite materials :

Laminate composite materials are a type of composite material that consists of layers of two or more different materials, such as fibers and a matrix, bonded together to create a single material. Each layer is referred to as a "lamina" and can have different material properties and orientations.

If all layers or plies in a composite material are stacked in the same orientation, it is referred to as a lamina. On the other hand, if the plies are stacked at different angles, it is called a laminate. Laminated materials, such as continuous-fiber composites (as shown in Fig 2.9), typically have layers, plies, or laminae oriented in a manner that enhances strength in the primary load direction [17].
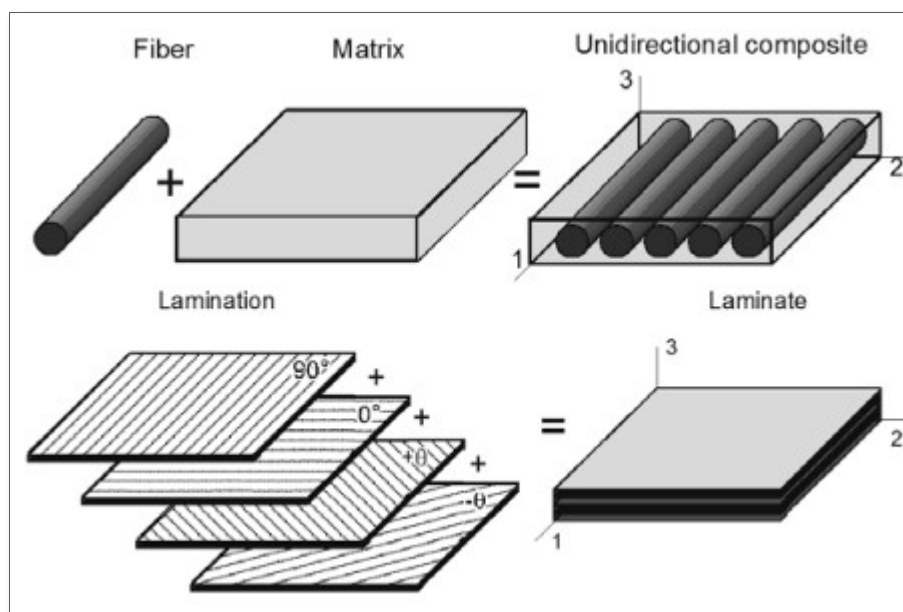
Fig 2. 9: unidirectional and laminate composite materials

However, the detachment of two plies, known as delamination, is the primary weak point of this type of material and explains their weak resistance to impact and, more generally, to out-of-plane stresses (whether direct or induced).

2.2.3.2 Sandwich composites:

Sandwich structures are composite materials that are experiencing significant growth in their use. These structures consist of three main layers with different mechanical characteristics (see Fig 2.10): two thin skins, typically laminated, with excellent mechanical properties (high modulus of elasticity and high compressive and tensile strength), which are bonded to a thick, lightweight core with weaker mechanical characteristics (e.g., foam, wood), whose primary role is to resist shear stresses. These layers are joined together through gluing or welding. The resulting structure is made of a lightweight, strong, and stiff material with good thermal and acoustic insulation properties. The objective of such a process is to constitute a structure that makes it possible to reconcile lightness and rigidity. Generally, the choice of materials is made with the initial objective of having a minimum mass, then taking into account the conditions of use (thermal conditions, corrosion, price, etc.).
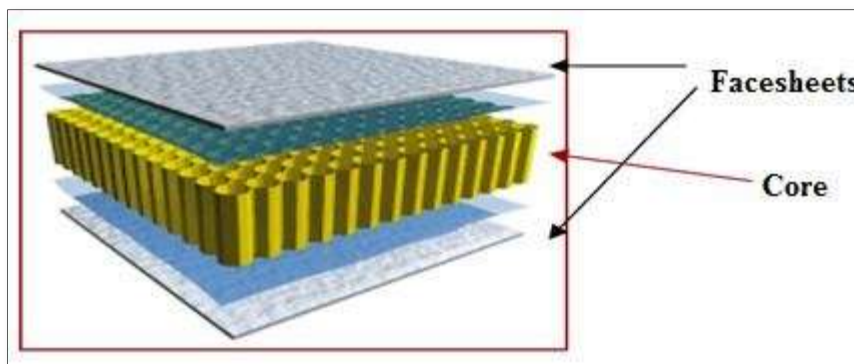
Fig 2. 10: Sandwich Structural Components

2.2.4 Composite materials behaviors :

The mechanical behavior of composites and metals differs fundamentally because composite materials are often heterogeneous and non-isotropic (orthotropic or anisotropic). You can say about a material that it is homogeneous if it has different properties at two different points. and be isotropic when it has the same characteristics in all directions. A fiber-reinforced composite lamina behaves like an orthotropic material, which means it has three mutually perpendicular

planes of symmetry known as principal material directions. On the other hand, anisotropic materials have varying properties in all directions and lack planes of symmetry. When normal stress is applied to anisotropic materials, it results in not only an extension in the direction of the stress but also a contraction perpendicular to it and a shearing deformation. Similarly, the application of shearing stress causes not only a distortion in the shearing direction but also an extension and contraction. This coupling between both types of loading and both types of deformation, known as shear-extension coupling, is a distinguishing feature of orthotropic materials under normal stress in a non-principal material direction. In addition, when normal or transverse stress is applied to a material, it results in coupling between different types of deformation, such as extension-twist or bending-twist. In a thin, symmetric laminated plate, there is no bending-extension coupling due to the symmetry of the middle surface. In contrast, unsymmetric laminated plates exhibit coupling between bending and extension. In this study, the material of each layer is assumed to be linearly elastic and orthotropic, with zero stress considered along the thickness directions. Additionally, all layers are perfectly bonded together.

2.2.5 Laminated composite plate theories :

Laminated plate theories are essential for providing an accurate analysis of laminated composite plates; hence, a number of laminated composite theories have been developed and provided with a great quantity of literature in order to provide an accurate analysis of laminated composite plates.[18]

To now, most applications involving the study of multilayer structures have favored the use of two-dimensional (2D) models. In reality, these models are more practical than 3D models in terms of modeling simplicity and necessary calculation efforts. In general, laminated plate theories may be classified into two basic categories [19]:

- Equivalent single-layer approach (ESL)
- layer-wise approach (LW).

2.2.5.1 Equivalent monolayer approach (ESL)

In the equivalent monochroving approach, which is the most adopted by researchers, the heterogeneous multilayer plaque is treated as a single homogeneous layer equivalent via the homogenization technique [20]. The ESL theories give a sufficiently precise explanation of the

global laminate response for many applications (e.g., transverse deflection, fundamental vibration frequency, critical buckling load, force, and moment resultants).

Because of the minimal number of dependent variables that must be accounted for, the main advantages of ESL models are their inherent simplicity and low computing costs.

However, ESL models are frequently insufficient for calculating the three-dimensional stress field at the ply level [21].

In this approach, three well-known theories can be distinguished, namely:

- Classical Plate Theory (CLPT)
- First order shear deformation theory (FSDT)
- Higher order theories (HSDT)

2.2.5.1.a. Classical Plate Theory (CLPT):

The Classical Laminate Theory (CLT) is a widely used engineering approach for analyzing the behavior of laminated composite materials, which are composed of two or more layers of different materials. It is a simplification of the more complex three-dimensional theory of elasticity and is based on the assumption that the laminate behaves as a homogeneous, anisotropic material. It was initiated by Kirchhoff [22] in 1850, then continued by Love [23] at the beginning of the 20th century.

The CLT assumes that the layers in a laminate are perfectly bonded to each other and that the laminate is thin relative to its other dimensions (the CLPT being applicable to any planar structural element having a thickness to width ratio smaller than 1/10 that acts as a plate [24, 25]). It also assumes that the stresses and strains in the thickness direction of the laminate are negligible compared to those in the plane of the laminate.

The CLPT theory is based on the assumption that lines normal to the median plane before deformation remain straight and perpendicular to the average surface after deformation (Fig. 2.11). which indicates that transverse shear strain and transverse normal strain are zero ($\sigma_z = 0$, $\varepsilon_z = 0, \varepsilon_{xz} = \varepsilon_{yz} = 0$).

Using these assumptions, the CLT can provide a simple way to calculate the mechanical properties of a laminate, such as its stiffness and strength, based on the properties of the

individual layers and their stacking sequence. The theory can also be used to predict the deformation and failure behavior of laminates under different loading conditions.

Despite its simplifications, the CLT is widely used in the design and analysis of composite structures in aerospace, automotive, and other industries due to its efficiency and accuracy in predicting the behavior of laminates.
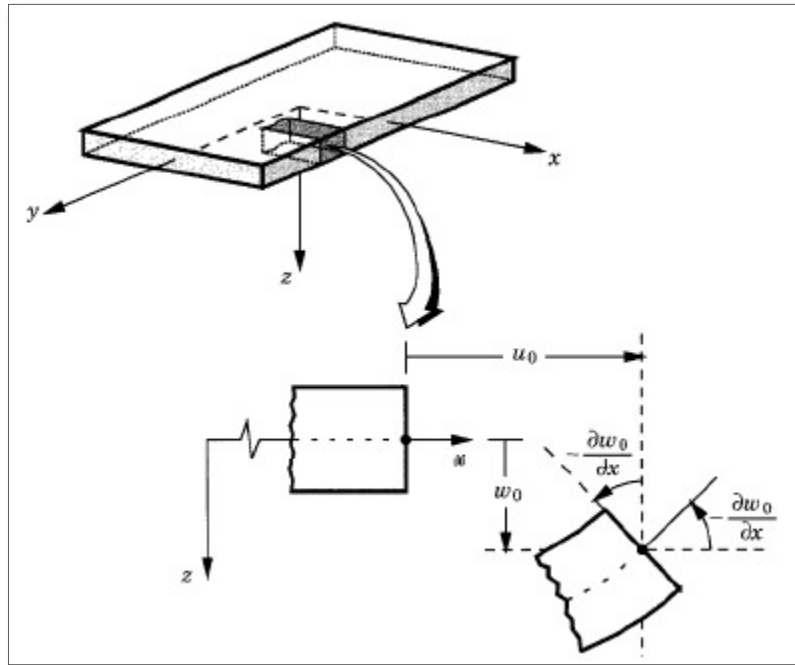
Fig 2. 11: Deformed and undeformed geometries of a plate edge under the Kirchhoff hypothesis [26]

The displacement field according to the CLT is given by the following equations:

$$u(x,y,z) = u_0(x,y) - z\frac{\partial w}{\partial x}$$
$$v(x,y,z) = v_0(x,y) - z\frac{\partial w}{\partial y}$$
$$w(x,y,z) = w_0(x,y)$$

Where u_0, v_0 and w_0 are the mid-plane displacement components of the plate element

Since Kirchhoff theory ignores transverse shear deformation, it cannot be applied to thick plates, where shear deformation effects are more significant. Thus, it is only suitable for thin plates [27].

2.2.5.1.b First Order Shear Deformation (FSDT):

First-order shear deformation theories (FSDTs) are enhancements over the classical laminate theory (CLT) [27]. This theory takes into account the shear deformation effects that occur in such structures, which are not considered in classical beam and plate theories.

This theory is essentially based on the following Reissner-Mindlin hypothesis: the transverse straight lines before deformation will still be straight after deformation, but they are not normal to the mid-plane after deformation. (because of the effect of transverse shear) [28, 29] (Fig. 2.12).
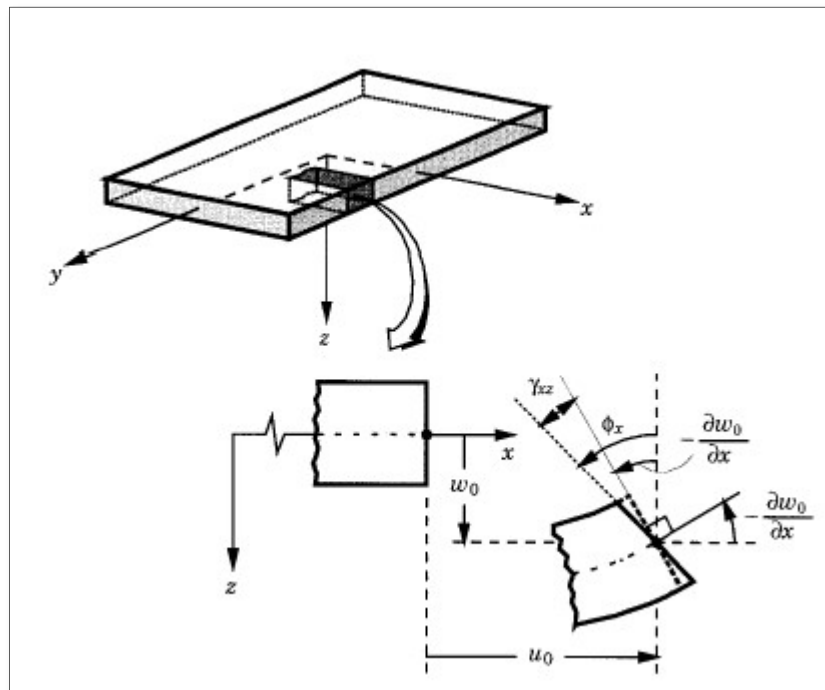
Fig 2. 12: Deformed and undeformed geometries of a plate edge under the Reissner-Mindlin hypothesis [26]

The displacement field of the first-order theory is written as follows:

$$u(x,y,z) = u_0(x,y) + z\phi_x(x,y)$$
$$v(x,y,z) = v_0(x,y) + z\phi_y(x,y)$$
$$w(x,y,z) = w_0(x,y)$$

Where ϕ_x and ϕ_y are the rotations of the normal around the axes (x, y), respectively.

♦ **Shear correction factors:**

A shear correction factor, denoted k, is added to correct for the mismatch between the actual (3D) transverse shear stress distribution and those assumed in the first-order theory. These factors are introduced as parameters in the constitutive relationships between transverse shear forces and transverse shear strains. For homogeneous, isotropic materials, the first concept of FC was presented by Reissner [30-32]. He proposed a value of 5/6 which is widely used, employing a calculation method based on considerations of static equilibrium and energy equivalence.

2.2.5.1.c. Higher-order shear deformation theories (HSDT):

Many researchers [33, 34] have proposed refined theories called "higher order shear deformation theories" (HSDT) to overcome the limitations of the previous theories. These limitations include the difficulty in determining the stresses and their distributions with respect to the plate's thickness. The HSDT theories utilize a non-linear variation of the displacement field, which is depicted in Fig 2.13, to more accurately represent the deformations and transverse shear stresses without needing to use CF correction factors. Additionally, the HSDT theories can take into account the possibility of warping of the plate's cross-section during deformation [35].
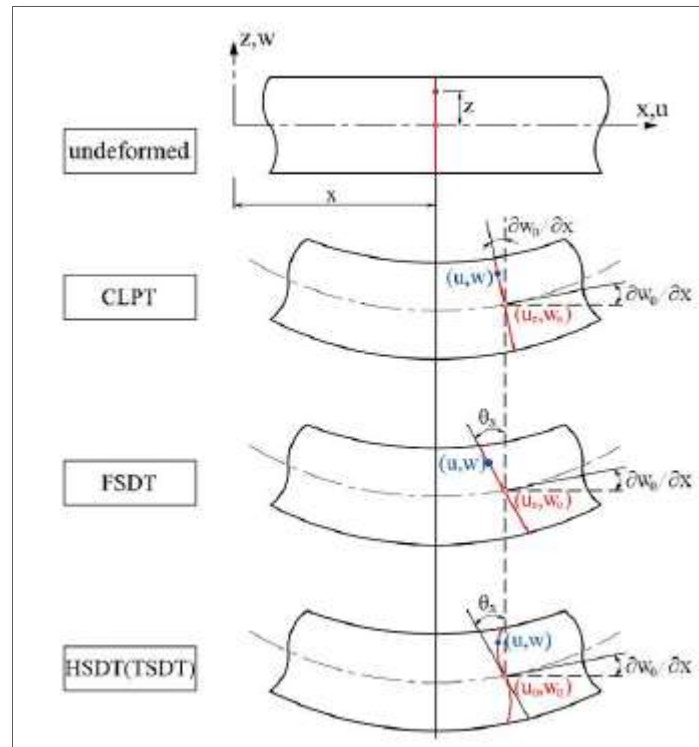
Fig 2. 13: Kinematics of deformation in different ESL theories (CLPT, FSDT,HSDT)

2.2 Literature Review

2.2.1 Failure loads:

The most significant criterion for laminated composite structure safety design is failure. Failure analysis of laminated composite materials is far more complicated than failure analysis of isotropic materials. The strength of a laminate is affected by several parameters, such as the laminate orientation angle, stacking sequence, load, stiffness, and hygrothermal environmental conditions, which impact stresses that affect laminate strength. For this reason, a laminate's failure analysis is more difficult than that of a single laminate; it necessitates the correct prediction of the strength of each laminate by measuring stresses on its local axis in each laminate and applying appropriate failure criteria. When a single laminate fails, it does not signify that the entire laminate fails; rather, it marks the start of the failure process, and it is called the first ply failure (FPF) load, which is defined as the load in which the first ply fails.

The failure criteria are divided into two groups: interactive and non-interactive. Non-interactive failure criteria are a type of failure criterion that assumes that the different failure

modes that a material or structure can undergo, such as tensile failure, compressive failure, or shear failure, are independent of each other (there is no interaction between the lamina stresses). This simplicity makes non-interactive failure criteria more commonly used in practice, especially in situations where it is difficult to predict how different failure modes might interact. While non-interactive failure criteria are generally simpler to use, they do have some limitations. Because they assume that different failure modes are independent of each other, they may not be accurate in all situations. In some cases, interactive failure criteria may be necessary to accurately predict failure in complex structures or materials. Interactive failure criteria are a type of failure criterion that takes into account the interactions between strengths from multiple directions that a material or structure can undergo (there is an interaction between the lamina stresses). These criteria are more complex than non-interactive failure criteria but are necessary in situations where it is important to understand how different failure modes might interact.

Various analytical approaches have been developed in the literature to characterize and model the failure behavior of composite plates. Some of these approaches focus on the behavior of each component of the material, such as the fiber/matrix interaction called "macro" , to understand their interactions and influence on the overall behavior of the plate. Conversely, "macro" approaches are based on global failure criteria at the structure's scale, such as the First-Ply Failure Theories. These methods help to identify the "damage" zones of the structure and provide an overall rating for each layer.

In general, the creation of laminated composite plates necessitates a thorough understanding of the damage to failure and an accurate modeling. Until now, many failure criteria have been offered in order to predict the behavior of composite structures Tsai–Wu [36], Tsai–Hill [37], Hoffman [38], Maximum stress [39], maximum strain [39], quadric surfaces [40] and modified quadric surfaces [41] are the most extensively utilized failure theories. They cannot forecast the failure mode of composite constructions (fiber or matrix). Failure theories such as Hashin [42], Norris [43], Hart-Smith [44], Sun [45] and Davila. [46], Puck [47] and Catalanotti [48] used these criterion to forecast fiber-dominated and matrix-dominated composite structure failures.

Tsai-Hill failure criterion directly adapts to the von-Mises criterion [49]. R. Hill introduced one of the first interactive failure criteria applicable to anisotropic materials [10, 50]. In the case of unidirectional composite materials, V.D. Azzi and S.W. Tsai [51] simplified the Hill fracture criterion in-plane stresses. In 1973, Hashin proposed two different failure

criterions, the first related to fiber failure and the second to matrix failure. In order to improve the prediction capabilities of the Hachin criteria, many researchers, including Sun and Puck, have proposed some modifications. Sun et al. [45] proposed an amendment to the failure of matrix compression for the Hachin criteria. Puck [47, 49] proposed a three-dimensional criterion that considers the tractions interaction on the fracture plane. In the same context, Davila [46] proposed new failure criteria for polymer laminates reinforced by fiber, which are denoted LaRC03. This criterion can predict matrix and fiber failure and fracture angle (are used Mohr-Coulomb effective stresses for determining the angle of fracture plane) for matrix failure under transverse compression by maximizing the Mohr-Coulomb effective stresses. Kim et al. [52] used a beam finite element method with layer-wise constant shear (BLCS) under bending loads to study the progressive failure of laminated composite beams using Tsai–Wu and Maximum stress failure criteria to predict the failure at Gaussian points of each damaged beam. On the other hand, Nazargah et al. [53] developed a four-node quadrilateral partial mixed plate element with few degrees of freedom. This finite element model is based on a parametrized mixed variational concept established recently by for static and free vibration analysis of functionally graded material (FGM) plates supported by Winkler-Pasternak elastic foundations. The provided model was validated by comparing it to the results of the three-dimensional (3D) theory of elasticity as well as the results of the classical and high-order plate theories available in the literature. In addition, a high-performance finite element model for bending and vibration analysis of thick plates has been developed by Nazargah [54] based on the parametrized mixed variational principle. For the bending and vibration analysis of multi-layered composite plates, Nazargah et al. [55] presented a unique mixed-field theory with a small number of unknown variables [55]. Irhirane et al. [56] have studied bending failure for graphite-epoxy laminates. The laminate composites have been modeled using eight-node isoparametric plate bending elements using first-order shear deformation theory (FSDT). On the other hand, different failure criteria theories are used to predict damage. Moncada et al. [57] used various failure theories to study the progressive failure of laminated composites and compared the results obtained by each of them. The generalized and high-fidelity generalized of cells micromechanics method, coupled with classical laminated theory, are used. It was shown that the numerical results agree with the experimental results. In addition, Hasan et al. [58] studied the failure analysis and shape control of smart laminated composites containing different types of piezoelectric materials under coupled thermal, electrical, and mechanical stimuli. They used various failure criteria, such as Tsai-Wu, Tsai-Hill, and Maximum stress criteria, to predict the first-ply failure FPF and ultimate laminate failure. Daniel [59] proposed a new nonlinear constitutive model to

describe composites' behavior and failure criteria under static and dynamic loading. M. Lezgy-Nazargah [60] investigated composite laminated beams' progressive failure analysis. The RHGB (refined high-order global-local beam) theory is used in his finite element formulation. Several failure criteria were used to describe the failure behavior of laminated composites and predict the FPF and UFP (ultimate failure load) of composite laminates with different loads, fiber orientation, and boundary conditions.

Moreover, composite laminates experience various thermal and moisture conditions during manufacturing and storage, which create stress and strain. Changes in temperature and moisture affect the stiffness and strength of composites, resulting in complex stress and strain in the plates. The elastic modulus and strength of composite laminates decrease as temperature and moisture concentrations increase, leading to the formation of hygrothermal internal tensions. These tensions can cause significant deformation and even structural failure. Hygrothermal stresses, which affect the performance of composite laminates, are generated due to exposure to moisture and temperature fluctuations. If a mechanical load is applied to the same laminate, it creates thermomechanical stress. Moreover, when the laminate is exposed to moisture, in addition to thermal and mechanical strain, it generates hygro-thermo-mechanical stress.

The thermal and hygrothermal behavior of laminated composite materials has received much attention by many investigators. Wu et Tauchert.[61, 62] studied the analysis of symmetric and antisymmetric plates subjected to a 3D variation of temperature (constant and linear varying thermal fields) using the classical laminated theory (CLT). They found that the effects of thermal membrane-bending coupling were significant in laminated plates with a small number of layers when compared to those with a high number of layers. Reddy and Hsu [63] used a finite-element formulation based on the FSDT for analyzing composite laminated plates subjected to uniform and sinusoidal temperature variations. They used several parameters (fiber orientation, aspect ratio, side-to-thickness ratio, and boundary condition) to show the effects on deflections and stresses of the plate. Ram et al. [64] investigated the effects of moisture and temperature on the bending behavior of laminated composite plates using a quadratic, eight-noded, isoparametric element with five degrees of freedom at each node. An anti-symmetric cross-ply laminate was used to obtain the deflection and stress resultants for a simple and clamped boundary condition at different moisture concentrations and temperatures. Chen [65] studied the thermal deformation and stress analysis of composite laminated plates using the finite element method.

25

Ray et al. [66] used an isoparametric element with eight nodes based on the first-order shear deformation theory (FSDT) to investigate the first-ply failure of symmetric and antisymmetric laminated composites under linear temperature loading. To achieve this goal, Tsai-Wu and Hoffman failure criteria are used. In a similar context, Zhang et al.[67] conducted a progressive failure analysis of composite materials in hygrothermal environments (i.e., temperature and moisture) to predict the failure of composite laminates. The model included constitutive equations accounting for hygrothermal strains. Additionally, A. Choudhury and colleagues [68] investigated the failure analysis of laminated composite plates under thermomechanical and hygro-thermo-mechanical loads for various parameters (i.e., stacking sequences, thicknesses, and fiber orientation angles). They employed different failure criteria, such as maximum stress, maximum strain, Tsai-Wu, and Tsai-Hill. Furthermore, they calculated the first-ply failure and the last-ply failure loads.

In order to test the reliability and accuracy of the computational tools used for analyzing the structural integrity, Hinton, Kaddour, and Soden [69, 70] conducted a comprehensive investigation to characterize the accuracy and validity of numerous failure predictions in composite laminates. This project is known as the "First World Wide Failure Exercise (WWFE-I)."

The WWFE-I aimed to bring together experts from around the world to compare and evaluate the accuracy and reliability of different computational tools used to predict the failure behavior of polymer composite laminates when subjected to complex loads . The exercise was designed to provide a platform for international collaboration and sharing of knowledge

In addition to testing the computational tools, the WWFE-I also aimed to identify any weaknesses or areas for improvement in the tools and to make recommendations for future research and development. By establishing a standardized and collaborative approach to evaluating the reliability and accuracy of computational tools.

Among the most commonly used and common failure criteria that can be mentioned are :

Maximum stress and strain failure criteria

Two commonly used failure criteria for modern composites are the maximum stress criterion and the maximum strain criterion. These criteria originated from conventional failure criteria for isotropic materials that were established long before the availability of modern composites.

These criteria were derived from conventional failure criteria for isotropic materials predating the availability of modern composites. They have found their way into contemporary engineering design tools like Abaqus and Ansys. These criteria are favored in certain applications due to their simplicity, particularly when a quick estimate is needed. They also provide clear insights into failure modes and can be applied to genuinely orthotropic materials, not just transversely isotropic materials. However, criticisms of these criteria stem from the absence of interactions among stress or strain components, leading to less accurate predictions, especially in situations involving competing stress or strain factors. Nevertheless, researchers have made efforts to adapt or modify these criteria to address their specific limitations [71]. The maximum stress criterion, being less complex, is widely employed to predict composite material failure. It is a linear, stress-based criterion that is dependent on failure mode and does not consider stress interactions (The mathematical formula is detailed in Chapter 3).

Tsai-Wu failure criteria

The Tsai-Wu failure criteria is a widely used material failure theory used in composite material analysis. It is named after two researchers, Edward Tsai and Alan Wu, who proposed this theory in 1971. The Tsai-Wu failure criteria uses a quadratic polynomial expression to predict the failure of composite materials.Usually, these equations are derived by adjusting them to experimental test results [72]. The theory uses the principal strains and stresses of a composite material to calculate the values of various parameters such as F_i, F_{ij}, and F_{ijk}. These parameters are related to the strengths of the material in its principal directions. The third-order tensor F_{ijk} is usually neglected in practice due to the large number of material constants required. The Tsai-Wu failure criteria equation takes into account the interaction between the various stresses and strains that a material may experience, this criteria is unrelated to failure modes.

Tsai and Wu's [36]Tensor Polynomial Criterion is the most comprehensive polynomial criterion for composite materials, and it can be expressed in tensor notation as :

$$F_i\sigma_i + F_{ij}\sigma_i\sigma_j + F_{ijk}\sigma_i\sigma_j\sigma_j \geq 1 \tag{2.1}$$

In a 3-D case, i, j, and k take values from 1 to 6 (i, j, k = 1, ... , 6). The parameters F_i, F_{ij}, and F_{ijk} are connected to the strengths of the lamina in its principal directions. However, due to the significant number of material constants required, the third-order tensor Fijk is often ignored for practical purposes. As a result, the overall polynomial criterion becomes a simpler quadratic expression, according to a commonly used approach given by :

$$F_i\sigma_i + F_{ij}\sigma_i\sigma_j \geq 1 \qquad (2.2)$$

Equation (2.2) is written in expanded form as follows:

$$
\begin{aligned}
&F_1\sigma_1 + F_2\sigma_2 + F_3\sigma_3 + F_4\sigma_4 + F_5\sigma_5 + F_6\sigma_6 \\
&+F_{11}\sigma_1^2 + 2F_{12}\sigma_1\sigma_2 + 2F_{13}\sigma_1\sigma_3 + 2F_{14}\sigma_1\sigma_4 + 2F_{15}\sigma_1\sigma_5 + 2F_{16}\sigma_1\sigma_6 \\
&+F_{22}\sigma_2^2 + 2F_{23}\sigma_2\sigma_3 + 2F_{24}\sigma_2\sigma_4 + 2F_{25}\sigma_2\sigma_5 + 2F_{26}\sigma_2\sigma_6 \\
&+F_{33}\sigma_3^2 + 2F_{34}\sigma_3\sigma_4 + 2F_{35}\sigma_3\sigma_5 + 2F_{36}\sigma_3\sigma_6 \\
&+F_{44}\sigma_4^2 + 2F_{45}\sigma_4\sigma_5 + 2F_{46}\sigma_4\sigma_6 \\
&+F_{55}\sigma_5^2 + 2F_{56}\sigma_5\sigma_6 \\
&+F_{66}\sigma_6^2 \geq 1
\end{aligned}
\qquad (2.3)
$$

Where $\sigma_1 = \sigma_{11} = \sigma_L$, $\sigma_2 = \sigma_{22} = \sigma_T$, $\sigma_3 = \sigma_{33} = \sigma_{T'}$, $\sigma_4 = \sigma_{23} = \sigma_{TT'}$, $\sigma_5 = \sigma_{13} = \sigma_{LT'}$,

$\sigma_6 = \sigma_{12} = \sigma_{LT}$

In the case of an orthotropic composite material subjected to a plane stress state in the planes (1, 2) = (L, T), the relationship (2.3) is written as

$$F_1\sigma_1 + F_2\sigma_2 + F_6\sigma_6 + F_{11}\sigma_1^2 + 2F_{12}\sigma_1\sigma_2 + F_{22}\sigma_2^2 + F_{66}\sigma_6^2 \geq 1 \qquad (2.4)$$

The parameters F_i and F_{ij} can be expressed using the breaking stresses, measured in various tests.
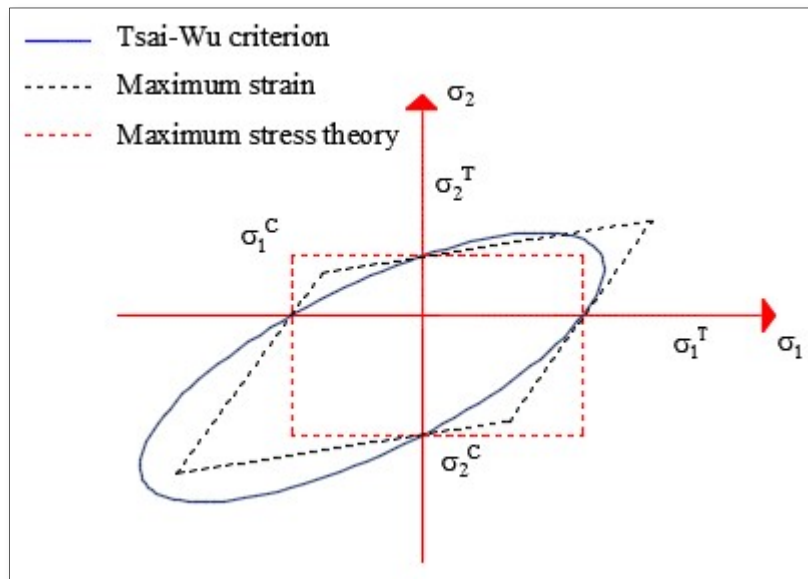
Fig 2. 14: Failure criterion from the maximum stress and maximum
strain and Tsai-We criteria, respectively.

Tsai-Hill failure criteria :

The Tsai-Hill failure criteria is a widely used method for predicting failure in composite materials. This criteria was developed by Tsai and Hill in 1965 and has been refined and extended over the years. This failure criterion considers the interaction between the stress components.

Based on the distortion energy theory, Tsai and Hill proposed that a lamina has failed if:

$$(G_2 + G_3)\sigma_1^2 + (G_1 + G_3)\sigma_2^2 + (G_1 + G_2)\sigma_3^2 - 2G_3\sigma_1\sigma_2 - 2G_2\sigma_1\sigma_3$$
$$-2G_1\sigma_2\sigma_3 + 2G_4\tau_{23}^2 + 2G_5\tau_{13}^2 + 2G_6\tau_{12}^2 \leq 1$$

(2.5)

The parameters G_1, G_2, G_3, G_4, G_5, and G_6 are characteristic parameters of the material being considered, which are linked to the ultimate strengths X, Y, and S of the material, according to the relationships established below.

In the case of a tensile (or compression) test in direction 1 (L), the Tsai-Hill criterion is reduced to:

$$(G_2 + G_3) = \frac{1}{X^2}$$

(2.6)

where X is the longitudinal strength in tension and compression in the direction L. Similarly, we find:

$$(G_1 + G_3) = \frac{1}{Y^2}$$

(2.7)

$$(G_1 + G_2) = \frac{1}{Z^2}$$

(2.8)

Where Y and Z are the transverse strengths in tension and compression in the direction T and T'.

In the case of a shear test in the plane (L,T), the Tsai-Hill criterion is reduced to:

$$2G_6 = \frac{1}{S_{12}^2}$$

(2.9)

$$2G_5 = \frac{1}{S_{13}^2} \qquad\qquad (2.10)$$

$$2G_4 = \frac{1}{S_{23}^2} \qquad\qquad (2.11)$$

Where S_{12} , S_{13} and S_{23} are the shear strengths in the plane (L, T$'$) and (T ,T').

Expressions (2.7) to (2.8) make it possible to determine the fracture parameters G_1, G_2, G_3, G_4, G_5, and G_6 to write Tsai-Hill's criterion in the form:

$$\left(\frac{\sigma_1}{X}\right)^2 + \left(\frac{\sigma_2}{Y}\right)^2 + \left(\frac{\sigma_3}{Z}\right)^2 - \left(\frac{1}{X^2} + \frac{1}{Y^2} - \frac{1}{Z^2}\right)\sigma_1\sigma_2$$
$$- \left(\frac{1}{X^2} + \frac{1}{Y^2} - \frac{1}{Z^2}\right)\sigma_1\sigma_3 - \left(\frac{1}{Y^2} + \frac{1}{Z^2} - \frac{1}{X^2}\right)\sigma_2\sigma_3 \qquad (2.12)$$
$$+ \left(\frac{\sigma_{12}}{S_{12}}\right)^2 + \left(\frac{\sigma_{13}}{S_{13}}\right)^2 + \left(\frac{\sigma_3}{S_{23}}\right)^2 \leq 1$$

In the case of a plane stress state in the plane (L, T) of the layer of composite material:

$$\left(\frac{\sigma_1}{X}\right)^2 + \left(\frac{\sigma_2}{Y}\right)^2 - \left(\frac{\sigma_1\sigma_2}{X^2}\right) + \left(\frac{\sigma_{12}}{S_{12}}\right)^2 \leq 1 \qquad\qquad (2.13)$$

2.2.2 Stress concentration :

The assembly of composite elements into a structure frequently; necessitates the creation of holes for receiving bolts or rivets or the passage of electrical or phone wires. Openings are used in large number of structural elements, such as plates and shells. In civil engineering, openings are used as doors, windows, power lines, or sometimes just to allow weight reduction. Cutouts alter the behavior of materials and create a very undesired stress concentration around these holes [73].

Often, the designer is concerned about stress concentration and the stress distribution around openings that must be defined in order to forecast failure load. For this reason, Numerous investigators have studied the distribution of stress in perforated plates using different methods such as analytical analysis, finite element analysis (FEA), and experimental techniques. Analytical methods have been commonly used to determine the stress distribution by solving a

set of differential equations and obtaining a closed-form analytical solution using stress functions or other mathematical techniques. However, the complexity of some problems may prevent an analytical solution from being found. As a result, the finite element method (FEM) is currently one of the most popular methods for stress analysis due to its ability to provide accurate solutions for problems with no analytic solution. Additionally, recent advancements in experimental methods have produced new techniques, including photo-elasticity, brittle coating, electrical strain gauges, and digital image correlation (DIC), for analyzing the stress field.

2.2.2.1 Analytic stress analysis :

2.2.2.1.a Stress concentration of perforated isotropic plates subjected to in-plane loading :

The concept of stress concentration was first introduced in Gabriel Lame's book on elasticity theory [74], where he addressed the problem of stress distribution in a plate with a round hole under a constant uniform tension. Airy [75] later discovered that, in the absence of body forces, there always exists a single auxiliary function, known as a stress function, that can express stresses. This stress function is now known as Airy's function. In 1966, Muskhelishvili [76]used complex variables to represent Airy's stress function [75], which has become one of the most effective methods for analytically calculating stress distribution, particularly around openings in an infinite elastic plate. The complex function theory developed by Muskhelishvili is considered a powerful tool for stress analysis.

Furthermore, Howland [77] provided an analysis of stress concentration in a finite plate that has a circular opening. In his study, an isotropic plate is considered with a hole located halfway between two parallel edges, and sought a solution for the uniaxial tension problem through a successive approximation method. Howland presented the results of this analysis for different ratios of the diameter of the hole to the width of the plate.

Lekhnitskii [78] and Savin [79] developed the "Lekhnitskii Formalism," which provides solutions for circular, elliptical, triangular, and square holes in orthotropic plates. Their approach is based on Muskhelivshili's method. Lekhnitskii[78] used Fourier series to derive the stress functions, while Savin [79] used Schwarz-Christoffel integral mapping. However, their solutions are the same. Lekhnitskii [78] focused on anisotropic plates with regular-shaped holes under in-plane or bending loading, while Savin [79] focused on simply or multiply connected domains in isotropic plates. Since the introduction of the formalism and increased

computing power, researchers have expanded their findings to include multiple holes, different discontinuities, and various loading conditions. Theocaris and Petrou [80, 81]used the Schwartz-Christoffel transformation to map a triangular hole and its exterior onto the interior of a unit circle to obtain the stress distribution in an isotropic plate.

2.2.2.1.b Stress concentration of perforated anisotropic plates subjected to in-plane loading :

Often, the designer is concerned about stress concentration and the stress distribution around openings that must be defined in order to forecast failure load. For this reason, several researchers have sought to determine the SCF for various kinds of geometric cutting under various types of stresses using different methods and different analytical approaches [82-84]. Green and Zerna [85] studied the anisotropic plates that contained the cutout to address issues of values in two-dimensional elasticity. This study was one of the earliest theoretical studies. In the same context, Greszczuk's [86] provided a theoretical solution for studying the stress concentrations and failure strengths in orthotropic and anisotropic plates under different in plan-loading using the Green and Zerna method. Lekhnitskii [78] and Savin [79] calculated the stress function for circular, elliptical, square , and triangular openings in infinite orthotropic plates under in-plane and bending loadings.

V.G. Ukadgaonker et al. [87] examined the stress concentration factor (SCF) in orthotropic laminates and anisotropic plates around regular and irregular shaped holes under different in-plane loading conditions using an analytical approach of solution. The results are similar to those obtained by FEM solutions. J. Rezaeepazhand and M.[88] proposed an analytical solution to study the stress distribution in a plate under a uniaxial tension load with various cutouts forms. The analytical solution results are compared to the FEM results. Furthermore, They investigated the influence of different parameters, such as material properties, fiber orientation, and cutout shapes, on perforated plates, whereas Shivaji Toralkar et al. [89] used analytical and FEM to study the influence of fiber orientation, E1/E2 ratio, diameter of the hole, length of the plate on the SCF of the laminated plate containing a circular cutout.

Rybicki and Schmueser [90] studied the stress behavior along the edge of a circular hole in a laminated plate using a 3D finite element stress analysis. To ensure the validity of this study, the tangential strain distribution around a circular cutout for a $[0/\pm45/0]_s$ plate exposed to uniaxial stress was calculated and the results obtained were compared with laboratory results. The distribution of interlaminar normal stress around the circular cutout is then studied, as well as the influence of modifications in lay-up angle and stacking sequence. On the other hand,

Rezaeepazhand and Jafari [91, 92] conducted an analytical study to examine the influence of hole shape and material qualities on the maximum stress concentration (SCF) value and position. Lekhnitskii's method [93] was used to calculate the stresses. In the same context, Khechai et al. [94] investigated the SCF at the edge of a circular opening in a laminated composite plate under uniaxial loading. The finite element method was used based on the CLT, and the first-ply failure (FPF) was calculated as well. Many parameters, such the E_1/E_2 ratio and fiber orientation angles are studied to understand their influence on stress concentration. In addition, Khechai et al. [73] expanded Greszczuk's analytical solution for determining the stress distribution of a composite laminated plate under arbitrarily oriented in-plane loading conditions.

Lekhnitskii [78] and Savin [79] determined the stress function around circular, elliptical, square, and triangular opening in infinite orthotropic plates under various in-plane and bending loadings. Ukadgaonker et al [87]. analyzed the stress distribution around irregular forms of opening in an infinite orthotropic plate subjected to various in-plane loading conditions using Savin's method. The FEM solution is employed to validate the results. In addition to this Ukadgaonker et Rao[95] studied the stress distribution around triangulair opening in isotropic and orthotropic plate subjected to various loading at infintity (uniaxial, biaxial, and shear loading). The stress distribution around a triangular hole in an anisotropic plate subjected to uniaxial load is studied by Daoust [96] using an analytical solution. They investigated the influence of different parameters, such as various degrees of bluntness at the triangle vertex, various length/height ratios of the triangular cutout, as well as different orientations of the load, on the stress concentration. Whereas Xin Lin Gao [97] used the analytical solution (complex potential method) for solving the problem of stress concentration in an infinite plate containing an elliptical hole under arbitrary biaxial loading. SIMHA et al [98]studied the stress concentration around irregular opening using the analytical solution based on complex variable method. in the same context, Magar et al [99]. studied the stress distribution at the edge of an elliptical opening in an infinite laminated plate subjected to various in-plane loading in a hygrothermal environment using the complex variable method of Muskhelishvili. They studied several parameters, such as type of load, fiber angle, stacking sequence, temperature, volume fraction of fiber, and environmental conditions on stress distribution. Although this complex method is effective and powerful in solving flexibility problems, it is complex and must be reformulated whenever the type of load changes. Dharmin et al.[100] and Nagpal et al.[101] presented reviews on new analytical methods and techniques for calculating the stress concentration around the opening of a laminated composite plate.

Designers often avoid unsymmetrical laminates due to the difficulty of analyzing their behavior. These plates exhibit a distinct structural behavior that was not introduced within the classical materials. However, the behavior of these unsymmetrical plates has to be in aware. As the composite technology advances, the use of the unsymmetrical laminates to satisfy design requirements effectively and affordably has become more common.

Since the application of unsymmetrical laminates to structures differs from regular ones; solutions toward stress concentration problems for such laminates must be conducted. Among the researchers who studied unsymmetical plates. Chen et al. [102] used the complex potential approach developed by Chen and Shen [103] to study the moments and stress resultants at the edge of opening of infinite unsymmetrical composite laminates subjected to remote uniform loading, in addition, they studied the behavior of unsymmetric laminate plates with an elliptical hole [104]. Furthermore, Dave et al. [105] used the complex variable approach to achieve a solution for stress distribution at the boundary of an oval hole in an infinite composite plate with unsymmetric material characteristics, employing several forms and sizes such as a rectangle , a square, a circle, an ellipse, and an eye form. And several parameters such as the fiber orientation and loading angle are also investigated. In the same context, Sharma et al. [82] used Muskhelishvili's complex variable method for calculating the distribution of stress concentration at the edge of different shapes of opening (circular, elliptical, triangular hole) in an infinite composite plate under biaxial loading at infinity. The effects of some parameters, such as fiber orientation, stacking sequence, load angle, and shape of hole, are studied.

The present work focuses on calculating the (SCF) and stress resultant in an infinite plate with an unsymmetrical stacking sequence.These last contained a circular hole of multiple sizes under arbitrary axial, biaxial, and shear loading at infinity using a general analytical solution. The current study starts with fundamental analytical solution for calculating the stress concentration in a single ply. Then, general solution is presented to calculate the stress distribution in infinite symmetric laminated plates, including the influence of load direction, also the formulations of the effective moduli of unsymmetrical laminated plates generated by layer lumping are presented.

2.2.2.2 Finite element analysis :

The finite element method (FEM) is a numerical method used in engineering to solve a wide range of problems. In situations where the problems involve intricate geometries and material characteristics, analytical solutions may not be feasible, and numerical methods become necessary. As a result, engineers depend on numerical techniques like FEM to obtain acceptable solutions. The basic idea of the finite element method is to divide a complex system into smaller, simpler parts called "finite elements." Each element is defined by a set of nodes or vertices, and its behavior is governed by a set of mathematical equations that describe its physical properties. After obtaining the solutions for each element, the next step is to combine them by assembling the sub-domains and applying the boundary conditions to obtain the solution for the complete system.

FEM has many advantages over other numerical methods, including its ability to handle complex geometries, irregular boundaries, and nonlinear material behavior. It is also flexible and can be used to solve a wide range of problems in different fields.

However, FEM also has some limitations. It requires a high level of mathematical expertise and computational resources, and the accuracy of the results depends on the quality of the mesh and the selection of appropriate elements and numerical methods.

The Finite Element Method (FEM) is a commonly used numerical technique for analyzing material behavior, including stress, strain, and failure. As previously mentioned in the section above, several studies have utilized FEM to evaluate the strength of failure using different criteria. FEM has also been applied in various investigations to calculate and analyze the stress distribution in perforated plates. In the following section, we will highlight some studies that have employed FEM to analyze the stress distribution in perforated plates. The Finite Element Method (FEM) is utilized in another major class of mathematical approaches for analyzing stress distribution in perforated plates.

Several researchers have investigated the problem of stress distribution around holes in composite plates using FEM. Louhghalam et al [106]. studied the stress concentration around rectangular openings using a complex-variable conformal mapping approach coupled with the FEM. Talib et al. [107] used the FEM to study the effect of a circular cutout on Kevlar-29/epoxy composite laminated plates. The different orientation angles of Kevlar-29 fiber were

investigated. An experimental investigation was also carried out to investigate the performance of these effects under compressive and tensile loads. Chen [108] developed a special finite element for evaluating the stress concentration around a circular hole in complex structures and used the complex variable formulation to derive a special set of stress functions that embody the stress concentration effects of a hole. In addition, to solve stress concentration problems in plane elasticity, Piltner [109] proposes a special finite element formulation with circular and elliptical holes and internal cracks. A special hole element were developed by Wang et al. [110] to analyse the stress concentration of an infinite isotropic solid with elliptical hole, using the special fundamental solutions for an infinite domain containing a single elliptical hole which are derived based on complex conformal mapping and Cauchy integrals. This element was specifically used in the region near the hole boundary, while regular elements were used at other locations. Additionally, the stress concentration factors for cracks are also calculated by using these special finite elements.

Conclusion

This second chapter is dedicated to the acquisition of the knowledge necessary about composite materials to study our problem. In the first, we presented some general notions concerning composite materials as well as a brief review of approaches and theories used to analyze the behavior of multilayer composite structures. In the second part of this chapter, a compilation of exclusive research papers is presented that reviews the failure strength, some failure criteria found in the literature, and stress concentration of composite materials

Chapter

3

MATHEMATICAL

FORMULATION

Chapter 3

Mathematical Formulation

3.1. Introduction

The purpose of this chapter is to expose the mathhematical formulation of the finite element used in order to study the failure mechanisms and the first ply failure (FPF) load. The FPF analysis is performed using a rectangular plate element with 6 degrees of freedom at each node. The present element is formulated based on the classical lamination theory (CLT) to calculate the in-plane stresses. To achieve this goal, several failure criterions, including Tsai-Wu, Tsai-Hill, Hashin, and Maximum Stress criteria, are used to predict failure mechanisms. These criterions are implemented within the finite element code to predict the different failure damages and responses of laminated beams from the initial loading to the final failure.

Sometimes designers need to make holes in different shapes in the laminate in order to meet the design requirements and for various practical reasons. For this, understanding the behavior of perforated laminates is necessary for the design of these complex structures. The second part in this work focuse to study the stress concentration factor in an infinite plate with an unsymmetrical stacking sequence of plates that include a circular hole under arbitrary loading at infinity using a general analytical solution. The Greszczuk's method is extended by first introducing different arbitrarily oriented in-plane loads. Then, in the current solution, the formulations of the effective moduli of symmetrical and unsymmetrical composite laminated plates are presented this solution used only if the assumption that the plate is infinite in size. However, to emulate as much as possible the true structural behavior when the plates are not infinite, the finite-width correction factor given by Tan [111] is added.

3.2 Finite element formulation

The finite element used in this investigation is a rectangular element of 24 degrees of freedom per element. Fig 3.1 shows the geometry and nodal variables of the element
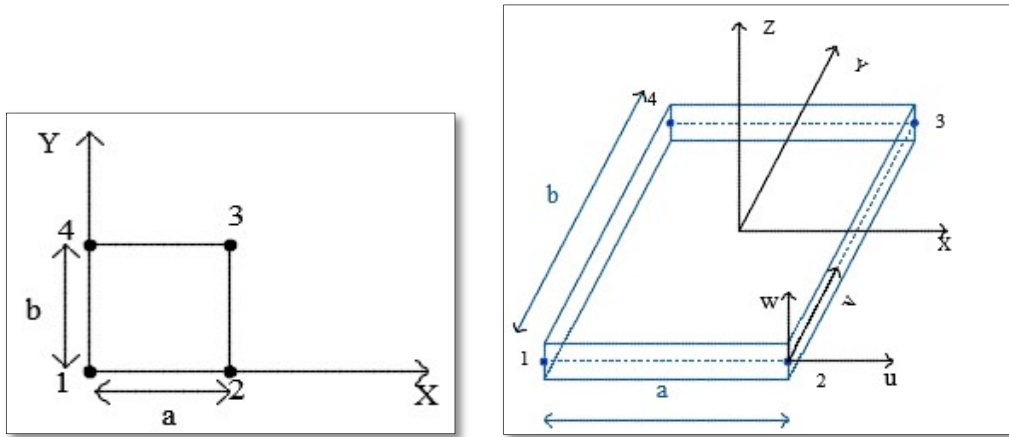
Fig 3. 1 : Geometry and nodal variables of the element (Rectangular plate element)

The current element has four (4) nodes, each with six degrees of freedom. The nodal degrees of freedom of the present element are

$$\{q\} = \left\{ u_i, v_i, w_i, \frac{\partial w_i}{\partial x}, \frac{\partial w_i}{\partial y}, \frac{\partial^2 w_i}{\partial x \partial y} \right\}_{i=1,4}$$

✓ two degrees of freedom in the plane (x, y) which are (u, v).

✓ four out-of-plane degrees of freedom, which are $(w, \frac{\partial w}{\partial x}, \frac{\partial w}{\partial y}, \frac{\partial^2 w}{\partial x \partial y})$

The presented element is a combination of a membrane element and a rectangular plate element with a high degree of accuracy. The membrane displacement of the developed element, through the element, can be expressed in terms of the interpolation functions as

$$\begin{Bmatrix} u(x,y) \\ v(x,y) \end{Bmatrix} = \begin{bmatrix} -\frac{x}{a} - \frac{y}{b} + \frac{xy}{ab} + 1 & 0 & \frac{x}{a} - \frac{xy}{ab} & 0 & \frac{xy}{ab} & 0 & \frac{y}{b} - \frac{xy}{ab} & 0 \\ 0 & -\frac{x}{a} - \frac{y}{b} + \frac{xy}{ab} + 1 & 0 & \frac{x}{a} - \frac{xy}{ab} & 0 & \frac{xy}{ab} & 0 & \frac{y}{b} - \frac{xy}{ab} \end{bmatrix} \{\delta_m^e\}$$
(3.1)

Where $\{\delta_m^e\}$ is the membrane displacement vector of the element. The Eq. (3.1) can be written as

$$\begin{Bmatrix} u(x,y) \\ v(x,y) \end{Bmatrix} = \begin{bmatrix} N_1^m & 0 & N_2^m & 0 & N_3^m & 0 & N_4^m & 0 \\ 0 & N_1^m & 0 & N_2^m & 0 & N_3^m & 0 & N_4^m \end{bmatrix} \{\delta_m^e\}$$
(3.2)

The interpolation functions can be used to express the membrane strain-displacement relation as

$$\{\varepsilon(x, y)\} = [B_m]\{\delta_m^e\} \tag{3.3}$$

$$[B_m] = \begin{bmatrix} -\dfrac{1}{a} + \dfrac{y}{ab} & 0 & \dfrac{1}{a} - \dfrac{y}{ab} & 0 & \dfrac{y}{ab} & 0 & -\dfrac{y}{ab} & 0 \\ 0 & -\dfrac{1}{b} + \dfrac{x}{ab} & 0 & -\dfrac{x}{ab} & 0 & \dfrac{x}{ab} & 0 & \dfrac{1}{b} - \dfrac{x}{ab} \\ -\dfrac{1}{b} + \dfrac{x}{ab} & -\dfrac{1}{a} + \dfrac{y}{ab} & -\dfrac{x}{ab} & \dfrac{1}{a} - \dfrac{y}{ab} & \dfrac{x}{ab} & \dfrac{y}{ab} & \dfrac{1}{b} - \dfrac{x}{ab} & -\dfrac{y}{ab} \end{bmatrix} \tag{3.4}$$

$$[B_m] = \begin{bmatrix} \dfrac{\partial N_1^m}{\partial x} & 0 & \dfrac{\partial N_2^m}{\partial x} & 0 & \dfrac{\partial N_3^m}{\partial x} & 0 & \dfrac{\partial N_4^m}{\partial x} & 0 \\ 0 & \dfrac{\partial N_1^m}{\partial y} & 0 & \dfrac{\partial N_2^m}{\partial y} & 0 & \dfrac{\partial N_3^m}{\partial y} & 0 & \dfrac{\partial N_4^m}{\partial y} \\ \dfrac{\partial N_1^m}{\partial y} & \dfrac{\partial N_1^m}{\partial x} & \dfrac{\partial N_2^m}{\partial y} & \dfrac{\partial N_2^m}{\partial x} & \dfrac{\partial N_3^m}{\partial y} & \dfrac{\partial N_3^m}{\partial x} & \dfrac{\partial N_4^m}{\partial y} & \dfrac{\partial N_4^m}{\partial x} \end{bmatrix} \tag{3.5}$$

The transverse displacement w of the element is expressed as

$$w(x, y) = \begin{bmatrix} \alpha_1 + \alpha_2 x + \alpha_3 y + \alpha_4 x^2 + \alpha_5 xy + \alpha_6 y^2 + \alpha_7 x^3 + \alpha_8 x^2 y + \alpha_9 xy^2 + \alpha_{10} y^3 + \alpha_{11} x^3 y + \\ \alpha_{12} x^2 y^2 + \alpha_{13} xy^3 + \alpha_{14} x^3 y^2 + \alpha_{15} x^2 y^3 + \alpha_{16} x^3 y^3 \end{bmatrix} \tag{3.6}$$

The displacement function of the plate element, given by Eq. (3.6), can be written in a vector form as

$$w(x, y) = \{P(x, y)\}\{\alpha\}^T \tag{3.7}$$

With $w(x, y)$ is the displacement function of the plate element and $\{\alpha\}^T$ is the constant parameters vector. As the plate element requires four degrees of freedom per node,

$$\delta_f^e = \left\{ w_i, \theta_{xi} = \frac{\partial w_i}{\partial x}, \theta_{yi} = \frac{\partial w_i}{\partial y}, \theta_{xyi} = \frac{\partial^2 w_i}{\partial x \partial y} \right\}_{i=1,4} \tag{3.8}$$

The plate displacements through the element can be expressed in terms of the nodal displacements as

$$w(x,y) = \{P(x,y)\}_{1 \times 16} [X]^{-1}_{16 \times 16} \{\delta_f^e\}_{16 \times 1}$$

(3.9)

So

$$w(x,y) = \begin{bmatrix} N_1^f & N_2^f & N_3^f & N_4^f & \cdots \cdots \cdots & N_{13}^f & N_{14}^f & N_{15}^f & N_{16}^f \end{bmatrix} \{\delta_f^e\}$$

(3.10)

Where the interpolation functions of the plate element are written as

$$w^*_1(x,y) = (1-3\frac{x^2}{a^2}+2\frac{x^3}{a^3})(1-3\frac{y^2}{b^2}+2\frac{y^3}{b^3})w_1 + (-x(\frac{x}{a}-1)^2)(1-3\frac{y^2}{b^2}+2\frac{y^3}{b^3})\theta_{x1} + (1-3\frac{x^2}{a^2}+2\frac{x^3}{a^3})y(\frac{y}{b}-1)^2\theta_{y1} +$$

$$(-x(\frac{x}{a}-1)^2)y(\frac{y}{b}-1)^2\theta_{xy1}$$

$$w^*_2(x,y) = (3\frac{x^2}{a^2}-2\frac{x^3}{a^3})(1-3\frac{y^2}{b^2}+2\frac{y^3}{b^3})w_2 + (-x(\frac{x^2}{a^2}-\frac{x}{a}))(1-3\frac{y^2}{b^2}+2\frac{y^3}{b^3})\theta_{x2} + (3\frac{x^2}{a^2}-2\frac{x^3}{a^3})y(\frac{y}{b}-1)^2\theta_{y2} +$$

$$(-x(\frac{x^2}{a^2}-\frac{x}{a}))y(\frac{y}{b}-1)^2\theta_{xy2}$$

$$w^*_3(x,y) = (3\frac{x^2}{a^2}-2\frac{x^3}{a^3})(3\frac{y^2}{b^2}-2\frac{y^3}{b^3})w_3 + (-x(\frac{x^2}{a^2}-\frac{x}{a}))(3\frac{y^2}{b^2}-2\frac{y^3}{b^3})\theta_{x3} + (3\frac{x^2}{a^2}-2\frac{x^3}{a^3})y(\frac{y^2}{b^2}-\frac{y}{b})\theta_{y3} +$$

$$(-x(\frac{x^2}{a^2}-\frac{x}{a}))y(\frac{y^2}{b^2}-\frac{y}{b})\theta_{xy3}$$

$$w^*_4(x,y) = (1-3\frac{x^2}{a^2}+2\frac{x^3}{a^3})(3\frac{y^2}{b^2}-2\frac{y^3}{b^3})w_4 + (-x(\frac{x}{a}-1)^2)(3\frac{y^2}{b^2}-2\frac{y^3}{b^3})\theta_{x4} + (1-3\frac{x^2}{a^2}+2\frac{x^3}{a^3})y(\frac{y^2}{b^2}-\frac{y}{b})\theta_{y4} +$$

$$(-x(\frac{x}{a}-1)^2)y(\frac{y^2}{b^2}-\frac{y}{b})\theta_{xy4}$$

(3.11)

The present element is based on the CLT, so the in-plane and out-of-plane displacements are given using eq. (3.14). On the other hand, based on the strain-displacement relation, the curvatures k can be given as

$$\{k(x,y)\} = -\begin{Bmatrix} \dfrac{\partial^2 w}{\partial x^2} \\ \dfrac{\partial^2 w}{\partial y^2} \\ 2\dfrac{\partial^2 w}{\partial x \partial y} \end{Bmatrix} = -\begin{bmatrix} \dfrac{\partial^2}{\partial x^2} \\ \dfrac{\partial^2}{\partial y^2} \\ 2\dfrac{\partial^2}{\partial x \partial y} \end{bmatrix} \{P(x,y)\}[X]^{-1}\{\delta_f^e\} = -\begin{bmatrix} \dfrac{\partial^2\{P(x,y)\}}{\partial x^2} \\ \dfrac{\partial^2\{P(x,y)\}}{\partial y^2} \\ 2\dfrac{\partial^2\{P(x,y)\}}{\partial x \partial y} \end{bmatrix} [X]^{-1}\{\delta_f^e\}$$

(3.12)

$$\{k(x,y)\} = [Q]_{3 \times 16} [X]^{-1}_{16 \times 16} \{\delta_f^e\}_{16 \times 1} = [B_f]_{3 \times 16} \{\delta_f^e\}$$

(3.13)

3.2.3 Kinematics relation

Based on Kirchhoff assumptions, the displacement field [94, 112] according to the CLT is given by the following equations:

$$u(x, y, z) = u_0(x, y) - z \frac{\partial w}{\partial x}$$
$$v(x, y, z) = v_0(x, y) - z \frac{\partial w}{\partial y}$$
$$w(x, y, z) = w_0(x, y) \tag{3.14}$$

Where u_0, v_0 and w_0 are the mid-plane displacement components of the plate element. The strain-displacement relations can be expressed as

$$\varepsilon_x = \frac{\partial u}{\partial x} = \frac{\partial u_0}{\partial x} - z \frac{\partial^2 w}{\partial^2 x} = \varepsilon_x^0 + z k_x$$

$$\varepsilon_y = \frac{\partial v}{\partial y} = \frac{\partial v_0}{\partial y} - z \frac{\partial^2 w}{\partial^2 y} = \varepsilon_y^0 + z k_y \tag{3.15}$$

$$2\varepsilon_{xy} = \frac{\partial u}{\partial y} + \frac{\partial v}{\partial x} = \frac{\partial u_0}{\partial y} + \frac{\partial v_0}{\partial x} - 2z \frac{\partial^2 w}{\partial x \partial y} = \gamma_{xy}^0 + z k_{xy}$$

3.3 Composite materials

By adopting the classical laminate assumptions, the resultant forces N and moments M are related to the mid-surface strains ε^0 and to the curvatures k by:

$$\begin{Bmatrix} N \\ M \end{Bmatrix} = \begin{bmatrix} A & B \\ B & D \end{bmatrix} \begin{Bmatrix} \varepsilon^0 \\ k \end{Bmatrix} \tag{3.16}$$

Where the matrices $[A]$, $[B]$, and $[D]$ are known as extensional, coupling, and bending rigidity matrices, respectively. These rigidities can be defined by:

$$\{A, B, D\}^T = \int_{-h/2}^{+h/2} [\bar{Q}_{ij}] (1, z, z^2) dz \tag{3.17}$$

With $\bar{Q}_{ij}$ denoting the coefficients of elasticity of a layer in the global coordinate system (x, y, z) of the laminate forming an angle θ with the local coordinate system. The finite element used in this investigation is a rectangular element of 24 degrees of freedom per element. Figure 1 shows the geometry and nodal variables of the element

The relationship between stress and strain can be written as

$$\begin{Bmatrix} \sigma_1 \\ \sigma_2 \\ \tau_{12} \end{Bmatrix} = \begin{bmatrix} Q_{11} & Q_{12} & 0 \\ Q_{12} & Q_{22} & 0 \\ 0 & 0 & Q_{66} \end{bmatrix} \begin{Bmatrix} \varepsilon_1 \\ \varepsilon_2 \\ \gamma_{12} \end{Bmatrix}$$

(3.18)

The Q_{ij} reduced stiffness components are expressed by :

$$Q_{11} = \frac{E_1}{1-v_{12}v_{21}} \ , \quad Q_{12} = \frac{v_{12}E_1}{1-v_{12}v_{21}} \ , \quad Q_{22} = \frac{E_2}{1-v_{12}v_{21}}, \quad Q_{66} = G_{12}$$

(3.19)

The stress-strain relations for a layer k, expressed in the global coordinate system of laminated, are thus written:

$$\begin{Bmatrix} \sigma_x \\ \sigma_y \\ \tau_{xy} \end{Bmatrix} = \begin{bmatrix} \overline{Q}_{11} & \overline{Q}_{12} & \overline{Q}_{16} \\ \overline{Q}_{12} & \overline{Q}_{22} & \overline{Q}_{26} \\ \overline{Q}_{61} & \overline{Q}_{62} & \overline{Q}_{66} \end{bmatrix} \begin{Bmatrix} \varepsilon_x + zk_x \\ \varepsilon_y + zk_y \\ \gamma_{xy} + zk_{xy} \end{Bmatrix}$$

(3.20)

where $\overline{Q}_{ij}$ are the coefficients of the stiffness matrix of a given layer k. They are expressed by the following relationships:

$$\begin{aligned}
\overline{Q}_{11} &= Q_{11}c^4 + Q_{22}s^4 + 2(Q_{12} + 2Q_{66})s^2c^2 \\
\overline{Q}_{12} &= (Q_{11} + Q_{22} - 4Q_{66})s^2c^2 + Q_{12}(s^2 + c^4) \\
\overline{Q}_{16} &= (Q_{11} - Q_{12} - 2Q_{66})sc^3 - (Q_{22} - Q_{12} - 2Q_{66})s^3c \\
\overline{Q}_{22} &= Q_{11}s^4 + Q_{22}c^4 + 2(Q_{12} + 2Q_{66})s^2c^2 \\
\overline{Q}_{26} &= (Q_{11} - Q_{22} - 2Q_{66})s^3c - (Q_{22} - Q_{12} - Q_{66})sc^3 \\
\overline{Q}_{66} &= (Q_{11} + Q_{22} - 2Q_{12} - 2Q_{66})s^2c^2 + Q_{66}(s^4 + c^4)
\end{aligned}$$

(3.21)

With $s = \sin\theta$ and $c = \cos\theta$

3.3.1 Plate subjected to hygrothermal environmental loading (temperature and moisture)

The stress–strain relation of the composite laminated plate subjected to hygrothermal load (temperature rise ΔT and moisture rise ΔC) in the local coordinate is given by

$$\begin{Bmatrix} \sigma_1 \\ \sigma_2 \\ \tau_{12} \end{Bmatrix} = \begin{bmatrix} Q_{11} & Q_{12} & 0 \\ Q_{12} & Q_{22} & 0 \\ 0 & 0 & Q_{66} \end{bmatrix} \left(\begin{Bmatrix} \varepsilon_1 \\ \varepsilon_2 \\ \gamma_{12} \end{Bmatrix} - \begin{Bmatrix} \varepsilon_1^t \\ \varepsilon_2^t \\ 0 \end{Bmatrix} - \begin{Bmatrix} \varepsilon_1^m \\ \varepsilon_2^m \\ 0 \end{Bmatrix} \right) \qquad (3.22)$$

Where ε^t and ε^m are the thermal and moisture deformations, respectively, and which are given by relation:

$$\begin{Bmatrix} \varepsilon_1^t \\ \varepsilon_2^t \\ 0 \end{Bmatrix} = \Delta T \begin{Bmatrix} \alpha_1 \\ \alpha_2 \\ 0 \end{Bmatrix} \quad \text{and} \quad \begin{Bmatrix} \varepsilon_1^m \\ \varepsilon_2^m \\ 0 \end{Bmatrix} = \Delta C \begin{Bmatrix} \beta_1 \\ \beta_2 \\ 0 \end{Bmatrix} \qquad (3.23)$$

Where α_1, α_2, β_1 and β_2 are thermal and moisture expansion coefficients, respectively. And ΔT and ΔC are the temperature and humidity or moisture rise, respectively .

The stress–strain relation of each layer of the composite laminated plate subjected to hygrothermal load (temperature rise ΔT and moisture rise ΔC) in the globale coordinate is given by

$$\begin{Bmatrix} \sigma_x \\ \sigma_y \\ \tau_{xy} \end{Bmatrix}_k = \begin{bmatrix} \overline{Q}_{11} & \overline{Q}_{12} & \overline{Q}_{16} \\ \overline{Q}_{12} & \overline{Q}_{22} & \overline{Q}_{26} \\ \overline{Q}_{61} & \overline{Q}_{62} & \overline{Q}_{66} \end{bmatrix}_k \left[\begin{Bmatrix} \varepsilon_x \\ \varepsilon_y \\ \gamma_{xy} \end{Bmatrix}_k - \Delta T \begin{Bmatrix} \alpha_x \\ \alpha_y \\ \alpha_{xy} \end{Bmatrix}_k - \Delta C \begin{Bmatrix} \beta_x \\ \beta_y \\ \beta_{xy} \end{Bmatrix}_k \right] \qquad (3.24)$$

⬥ Stress Resultants

The mid-plane forces of a plate and the moments are related to the deformations and curvatures by the following expressions:

$$\begin{Bmatrix} N_x \\ N_y \\ N_{xy} \\ M_x \\ M_y \\ M_{xy} \end{Bmatrix} = \begin{bmatrix} A_{11} & A_{12} & A_{16} & B_{11} & B_{12} & B_{16} \\ A_{12} & A_{22} & A_{26} & B_{12} & B_{22} & B_{26} \\ A_{16} & A_{26} & A_{66} & B_{16} & B_{26} & B_{66} \\ B_{11} & B_{12} & B_{16} & D_{11} & D_{12} & D_{16} \\ B_{12} & B_{22} & B_{26} & D_{12} & D_{22} & D_{26} \\ B_{16} & B_{26} & B_{66} & D_{16} & D_{26} & D_{66} \end{bmatrix} \begin{Bmatrix} \varepsilon_x^0 \\ \varepsilon_y^0 \\ \gamma_{xy}^0 \\ \kappa_x \\ \kappa_y \\ \kappa_{xy} \end{Bmatrix} - \begin{Bmatrix} N_x^t \\ N_y^t \\ N_{xy}^t \\ M_x^t \\ M_y^t \\ M_{xy}^t \end{Bmatrix} - \begin{Bmatrix} N_x^m \\ N_y^m \\ N_{xy}^m \\ M_x^m \\ M_y^m \\ M_{xy}^m \end{Bmatrix} \qquad (3.25)$$

And can be written as:

$$\begin{Bmatrix} N \\ M \end{Bmatrix} = \begin{bmatrix} A & B \\ B & D \end{bmatrix} \begin{Bmatrix} \varepsilon^0 \\ k \end{Bmatrix} - \begin{Bmatrix} N^t \\ M^t \end{Bmatrix} - \begin{Bmatrix} N^m \\ M^m \end{Bmatrix} \tag{3.26}$$

The thermal force and moment resultants are defined by:

$$N^t = \int_{-\frac{h}{2}}^{\frac{h}{2}} \left[\bar{Q}_{ij} \right]_k \left[\Delta T \{\alpha\}^T \right] dz \quad , \qquad M^t = \int_{-\frac{h}{2}}^{\frac{h}{2}} \left[\bar{Q}_{ij} \right]_k \left[\Delta T \{\alpha\}^T \right] z dz \tag{3.27}$$

The moisture force and moment resultants are defined by:

$$N^m = \int_{-\frac{h}{2}}^{\frac{h}{2}} \left[\bar{Q}_{ij} \right]_k \left[\Delta C \{\beta\}^T \right] dz \quad , \qquad M^m = \int_{-\frac{h}{2}}^{\frac{h}{2}} \left[\bar{Q}_{ij} \right]_k \left[\Delta C \{\beta\}^T \right] z dz \tag{3.28}$$

❖ *stiffness matrix*

The total potential energy of a plate subjected to a distributed transverse loading is given by:

$$\Pi = U + V' \tag{3.29}$$

The equilibrium configuration is defined by the minimization of the total potential energy which means the cancellation of its first variation.

$$\delta\Pi = \delta U + \delta V = 0 \tag{3.30}$$

The element stiffness matrix $\left[K^e \right]$ can be obtained as

$$\left[K^e \right] = \iint \left\{ [B_m]^T [A][B_m] + [B_m]^T [B][B_f] + [B_f]^T [B][B_m] + [B_f]^T [D][B_f] \right\} ds \tag{3.31}$$

The matrix $\left[K^e \right]$ can be written in the form:

$$\left[K^e \right] = \left[K_1^e \right] + \left[K_2^e \right] + \left[K_3^e \right] + \left[K_4^e \right] \tag{3.32}$$

With :

$\left[K_1^e \right] = [B_m]^T [A][B_m]$: Elementary membrane stiffness matrix.

$\left[K_2^e \right] = [B_m]^T [B][B_f]$: Elementary membrane-bending coupling stiffness matrix

$\left[K_3^e \right] = [B_f]^T [B][B_m]$: Elementary bending-membrane coupling stiffness matrix

$$\left[K_4^e\right]=\left[B_f\right]^T\left[D\right]\left[B_f\right] : \text{Elementary bending stiffness matrix}$$

To obtain the total stiffness matrix of the structure, the elementary stiffness matrices are assembled.

3.4 The steps to calculate Strain and stresses in a laminated

A computer program is developed for calculating local strains and stress distributions in a laminated beam, subjected to the applied forces and moments, using the steps listed below:

1- Calculate the values of the reduced stiffness matrix $[Q]$ for each ply using its three elastic moduli, E_1, E_2, G_{12} and v_{12}.

2- Use the $[Q]$ matrix produced in step 1 and the ply angle to determine the value of the transformed global reduced stiffness matrix $[\overline{Q}_{ij}]$ for each ply.

3- Knowing the thickness t_k, of each layer, find the coordinates of the top and bottom of each layer h_i, $i = 1..., n$, and the total thickness h of the laminate using the following equations

$$h = \sum_{k=1}^{n} t_k$$

(3.33)

4- The location of the mid-plane is $h/2$ from the top or the bottom surface of the laminate. The z-coordinate of each ply k surface (top and bottom) is given by

- Ply 1:

$$h_0 = -h/2 \quad \text{(top surface)}$$

$$h_1 = -h/2 + t_1 \quad \text{(bottom surface).}$$

- Ply k: (k= 2, 3,.., n-2, n-1)

$$h_{k-1} = -h/2 + \sum_{=1}^{k-1} t \quad \text{(top surface).}$$

$$h_k = -h/2 + \sum_{=1}^{k} t \quad \text{(bottom surface).}$$

- Ply n:

$h_{n-1} = h/2 - t_n$ (top surface).

$h_n = h/2$ (bottom surface).

5- Using the matrix from step 2 and the position of each layer from step 3, to calculate the three stiffness matrices $[A]$, $[B]$, and $[D]$ using Eq. 3.17.

6- Substitute the stiffness matrix values found in step 4 and the applied forces and moments in Eq. 3.16.

7- Solve the six simultaneous equations, Eq. 3.16, to find the mid-plane strains and curvatures.

8- Now that the position of each layer is known, find the global strain in each layer using the following expression

$$\begin{Bmatrix} \varepsilon_x \\ \varepsilon_y \\ \gamma_{xy} \end{Bmatrix} = \begin{Bmatrix} \varepsilon_x^0 \\ \varepsilon_y^0 \\ \gamma_{xy}^0 \end{Bmatrix} + z \begin{Bmatrix} k_x \\ k_y \\ k_{xy} \end{Bmatrix}$$

(3.34)

9- To find the global stresses in each lamina, use the following stress-strain expression:

$$\begin{Bmatrix} \sigma_x \\ \sigma_y \\ \tau_{xy} \end{Bmatrix} = \begin{bmatrix} \overline{Q_{ij}} \end{bmatrix} \begin{Bmatrix} \varepsilon_x \\ \varepsilon_y \\ \gamma_{xy} \end{Bmatrix}$$

(3.35)

10- To find the local strains, use the following transformation equation:

$$\begin{Bmatrix} \varepsilon_1 \\ \varepsilon_2 \\ \gamma_{12}/2 \end{Bmatrix} = [T]^{-1} \begin{Bmatrix} \varepsilon_x \\ \varepsilon_y \\ \gamma_{xy}/2 \end{Bmatrix}$$

(3.36)

11- For finding the local stresses, use following the transformation equation

$$\begin{Bmatrix} \sigma_1 \\ \sigma_2 \\ \tau_{12} \end{Bmatrix} = [T]^{-1} \begin{Bmatrix} \sigma_x \\ \sigma_y \\ \tau_{xy} \end{Bmatrix}$$

(3.37)

3.5 Failure Criterion

As mentioned previously, the main objective of this study is to determine the failure load of laminated beams subjected to various bending conditions. Three different families of failure

criteria are adopted in this investigation. The first is the maximum stress criterion (there is no interaction between the lamina stresses). The second criteria are Tsai-Hill and Tsai-Wu (there is an interaction between the lamina stresses). The last one is the Hashin criterion.

3.5.1 Maximum stress failure criterion

The maximum stress failure criterion has the advantage of being simple in form and easy to apply, but this criterion ignores the interactions between different stress components (one can assume that there is no interaction between stresses or strain components). If one of the following conditions is verified, failure initiation begins.

$$\frac{\sigma_1}{X_t} = 1 \text{ for } \sigma_1 > 0 \quad \text{and} \quad \frac{\sigma_1}{X_c} = 1 \text{ for } \sigma_1 < 0;$$

$$\frac{\sigma_2}{Y_t} = 1 \text{ for } \sigma_2 > 0 \quad \text{and} \quad \frac{\sigma_2}{Y_c} = 1 \text{ for } \sigma_2 < 0;$$

$$\frac{|\tau_{12}|}{S} = 1$$

$$(3.38)$$

where σ_1, σ_2 and τ_{12} are the ply normal and shear stress components, X_t and X_c are the longitudinal strengths in tension and compression, respectively. Y_t and Y_c are the transverse strengths in tension and compression, respectively. S is the in-plane shear strength.

3.5.2 Tsai-Hill quadratic failure criterion

Tsai-Hill failure criterion directly adapts to the classic Von-Mises criterion [49]. Then, Tsai and Hill made some modifications to apply this criterion to anisotropic materials. Contrary to the maximum stress criterion, this failure criterion considers the interaction between the stress components.

$$\left(\frac{\sigma_1}{X}\right)^2 + \left(\frac{\sigma_2}{Y}\right)^2 - \frac{\sigma_1\sigma_2}{X^2} + \left(\frac{\tau_{12}}{S}\right)^2 = 1$$

$$(3.39)$$

3.5.3 Tsai–Wu failure criterion

The Tsai-Wu failure criterion is widely used in anisotropic materials and is based on the total strain energy failure theory [94]. This criterion takes account of the interaction between stresses. When a laminate's failure index approaches 1, the Tsai-Wu criterion predicts failure.

$$F_i\sigma_i + F_{ij}\sigma_i\sigma_j \geq 1, \quad i,j = 1,2,\ldots,6 \tag{3.40}$$

Based on this criterion, the failure load can be calculated using the following expression:

$$\sigma f_1\left(\frac{\sigma_1}{\sigma}\right) + \sigma f_2\left(\frac{\sigma_2}{\sigma}\right) + \sigma^2 f_{11}\left(\frac{\sigma_1}{\sigma}\right)^2 + \sigma^2 f_{22}\left(\frac{\sigma_2}{\sigma}\right)^2 + \sigma^2 f_{66}\left(\frac{\sigma_{12}}{\sigma}\right)^2 + 2\sigma^2 f_{12}\left(\frac{\sigma_1\sigma_2}{\sigma^2}\right) = 1 \tag{3.41}$$

By designating the value of σ that causes failure as σ_f, Eq. 3.41 can be rewritten as:

$$A\sigma_f^2 + B\sigma_f - 1 = 0 \tag{3.42}$$

Where

$$A = f_{11}\left(\frac{\sigma_1}{\sigma}\right)^2 + f_{22}\left(\frac{\sigma_2}{\sigma}\right)^2 + f_{66}\left(\frac{\sigma_{12}}{\sigma}\right)^2 + 2f_{12}\left(\frac{\sigma_1\sigma_2}{\sigma^2}\right)$$

$$B = f_1\left(\frac{\sigma_1}{\sigma}\right) + f_2\left(\frac{\sigma_2}{\sigma}\right)$$

$$f_{11} = \frac{1}{X_t X_c}, \quad f_{22} = \frac{1}{Y_t Y_c}, \quad f_{66} = \frac{1}{S^2},$$

$$f_1 = \frac{1}{X_t} - \frac{1}{X_c}, \quad f_2 = \frac{1}{Y_t} - \frac{1}{Y_c}, f_{12} \cong -0.5(f_{11}f_{22})^{1/2} \tag{3.43}$$

3.5.4 Hashin failure criterion

The Hashin criterion is a failure criterion that is physically based. This criterion can predict the failure modes and mechanisms of unidirectional composites. It is based on four main modes of material failure, as presented in Table 3.1.

Table 3. 1. Failure modes based on Hashin criterion

Failure modes	Mathematical expression
Fiber failure in tension $\sigma_{11} > 0$	$\left(\frac{\sigma_{11}}{X_t}\right)^2 + \left(\frac{\tau_{12}}{S}\right)^2 \geq 1$
Fiber failure in compression $\sigma_{11} < 0$	$\left(\frac{\sigma_{11}}{X_c}\right)^2 \geq 1$

Matrix failure in tension $\sigma_{22} > 0$	$\left(\dfrac{\sigma_{22}}{Y_t}\right)^2 + \left(\dfrac{\tau_{12}}{S}\right)^2 \geq 1$
Matrix failure in compression $\sigma_{22} < 0$	$\left(\dfrac{\sigma_{22}}{Y_c}\right)^2 + \left(\dfrac{\tau_{12}}{S}\right)^2 \geq 1$

3.6 Stress concentration

3.6.1 Stresses in infinite anisotropic plates containing a circular holes:

Greszczuk [86] provides the first rough analytical solution for an anisotropic single lamina subjected to uniaxial load as illustrated in Fig. 1a, employing Green and Zerna's [85] analytical solution. This solution enables us to determine the circumferential stress $\sigma_{\alpha\theta}$ at any location around the hole's periphery as:

$$\sigma_{\alpha\theta} = \left[\psi_1 + \psi_2 + \psi_3\right]\omega^{-1}\sigma_x \tag{3.44}$$

With

$$\psi_1 = (1+\gamma_1)(1+\gamma_2)\left[1+\gamma_1+\gamma_2-\gamma_1\gamma_2-2\cos 2(\alpha-\theta)\right]$$

$$\psi_2 = -4\left[\gamma_1+\gamma_2-(1+\gamma_1\gamma_2)\cos 2(\alpha-\theta)\right]\sin^2\alpha$$

$$\psi_3 = -4(\gamma_1\gamma_2-1)\sin 2(\alpha-\theta)\sin\theta\cos\theta \tag{3.45}$$

$$\omega = \left[1+\gamma_1^2-2\gamma_1\cos 2(\alpha-\theta)\right]\left[1+\gamma_2^2-2\gamma_2\cos 2(\alpha-\theta)\right]$$

The constants γ_1 and γ_2 are calculated as follows:

$$\gamma_1 = (\xi-1)/(\xi+1) \ , \ \gamma_2 = (\vartheta-1)/(\vartheta+1) \tag{3.46}$$

With

$$\xi = \left[\zeta+(\zeta^2-\eta)^{1/2}\right]^{1/2} \ , \quad \vartheta = \left[\zeta-(\zeta^2-\eta)^{1/2}\right]^{1/2} \ , \quad \zeta = \frac{E_2}{2G_{12}}-\nu_{12} \ , \quad \eta = \frac{E_2}{E_1} , \tag{3.47}$$

Where E_1, E_2 are the elastic modulus, G_{12} is shear modulus, ν_{12} Poisson's ratio in material. And θ is the fiber orientation angle.

The approximate analytical solution for cases of anisotropic plates under biaxial or shear loading conditions as illustrated in Figs 3.2(b) and 3.2(c) can be found by decomposing the applied stress into the stress components linked to the axes of symmetry of the material [113].
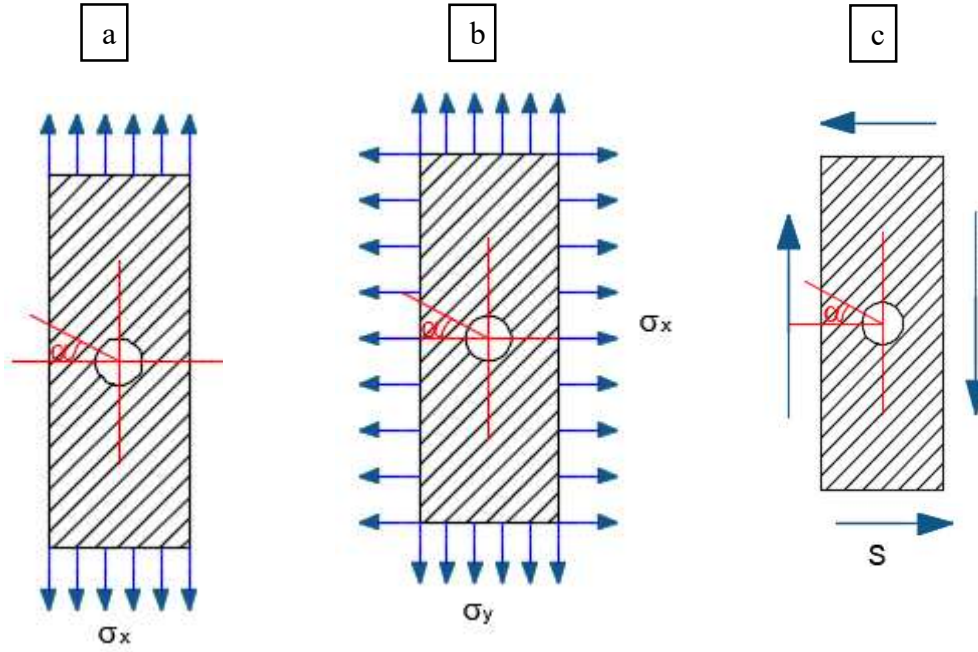
Fig 3. 2: anistropic composite single-ply with an opening under different kinds of loading: a: uniaxial load, b: biaxial load, c: shear loading

Arslan et al.[113] Greszczuk's[86] analytical solution for determining the circumferential stress at the edge of a circular cut. After superposition, the resulting formula for circumferential stress at a location α along the border of an aperture in anisotropic plates is

$$\sigma_\alpha = \left(M_1 N_1 + M_2 N_2 - M_3 N_3 \right) \omega^{-1} \tag{3.48}$$

With

$$N_1 = \left(1+\gamma_1\right)\left(1+\gamma_2\right)\left[1+\gamma_1+\gamma_2-\gamma_1\gamma_2-2\cos 2\left(\alpha-\theta\right)\right]$$

$$N_2 = \left(1-\gamma_1\right)\left(1-\gamma_2\right)\left[1-\gamma_1-\gamma_2-\gamma_1\gamma_2+2\cos 2\left(\alpha-\theta\right)\right]$$

$$N_3 = 4\left(\gamma_1\gamma_2-1\right)\sin 2\left(\alpha-\theta\right) \tag{3.49}$$

$$M_1 = \left[\sigma_x\left(1+\cos 2\theta\right)+\sigma_y\left(1-\cos 2\theta\right)\right]/2$$

$$M_2 = \left[\sigma_x\left(1-\cos 2\theta\right)+\sigma_y\left(1+\cos 2\theta\right)\right]/2$$

$$M_3 = \left[\left(\sigma_x - \sigma_y \right) \sin 2\theta \right] / 2$$

3.6.2 Stresses in infinite laminated plates containing circular holes:

The circumferential stress at the boundary of the opening in a laminated plate containing a several plys; with various material characteristics and various fiber orientation angles as well, can be roughly determined from the preceding given solutions when using the equivalent elastic constants corresponding to a symmetric laminated composite plate. Once the laminate's resultant stresses are understood, the multilayer plate theory is used to calculate the local stresses in each ply. Here, symmetry and a uniform thickness of the laminate are assumed. Each lamina is uniform, orthotropic, and precisely connected to the next. The stiffness moduli Aij values for symmetrically laminated plates [114] can be calculated based on the classical laminate theory CLT by taking $[A] = [a]^{-1}$

Where

$$[a] = H^{-1} \begin{bmatrix} a_{11}^* & a_{12}^* & a_{16}^* \\ a_{21}^* & a_{22}^* & a_{26}^* \\ a_{61}^* & a_{62}^* & a_{66}^* \end{bmatrix}, \quad V_{[1,2,3,4]} = \int_{-H/2}^{H/2} \left[\cos 2\theta, \cos 4\theta, \sin 2\theta, \sin 4\theta \right] dz \quad (3.50)$$

$$\begin{pmatrix} a_{11}^* \\ a_{22}^* \\ a_{12}^* \end{pmatrix} = \begin{bmatrix} U_1 & V_1 & V_2 \\ U_1 & -V_1 & V_2 \\ U_4 & 0 & -V_2 \end{bmatrix} \begin{pmatrix} H \\ U_2 \\ U_3 \end{pmatrix}, \quad \begin{pmatrix} a_{66}^* \\ a_{16}^* \\ a_{26}^* \end{pmatrix} = \begin{bmatrix} U_5 & 0 & -V_2 \\ 0 & 0.5V_3 & V_4 \\ 0 & 0.5V_3 & -V_4 \end{bmatrix} \begin{pmatrix} H \\ U_2 \\ U_3 \end{pmatrix} \quad (3.51)$$

Where H denotes the total thickness of the plate and U_j designates the laminate invariants in terms of reduced stiffness Q_{ij} matrix components, which are described as:

$$U_1 = \left(3Q_{11} + 3Q_{22} + 2Q_{12} + 4Q_{66} \right) / 8$$

$$U_2 = \left(Q_{11} - Q_{22} \right) / 2$$

$$U_3 = \left(Q_{11} + Q_{22} - 2Q_{12} - 4Q_{66} \right) / 8 \qquad (3.52)$$

$$U_4 = \left(Q_{11} + Q_{22} + 6Q_{12} - 4Q_{66} \right) / 8$$

$$U_5 = \left(Q_{11} + Q_{22} - 2Q_{12} + 4Q_{66} \right) / 8$$

These are the invariants provided for the entire laminate via the composite's reduced stiffness matrix components. The circumferential stresses at the boundary of the aperture (corresponding to the varied loads) for symmetric laminated plates can be found by replacing γ_1 and γ_2 in Eq (3.46) with x_1 and x_2 as follows:

$$x_1 = \left(\xi' - 1\right)/\left(\xi' + 1\right), \; x_2 = \left(\vartheta' - 1\right)/\left(\vartheta' + 1\right) \tag{3.53}$$

With:

$$\xi' = \left[\zeta' + \left(\zeta'^2 - \eta'\right)^{1/2}\right]^{1/2}, \; \vartheta' = \left[\zeta' - \left(\zeta'^2 - \eta'\right)^{1/2}\right]^{1/2}, \; \zeta' = \frac{E_y}{2G_{xy}} - v_{xy} \text{ and } \eta' = \frac{E_y}{E_x} \tag{3.54}$$

With E_x, E_y, G_{xy}, and v_{xy} denoted the equivalent elastic constants for the symmetric laminated plate.

Khechai et al. [73] extended the prior solutions of Greszczuk [86] and Arslan [113] to calculate the stress distribution in single layer and multilayered composite plates exposed to uniaxial, biaxial, and shear loading directed at an arbitrary angle β with respect to the x-axis (as shown in Fig 3.3).
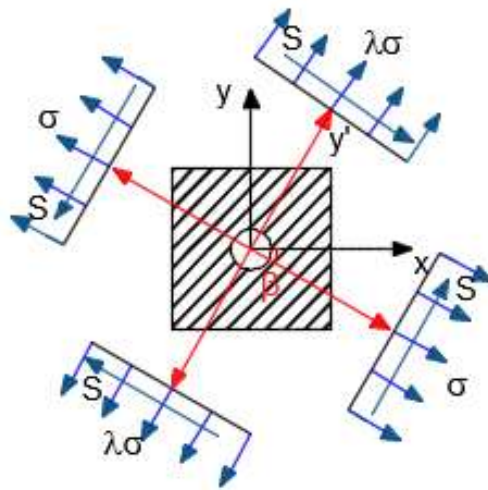
Fig 3. 3: Laminated plate with arbitrarily oriented fibers under general loading conditions

By using the static equilibrium equation, the stresses created in each layer of the laminate due to oriented fiber and loading must be resolved into components (along the fiber direction, transverse direction, and shear) related to the material's axes of symmetry.

The stress distribution function might then be calculated using superposition. The stress distribution for the multilayered composite plate under general-directed loading as illustrated in Fig 3.3, can be determined

$$\sigma_\alpha = \left[B_1 C_1 + B_2 C_2 - B_3 C_3 \right] C_4^{-1} \tag{3.55}$$

With

$$C_1 = (1 + x_1)(1 + x_2)\left[1 + x_1 + x_2 - x_1 x_2 - 2\cos 2(\alpha - \theta) \right]$$

$$C_2 = (1 - x_1)(1 - x_2)\left[1 - x_1 - x_2 - x_1 x_2 + 2\cos 2(\alpha - \theta) \right]$$

$$C_3 = 4(x_1 x_2 - 1)\sin 2(\alpha - \theta) \tag{3.56}$$

$$C_4 = \left[1 + x_1^2 - 2x_1 \cos 2(\alpha - \theta) \right]\left[1 + x_2^2 - 2x_2 \cos 2(\alpha - \theta) \right]$$

$$B_1 = \left[\sigma\{1 + \cos 2(\theta - \beta)\} + \lambda\sigma\{1 - \cos 2(\theta - \beta)\} \right]/2 + S\sin 2(\theta - \beta)$$

$$B_2 = \left[\sigma\{1 - \cos 2(\theta - \beta)\} + \lambda\sigma\{1 + \cos 2(\theta - \beta)\} \right]/2 + S\sin 2(\theta - \beta)$$

$$B_3 = \left[(\sigma - \lambda\sigma)\sin 2(\theta - \beta) \right]/2 + S\cos 2(\theta - \beta)$$

The laminate equivalent elastic constants are only for balanced and symmetric laminates. If the laminate is not balanced or symmetric, these solutions cannot be employed [5]

3.6.3 Effective Moduli for unsymmetrical laminated plates:

In the anisotropic plate, the constitutive equations of a lumped sub-laminated plate are obtained from the CLT as:

$$\begin{Bmatrix} \varepsilon^0 \\ k \end{Bmatrix} = \begin{bmatrix} a & b \\ b^T & d \end{bmatrix} \begin{Bmatrix} N \\ M \end{Bmatrix} \tag{3.57}$$

With

$$\begin{bmatrix} a & b \\ b^T & d \end{bmatrix} = \begin{bmatrix} A & B \\ B & D \end{bmatrix}^{-1} \tag{3.58}$$

With ε^0 and k are mid-plane strain and curvature, respectively. And N, M are the force and moment resultants, respectively. A, B, and D are extensional, coupling and bending stiffness of the lumped sub laminate, respectively.

Chen and Chan [115] derived equations for calculating the effective equivalent elastic modulus while accounting for shear and bending deformations. These equivalent moduli were determined by elements of the matrix P, which was described as follows:

$$[P]=[a]-[b][d]^{-1}[b]^{T} \tag{3.59}$$

The effective modulus, E_x and E_y can be calculating as

$$E_x = \frac{1}{\left(P_{11}-\dfrac{P_{16}^2}{P_{66}}\right)t}, \quad E_y = \frac{1}{\left(P_{22}-\dfrac{P_{26}^2}{P_{66}}\right)t} \tag{3.60}$$

Similarly, v_{xy} and G_{xy} can be written as

$$v_{xy} = -\frac{P_{12}-\dfrac{P_{16}P_{26}}{P_{66}}}{P_{11}-\dfrac{P_{16}^2}{P_{66}}}, \quad G_{xy} = \frac{1}{\left[P_{66}-\dfrac{1}{\left(P_{11}P_{22}-P_{12}^2\right)}\left(P_{16}^2 P_{22}-2P_{12}P_{26}P_{16}+P_{26}^2 P_{11}\right)\right]t} \tag{3.61}$$

With t is total thickness of the lumped layers.

3.6.4 The correction factors for finite-width for an anisotropic plate containing a circular hole :

In engineering design, we typically use the term "stress concentration factor" (SCF) K_T^{∞}, which is the ratio of the circumferential stress σ_α to the reference stress of the gross cross-section (applied stress), to assess the structural integrity of a material. The solutions mentioned above are only applicable if the size of the opening is small compared to the dimensions of the plate, under the assumption that the plate is infinite in size. However, to emulate as much as possible the true structural behavior when the plates are not infinite, the finite-width correction factor given by Tan [111] is added in the preceding solution.

Tan [111] calculated the finite width correction factor of anisotropic and orthotropic plate with a central elliptic opening. The finite width correction factor is given by (for orthotropic laminates)

$$\frac{K_T^{\infty}}{K_T} = 3(1-\varsigma)/[2+(1-\varsigma)^3]+\tfrac{1}{2}(\varsigma M)^6(K_T^{\infty}-3)[1-(\varsigma M)^2] \tag{3.62}$$

$$(\varsigma M)^2 = \frac{1}{2}\left\{\sqrt{1-8\left\{[3(1-\varsigma)/[2+(1-\varsigma)^3]]-1\right\}}-1\right\} \tag{3.63}$$

$$\varsigma = D/W \tag{3.64}$$

Chapter 4

RESULTS AND DISCUSSION - FAILURE LOAD OF NON-PERFORATED LAMINATED

Chapter 4

Results and Discussion - failure load of non-perforated laminated

4.1. Introduction :

This chapter presents the results of failure loads under both static and hygrothermal loading conditions, as well as their analyses. The first part of this chapter aims to validate the present element by calculating the displacement and first-ply failure load (FPF) under different loading conditions and boundary conditions, while also validating the stress and effort resultants under temperature and moisture. The refined rectangular plate element used in the analysis is formulated based on the classical lamination theory (CLT) to calculate in-plane stresses. Several failure criteria, including Tsai-Wu, Tsai-Hill, Hashin, and Maximum Stress criteria, are utilized to predict failure mechanisms, as discussed in the previous chapter. The numerical results obtained from the present element are compared favorably with those from analytical approaches and those found in the literature. In the second part of this chapter, a parametric study is conducted to investigate several parameters, such as fiber orientations, stacking sequences, boundary conditions, load types, and the effects of temperature and moisture, to understand their impact on the strength of these laminated beams.

4.2. Validation of the present element:

In order to assess the performance of the present element to convergence, various examples are studied considering symmetric laminated beams and plates with different stacking sequences, different loadings, geometry, and boundary conditions. The numerical results obtained are compared with analytical solutions and other numerical results found in literature based on high-order finite element models. Before beginning this examination, a convergence study of the current element should be performed to ensure that the present finite element performs. The

obtained results are extracted from FORTRAN and MATLAB codes written by the authors based on the proposed formulations mentioned in the preceding sections.

4.2.1 Simply supported cross-ply laminated beam [90₂/0]ₛ under a concentrated load

In the first example, a simply supported (*SS*) six-layer laminated beam subjected to a concentrated load *P*=100 kN is considered (see Fig 4.1). The concentrated load is applied at the mid-span of the beam (three-point bending test). The thickness of each layer is 2 mm.
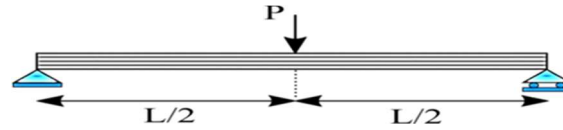
Fig 4. 1: Simply supported laminated beam [90₂/0]s under a concentrated load

The geometric and the mechanical characteristics of the laminated beam are presented in Table 4.1.

Table 4. 1: Geometrical parameters and mechanical proprieties

E_1 (MPa)	E_2 (MPa)	G_{12} (MPa)	v_{12}	P (kN)	*Length L* (mm)	*Width b* (mm)	*Thickness h* (mm)
123×10^7	8.5×10^7	4.1×10^7	0.25	100	1000	200	12

The numerical results obtained by the present element are compared with the analytical solution. The maximum value of the analytical displacement is calculated using the following relation

$$w=\frac{PL^3}{48E_{eq}I}$$

With $E_{eq} = \frac{12}{D_{11}h^3}$

The convergence of the transverse displacement, using different mesh sizes, is tabulated in Table 4.2.
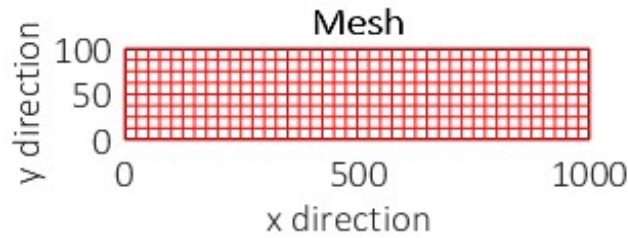
Fig 4. 2: The meshed configuration of the laminated beam

Table 4. 2: Displacement convergence of a simply supported beam subjected to a concentrated load.

Mesh size	4×2	8×4	10×4	12×6	20×8	40×8	Analytical displacement
Displacement	0.56671	0.56676	0.56677	0.56678	0. 5668	0.56681	0.567
Error (%)	5.114E^{-2}	4.232E^{-2}	4.056E^{-2}	3.880E^{-2}	3.52E^{-2}	3.35E^{-2}	-

As can be observed, the current finite element has a high convergence rate. By using only 10×4 elements, it is almost adequate to determine the maximum deflection of the laminated beam with enough engineering accuracy. In addition, for mesh size (40×8) elements, the error percentage of the transverse displacement predicted by employed element is around 3.35E-2% compared to the analytical solution. Based on prior convergence studies, it is clear that (40 × 8) elements are most sufficient to get more precise results. Therefore, all the subsequent results are obtained using (40×8) elements.

4.2.2. **FPF analysis of a simply supported cross-ply [$90_8/0_8$]$_s$ beams**

The second example is considered in order to verify the present element's ability and validity in predicting the FPF strength of beams with various geometrical parameters. In this example, the FPF load and its corresponding displacement of cross-ply laminated beams [$90_8/0_8$]$_s$ are predicted using the present element. The analyzed beams are *SS*, and a concentrated load is applied at the mid-span of the beams. The laminated beams are made of graphite/epoxy and the material characteristics, geometrical, and strength parameters are listed in Table.4.3.

Table 4. 3: Geometric and material properties of AS4/3502 graphite/epoxy.

E_1 (MPa)	E_2 (MPa)	G_{12} (MPa)	v_{12}	X_t (MPa)	X_c (MPa)	Y_t (MPa)	Y_c (MPa)	S (MPa)
141200	11500	6000	0.3	2343	1723	51	223	86
Laminate	*Length L* (mm)	*Width b* (mm)	*Thickness h* (mm)	Lay-up				
A1	139.7	24.84	4.648	[$90_8/0_8$]$_s$				

| A2 | 152.4 | 25.65 | 4.547 | $[90_8/0_8]_s$ |

The FPF analysis of the considered beams has also been examined by M. L. Nazargah [59] using a high-order global-local (HO-GL) finite element model, Kim et al. [52] using a beam finite element with LW constant shear, and the analytical results obtained by the CLT. One can see in Tables 4.4 and 4.5 that, by using different failure criteria, the predicted FPF loads and their corresponding deflections produced by the current element are in good agreement with the numerical and analytical results. Therefore, the performance of the developed element is confirmed both in terms of good accuracy and a quick rate of convergence.

Table 4. 4: FPF load (N) of the laminated graphite/epoxy beams.

Failure criteria	Analytical results based on CLT	Numerical results based on HO-GL model [60]	Numerical results based on LW theory [52]	Numerical results based on Present element	
A1					
Hashin	325	303	-	356	Layer 1
Maximum Stress	325	304	307	356	Layer 1
Tsai-Hill	325	304	-	356	Layer 1
Tsai-Wu	327	304	307	361	Layer 1
A2					
Hashin	295	274	-	325	Layer 1
Maximum Stress	295	275	307	325	Layer 1
Tsai-Hill	295	275	-	325	Layer 1
Tsai-Wu	297	275	307	329	Layer 1

Table 4. 5: Displacement (mm) using FPF load of the laminated graphite/epoxy beams.

Failure criteria	Analytical results based on CLT	Numerical results based on Present element
A1		
Hashin	3.210	3.513
Maximum Stress	3.210	3.513
Tsai-Hill	3.210	3.513
Tsai-Wu	3.229	3.562
A2		
Hashin	3.900	4.293
Maximum Stress	3.900	4.293
Tsai-Hill	3.900	4.293
Tsai-Wu	3.927	4.346

4.2.3. **Clamped supported cross-ply laminated plate [0/90]ₛ under a concentrated load**

study consists of square [0/90]ₛ laminated plates with sides a=b = 10 cm. The plates are clamped on the four sides (CC) and subjected to concentration load (Failure load = 1410 N). The elastic properties used in this study are given in Table 4.6. The convergence of the displacement obtained is presented in Table 4.7 and shown on Fig 4.3.

Table 4. 6: Material property.

E_1(MPa)	E_2 (MPa)	G_{12} (MPa)	v_{12}	a et b (mm)	h (mm)
141000	9340	4500	0.35	100	(0.5/0.5/0.5/0.5)
X_t (MPa)	Y_t (MPa)	X_C (MPa)	Y_C (MPa)	S (MPa)	
1500	180	1000	240	150	

Table 4. 7: Convergence of the displacement for a clamped laminated plate subjected to a concentrated load.

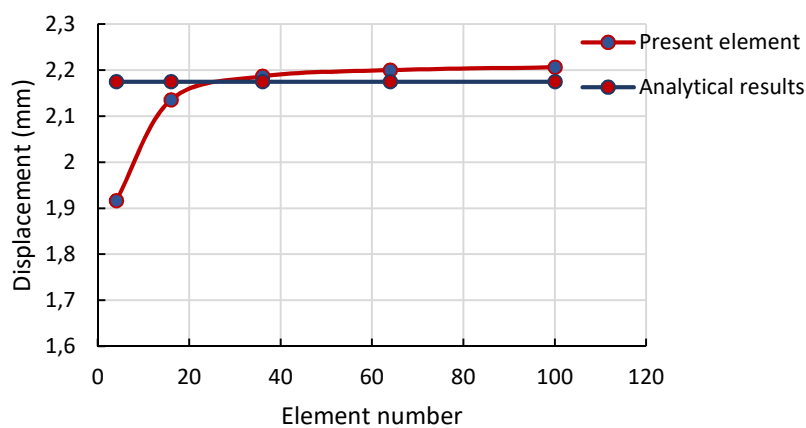| Mesh	Displacement (mm)
2*2	1,9166
4*4	2,1357
6*6	2,1867
8*8	2,2003
10*10	2,2066
Analytic displacement	2,1750

Fig 4. 3: Convergence of the displacement for a clamped laminated plate subjected to a concentrated load

One can see from table 4.7 and Fig.4.3 that, the numerical results obtained by the present element compare favorably with those obtained by the analytic solution. It is observed that the

results are very close to the reference results, which demonstrates the accuracy of the present element.

4.2.4. **Simply supported cross-ply laminated plate [0/90/0] under a uniforme loading**

In this example, a rectangular laminated plate is simply supported (SSSS) with fiber orientation [0/90/0] and subjected to uniform load; two thickness ratios are used: 0.01 and 0.02. The results obtained using the present element are compared with those obtained by Reddy [116] and the first-order shear deformation theory (FSDT). Table 4.8 shows the convergence of the transverse displacement using various mesh sizes. The mechanical characteristics are: $E_1 = 174.6$ GPa,

$E_2 = 7$ GPa, $G_{12} = G_{13} = 3.5$ GPa, $G_{23} = 1.4$ GPa, $\upsilon_{12} = \upsilon_{13} = 0.25$

The maximum value of the analytical displacement is calculated using the following relation

$$\overline{w} = \frac{w E_2 h^3}{q_0 a^4} 10^2$$

Table 4.8: Convergence of the displacement for a simply (SSSS) laminated plate subjected to uniform load. $\overline{w} = \frac{w E_2 h^3}{q_0 a^4} 10^2$

Mesh	Thickness ratio h/a	
	0.01	0.02
2×2	0.68103	0.6220
4×4	0.6696	0.6399
6×6	0.6694	0.6669
8×8	0.6693	0.65193
10×10	0.6693	0.6545
Reddy [116]	0.6705	0.6838
First-order shear deformation theory[116]	0.6697	-
higher-order theory[117]	0.6713	-

Table 4.8 shows that the results are quite close to those obtained by in addition to those found by first-order shear theory and higher-order theory [117] , indicating that the current element, in general, gives accurate results when compared to the literature. 10 * 10 mesh division was used for the entire plate analysis.

However, the second and third test examples are taken into consideration in order to verify the viability and capability of the present element and to assess the stress of beams subjected to uniform temperature and moisture.

4.3.Validation of plate subjected to Hygrothermal environmental condition

4.3.1 Simply supported cross-ply laminated plate subjected to uniforme temperature

A symmetric laminated plate $[0/90]_s$ simply supported (SS) subjected to a uniform temperature T = 50 °C the thickness of each layer is 0.5. A 10x10 mesh division has been adopted. The mechanical characteristics of the laminated plate are presented in Table 4.9. The stress and stress resultants of laminated materials are presented in Table 4.10 and compared with an analytical solution.

Table 4. 8: Geometrical parameters and mechanical proprieties.

E_1 (MPa)	E_2 (MPa)	G_{12} (MPa)	v_{12}	T (C°)	α_1	α_2	β_1	β_2
142000	10300	7200	0.27	50	-9e-7	2.7e-5	1e-2	2e-1
X_t (MPa)	X_c (MPa)	Y_t (MPa)	Y_c (MPa)	S (MPa)				
2280	1440	57	228	71				

Table 4. 9: Stress convergence of a simply supported beam subjected to uniform temperature.

	Nx	Ny	Nxy	σ_x	σ_y	σ_{xy}
Present element	11.2034	11.2034	0	12.924	12.924	0
Analtical	11.203	11.203	0	12.925	12.925	0

The results of stress and effort resultants on laminated materials are determined and compared with analytical results. The results show excellent agreement with the analytical solution.

4.3.2.Simply supported cross-ply laminated plate subjected to uniform moisture

A simply supported (SS) four-layer laminated plate subjected to uniform moisture $C=0.05$. The mechanical characteristics of the laminated plate are presented in Table 4.9. The stress and efforts resultant are presented in table 4.11

Table 4. 10: Stress convergence of a simply supported beam subjected to uniform moisture.

	Nx	Ny	Nxy	σ_x	σ_y	σ_{xy}
Present element	204.280	204.280	0	88.018	88.018	0
Analytical	204.281	204.281	0	88.018	88.018	0

The stress and effort results of a symmetrical beam subjected to uniform moisture equal to 5% are shown in Table 4.11. The results are compared with an analytical solution. This finding shows that the result obtained by the current element provides excellent agreement with the analytical solution, which indicates the performance and accuracy of the present element.

4.4.Parametric study:

4.4.1. Effect of boundary condition and stacking sequences on the FPF load in laminated plate:

After the convergence test, the accuracy of this element was validated. Now, one can use it to analyze the influence of boundary conditions and the direct influence of fiber orientation angle on the failure load and also determine the damage location. A Tsai-Wu failure criterion is used to determine the FPF load of plates with stacking sequence $[0/\theta]_s$ under concentrated load. Different boundary conditions are considered as given in table 4.12. The results are presented in table 4.13 and Figs 4.4 and 4.5.). The elastic properties used in this study are given in Table.4.6.

Table 4. 11: Boundary conditions employed in numerical tests.

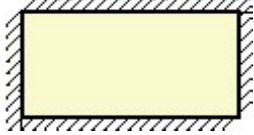| Boundary conditions		
CC	$u = 0; v = 0; w = 0; \dfrac{\partial w}{\partial x} = 0; \dfrac{\partial w}{\partial y} = 0; \dfrac{\partial^2 w}{\partial x \partial y} = 0$	
	$u = 0; v = 0; w = 0; \dfrac{\partial w}{\partial x} = 0; \dfrac{\partial w}{\partial y} = 0; \dfrac{\partial^2 w}{\partial x \partial y} = 0$	
SS	$u \neq 0; v \neq 0; w = 0; \dfrac{\partial w}{\partial x} \neq 0; \dfrac{\partial w}{\partial y} = 0; \dfrac{\partial^2 w}{\partial x \partial y} \neq 0$	
	$u \neq 0; v \neq 0; w = 0; \dfrac{\partial w}{\partial x} \neq 0; \dfrac{\partial w}{\partial y} = 0; \dfrac{\partial^2 w}{\partial x \partial y} \neq 0$	

Table 4. 12: The FPF strength of simply supported and clamped laminated plates with different stacking sequences.

| Boundary condition	Stacking sequences	Failure load		
		Analytical Results	Present element	Location
CC	[0°/0°]s	1650	1140	Bot 4
	[0°/15°]s	1680	1160	Bot 4
	[0°/30°]s	1732	1220	Bot 4
	[0°/45°]s	1800	1300	Bot 4
	[0°/60°]s	1850	1360	Bot 4
	[0°/75°]s	1880	1400	Bot 4
	[0°/90°]s	1880	1410	Bot 4
SS	[0°/0°]s	1210	905	Bot 4
	[0°/15°]s	1230	930	Bot 4
	[0°/30°]s	1290	990	Bot 4
	[0°/45°]s	1340	1040	Bot 4
	[0°/60°]s	1370	1080	Bot 4
	[0°/75°]s	1370	1100	Bot 4
	[0°/90°]s	1370	1102	Bot 4
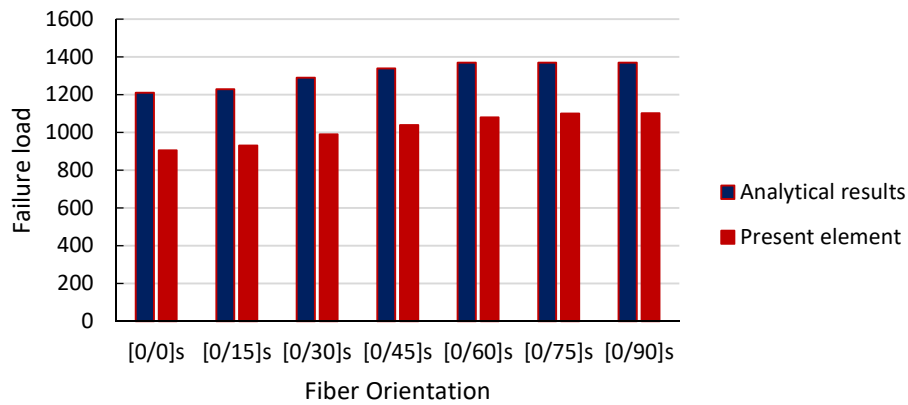
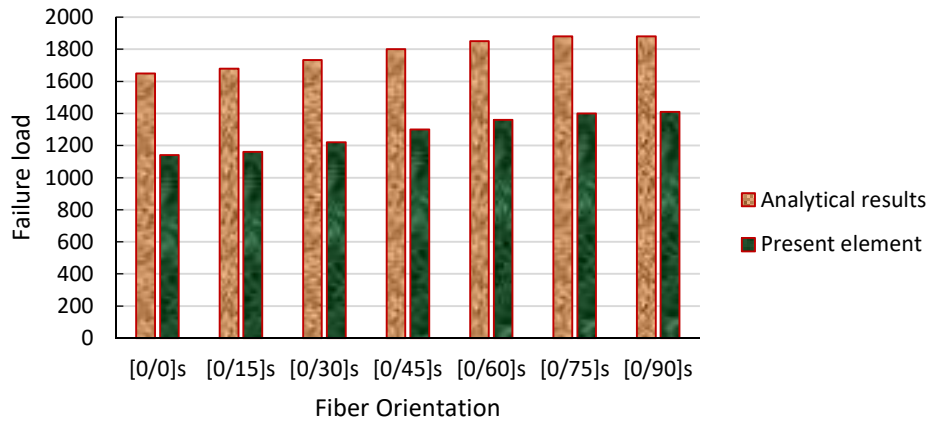Fig 4. 4: The FPF strength of simply supported laminated plates with different stacking sequences.

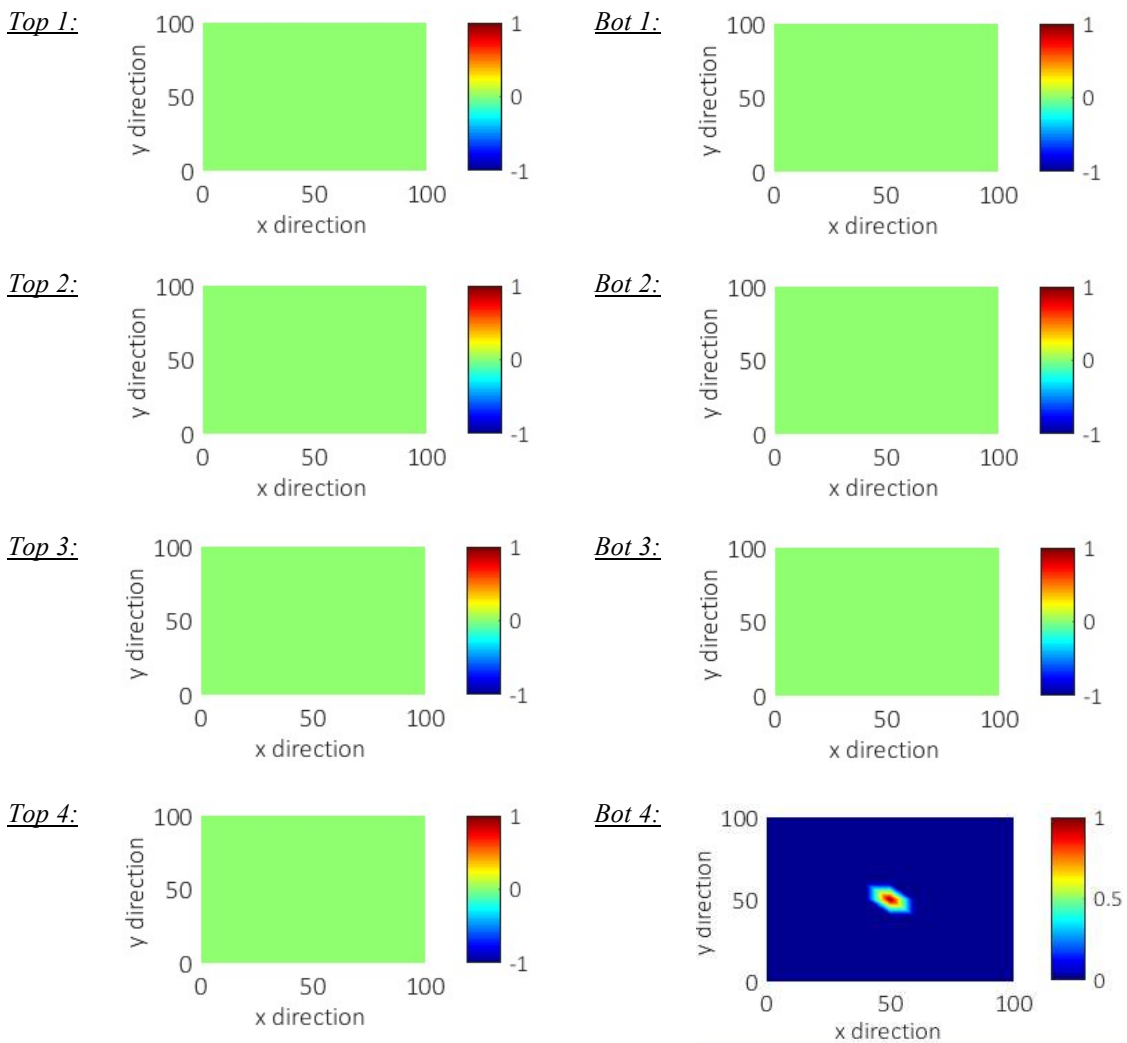Fig 4. 5: The FPF strength of clamped laminated plates with different stacking sequences.

Fig 4. 6: Damage distributions of fixed supported laminated plates [0/90]s under concentrated load.

It is observed that, for both boundary conditions, by increasing the fiber orientation angle, there is an increase in failure load, and when the stacking sequences are [0/75]s and [0/90]s, the failure loads are almost constant for both boundary conditions. The maximum failure load obtained using the present element is 1410 N for clamped plates and 1102 N for a simply supported laminated with [0/90]s. The first surface failure (FPF) is the bottom side of the fourth layer.
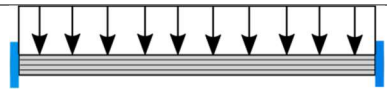
4.4.2. *The FPF load of Laminated Beams :*

After establishing the accuracy of the present element, a comprehensive analysis of bending, and damage of multilayered beams is carried out. The effects of loading, boundary conditions, number of layers, and stacking sequences are investigated and discussed in detail. The following analysis is focused on glass/epoxy beams using the present element, and the results are compared to the analytical solution based on the CLT.

4.4.2.1. *Effect of loading and boundary conditions on the FPF strength*

After validating the performance of the presented elements for the analysis of cross-laminated beams, this section considers a number of numerical tests to study the transverse deformation and FPF strength. Table 4.14 presents both loading and boundary conditions, for which the numerical results are obtained, where CC, SS, and CF respectively indicate: fully clamped, fully simply supported, and clamped from one side and free from the other, respectively.

Table 4. 13: Boundary conditions used in the numerical tests.

Abbreviations	Restrained edges	
CC	$u = 0, v = 0, w = 0, \dfrac{\partial w}{\partial x} = 0, \dfrac{\partial w}{\partial y} = 0, \dfrac{\partial^2 w}{\partial x \partial y} = 0$	
SS	$u \neq 0, v \neq 0, w = 0, \dfrac{\partial w}{\partial x} \neq 0, \dfrac{\partial w}{\partial y} = 0, \dfrac{\partial^2 w}{\partial x \partial y} \neq 0$	
CS	$u = 0, v = 0, w = 0, \dfrac{\partial w}{\partial x} = 0, \dfrac{\partial w}{\partial y} = 0, \dfrac{\partial^2 w}{\partial x \partial y} = 0$ $u \neq 0, v \neq 0, w = 0, \dfrac{\partial w}{\partial x} \neq 0, \dfrac{\partial w}{\partial y} = 0, \dfrac{\partial^2 w}{\partial x \partial y} \neq 0$	
CF	$u = 0, v = 0, w = 0, \dfrac{\partial w}{\partial x} = 0, \dfrac{\partial w}{\partial y} = 0, \dfrac{\partial^2 w}{\partial x \partial y} = 0$	

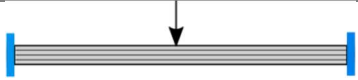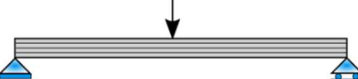| CC with two concentrated loads | $u = 0, v = 0, w = 0, \dfrac{\partial w}{\partial x} = 0, \dfrac{\partial w}{\partial y} = 0, \dfrac{\partial^2 w}{\partial x \partial y} = 0$ | |
| CC with a distributed load | $u = 0, v = 0, w = 0, \dfrac{\partial w}{\partial x} = 0, \dfrac{\partial w}{\partial y} = 0, \dfrac{\partial^2 w}{\partial x \partial y} = 0$ | |

The laminated beams are made of glass/epoxy, and their corresponding geometrical and material characteristics are given in Table 4.15.
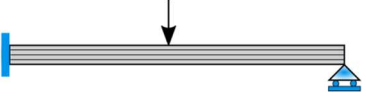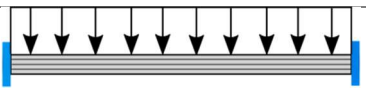
Table 4. 14: Geometric and material properties of glass/epoxy beams.

E_1 (MPa)	E_2 (MPa)	G_{12} (MPa)	v_{12}	X_t (MPa)	X_c (MPa)	Y_t (MPa)	Y_c (MPa)	S (MPa)
141000	9340	4500	0.35	1500	1000	180	240	150

Laminate	Length L (mm)	Width b (mm)	Thickness h (mm)	Lay-up
A3	1000	100	2	[0/90]$_s$

Table 4.16 presents the comparisons of maximum transverse displacement and FPF loads of glass/epoxy laminated beams using various failure criteria.

Table 4. 15: Displacement (mm) and FPF load (N) of glass/epoxy laminated beams.

Boundary condition	Failure theory	Displacement		FPF load	
		Analytical results based on CLT	Numerical results based on present element	Analytical results based on CLT	Numerical results based on present element
	Tsai-Wu	305.44	300.92	490.00	482.00
	Hashin	284.87	287.22	457.00	489.00
	Max Stress	284.87	242.89	457.00	389.00
	Tsai-Hill	286.74	242.89	460.00	389.00
	Tsai-Wu	649.40	611.52	260.00	245.00
	Hashin	606.94	534.15	243.00	214.00
	Max Stress	606.94	534.15	243.00	214.00
	Tsai-Hill	609.44	536.65	244.00	215.00
	Tsai-Wu	2515.52	2436.60	63.00	61.00
	Hashin	2315.88	2276.90	58.00	57.00
	Max Stress	2315.88	2316.80	58.00	58.00
	Tsai-Hill	2355.81	2316.80	59.00	58.00
	Tsai-Wu	365.06	360.38	327.00	330.00

	Hashin	340.50	334.19	305.00	306.00
	Max Stress	340.50	352.76	305.00	323.00
	Tsai-Hill	342.73	336.38	307.00	308.00
	Tsai-Wu	235.54	238.71	291.00	295.00
	Hashin	219.35	212.25	271.00	278.00
	Max Stress	219.35	239.74	271.00	314.00
	Tsai-Hill	220.97	213.01	273.00	279.00
	Tsai-Wu	237.48	234.55	0.0076	0.007
	Hashin	221.86	217.80	0.0071	0.0065
	Max Stress	221.86	237.90	0.0071	0.0071
	Tsai-Hill	221.86	217.80	0.0071	0.0065

On the other hand, the transverse deflection distributions of glass-epoxy laminated beams using various boundary conditions are presented in Fig 4.7.
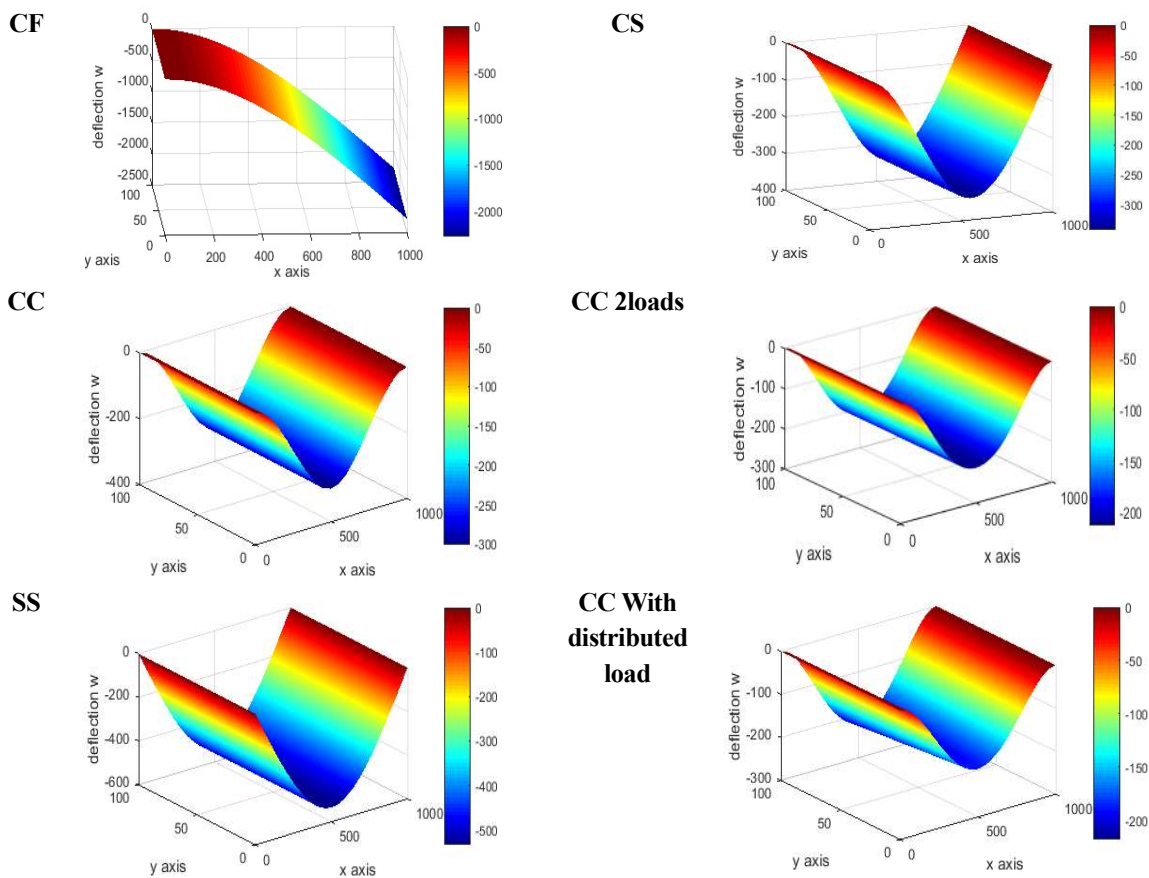

Fig 4. 7: The transverse displacement distribution of FPF for different boundary conditions in glass-epoxy laminated beams

The numerical results are obtained for various schemes of loading and different boundary conditions. These results are compared to those obtained by the analytical solution based on the CLT.

As can be seen in Table 9, for both displacement and FPF load results, there are no significant differences between the present results and the analytical solutions. For example, by using the Tsai-Wu failure theory, the maximum displacements obtained by the present element and CLT are almost the same, and they equal 300.92 mm and 305.44 mm, respectively. On the other hand, by considering the same example, the predicted FPF loads obtained using the Hashin criterions are 460.00 N and 457.00 N, respectively. Moreover, it can be observed that the BC and loading have a remarkable impact on the FPF loads.

4.4.2.2. *Effect of stacking sequences on the FPF strength and deflection of FPF*

In the present section, clamped and simply supported glass/epoxy multilayered beams are studied. The computational results are obtained for various symmetric stacking sequences. Two different configurations of stacking sequences, $[0°/\theta°]_s$ and $[90°/\theta°]_s$, are considered to see the direct effect of fiber orientation on FPF load and deflection of FPF. Furthermore, by using Hashin criterion, the damage mechanism and location can easily be detected. Tsai-Wu criterion is also adopted for comparison purpose. In these examples, we kept the same geometrical and mechanical properties of the previous beams and changing only fiber orientation and the support conditions.

The FPF results of glass/epoxy beams subjected to a concentrated load at the mid-span of the beams are highlighted in Tables 4.17, 4.18 and Figs 4.8 and 4.9 Tables 4.19, 4.20 and Figures 4.10 and 4.11 show the transverse deformation caused by the FPF load of glass/epoxy beams.

Table 4. 16: FPF loads (N) of clamped and simply supported [0°/θ°]ₛ glass/epoxy beams.

BC	Lay-up	Tsai-Wu criteria		Hashin criteria		
		Analytical results based on CLT	Numerical results based on the present element	Analytical results based on CLT	Numerical results based on the present element	
					Load	Dominant Failure Mode Type
CC	[0°/0°]ₛ	547.0	542.0	510.0	407.0	Fiber compression
	[0°/15°]ₛ	506.0	503.0	471.0	401.0	Interface
	[0°/30°]ₛ	477.0	475.0	444.0	393.0	interface

	[0°/45°]$_s$	478.0	475.0	446.0	389.0	interface
	[0°/60°]$_s$	484.0	480.0	451.0	388.0	interface
	[0°/75°]$_s$	488.0	482.0	455.0	389.0	interface
	[0°/90°]$_s$	490.0	482.0	457.0	389.0	Fiber compression
SS	[0°/0°]$_s$	284.0	269.0	270.0	231.0	Fiber compression
	[0°/15°]$_s$	271.0	258.0	265.0	228.0	Fiber compression
	[0°/30°]$_s$	252.0	243.0	254.0	221.0	Fiber compression
	[0°/45°]$_s$	246.0	237.0	246.0	215.0	Fiber compression
	[0°/60°]$_s$	251.0	239.0	243.0	213.0	Fiber compression
	[0°/75°]$_s$	257.0	243.0	243.0	213.0	Fiber compression
	[0°/90°]$_s$	260.0	245.0	243.0	214.0	Fiber compression

Table 4. 17: FPF loads (N) of clamped and simply supported [90°/θ°]$_s$ glass/epoxy beams.

BC	Lay-up	Tsai-Wu criteria		Hashin criteria		
		Analytical results based on CLT	Numerical results based on the present element	Analytical results based on CLT	Numerical results based on the present element	
					Load	Dominant Failure Mode Type
CC	[90°/0°]$_s$	207.0	206.0	193.0	186.0	Fiber compression
	[90°/15°]$_s$	148.0	142.0	137.0	131.0	Fiber compression
	[90°/30°]$_s$	130.0	121.0	121.0	111.0	Fiber compression
	[90°/45°]$_s$	107.0	98.0	100	94.0	Matrix tensile
	[90°/60°]$_s$	97.0	95.0	92.0	90.0	Matrix tensile
	[90°/75°]$_s$	98.0	98.0	94.0	92.0	Matrix tensile
	[90°/90°]$_s$	99.0	97.0	95.0	93.0	Matrix tensile
SS	[90°/0°]$_s$	109.0	104.0	102.0	95.0	Fiber compression
	[90°/15°]$_s$	111.0	106.0	103.0	96.0	Interface
	[90°/30°]$_s$	87.0	82.0	88.0	83.0	Matrix tensile
	[90°/45°]$_s$	65.0	62.0	66.0	63.0	Matrix tensile
	[90°/60°]$_s$	53.0	51.0	54.0	52.0	Matrix tensile
	[90°/75°]$_s$	50.0	49.0	50.0	48.0	Matrix tensile
	[90°/90°]$_s$	51.0	49.0	50.0	48.0	Matrix tensile

Table 4. 18: deflection of clamped and simply supported [0°/θ°]$_s$ glass/epoxy beams.

BC	Lay-up	Tsai-Wu criteria		Hashin criteria	
		Analytical results based on CLT	Numerical results based on the present element	Analytical results based on CLT	Numerical results based on the present element
CC	[0°/0°]$_s$	301.983	299,92	281,557	225,25

|	Lay-up			
	[0°/15°]ₛ	286.829	285,94	266.989	227,99
	[0°/30°]ₛ	283.879	282,89	264.24	234,11
	[0°/45°]ₛ	293.687	292,02	274.026	239,22
	[0°/60°]ₛ	301.156	299,110	280.622	241,82
	[0°/75°]ₛ	304.23	301,0	283.675	243,00
	[0°/90°]ₛ	305.437	300,92	284.866	242,89
SS	[0°/0°]ₛ	629.087	595,23	598.076	511,16
	[0°/15°]ₛ	614.999	584,27	601.383	516,34
	[0°/30°]ₛ	601.368	578,19	606.141	525,86
	[0°/45°]ₛ	609.634	585,81	609.634	531,45
	[0°/60°]ₛ	629.137	597,82	609.085	532,79
	[0°/75°]ₛ	643.149	607,38	608.114	532,40
	[0°/90°]ₛ	649.40	611,52	606.94	534,15

Table 4. 19: Deflection of clamped and simply supported [90°/θ°]ₛ glass/epoxy beams.

BC	Lay-up	Tsai-Wu criteria		Hashin criteria	
		Analytical results	Present element	Analytical results	Present element
CC	[90°/0°]ₛ	623.482	620,43	581.314	560,25
	[90°/15°]ₛ	532.822	512,07	493.22	472,49
	[90°/30°]ₛ	653.232	611,30	608.01	561,0
	[90°/45°]ₛ	706.818	651,10	660.578	624,96
	[90°/60°]ₛ	754.393	741,3	715.507	702,72
	[90°/75°]ₛ	812.226	813,20	779.074	763,65
	[90°/90°]ₛ	826.519	810.30	793.125	777,36
SS	[90°/0°]ₛ	1314.711	1253,5	1230.28	1145,0
	[90°/15°]ₛ	1501.663	1434.8	1393.435	1299,4
	[90°/30°]ₛ	1545.721	1460,9	1563.488	1478,7
	[90°/45°]ₛ	1577.599	1508.7	1601.870	1533,1
	[90°/60°]ₛ	1620.306	1561,0	1650.878	1591,6
	[90°/75°]ₛ	1661.383	1628,2	1661.383	1595,0
	[90°/90°]ₛ	1706.522	1639,1	1673.06	1605,7
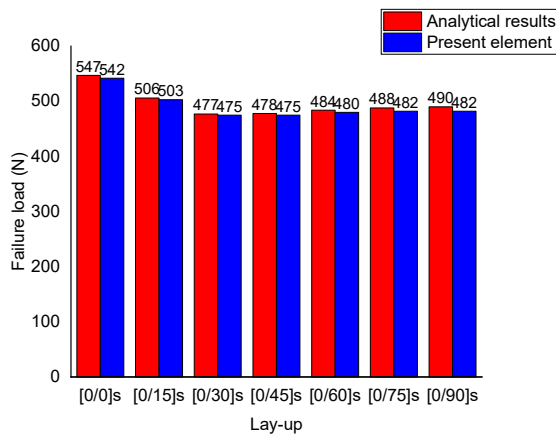
(a) CC Tsai-Wu   **(b) CC Hashin**
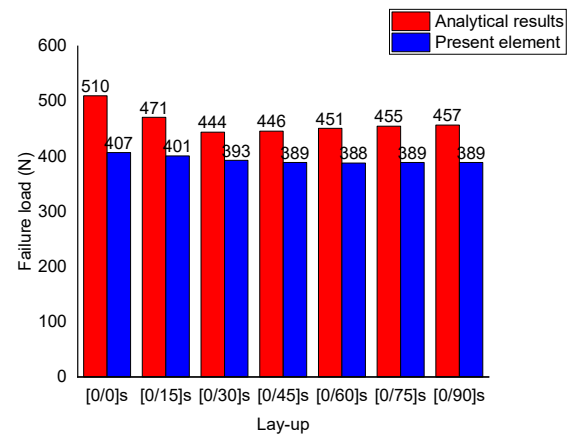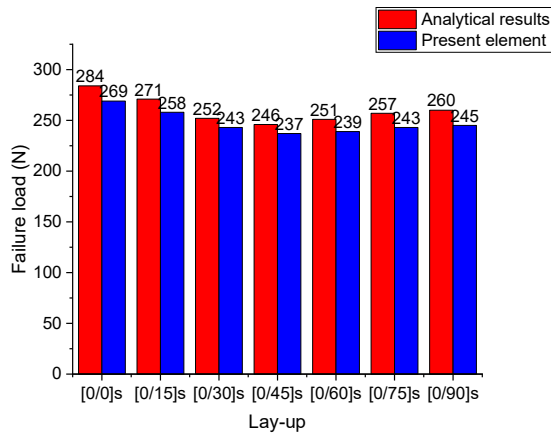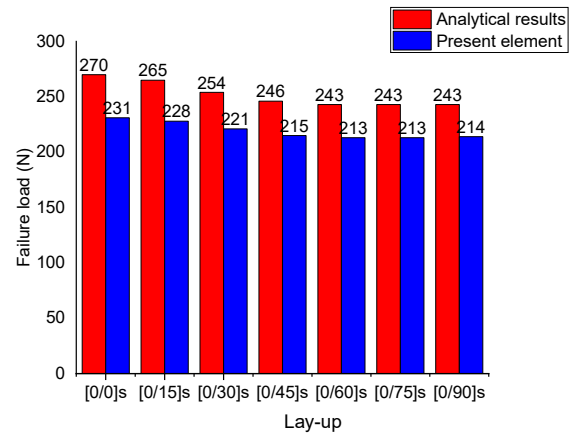
(c) SS Tsai-Wu   **(d) SS Hashin**

Fig 4. 8: FPF loads (N) of clamped and simply supported $[0°/\theta°]$s glass/epoxy beams using different failure criterion.
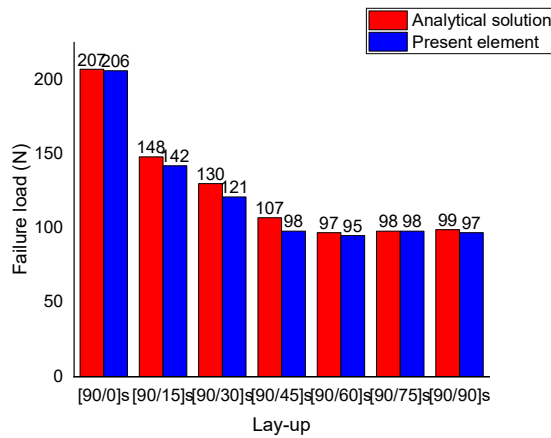
(a) CC Tsai-Wu   **(b) CC Hashin**
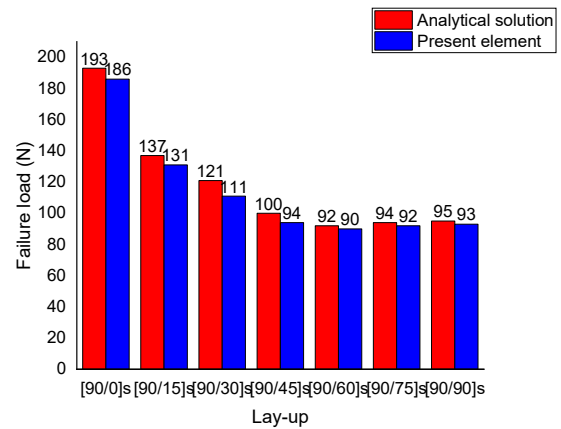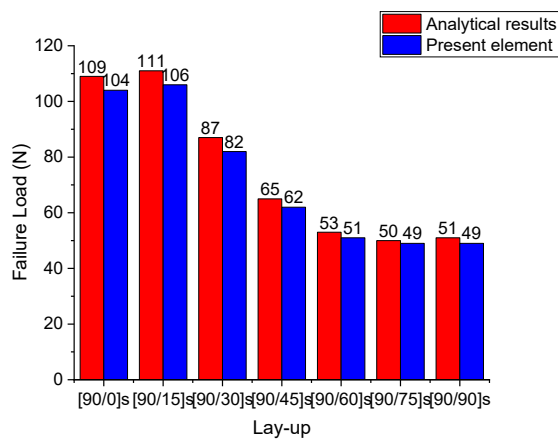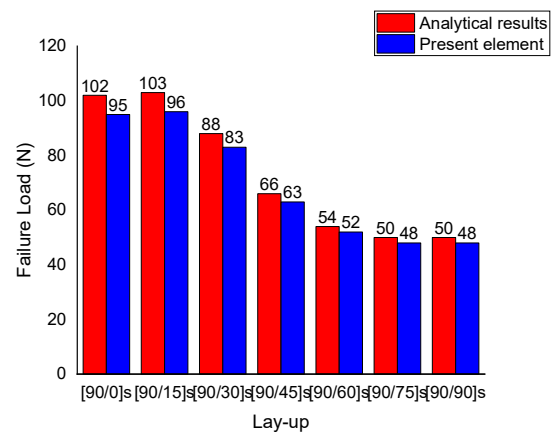
(c) SS Tsai-Wu   **(d) SS Hashin**

Fig 4. 9: FPF loads (N) of clamped and simply supported [90°/θ°]s glass/epoxy beams using different failure criterion.

(a)

(b)

Fig 4. 10: Deflection of FPF load of (a) clamped and (b) simply supported [0°/θ°]s glass/epoxy beams using Tsai-wu failure criterion.

(a)

(b)

Fig 4. 11: Deflection (w) of FPF loads (N) of (a) clamped and (b) simply supported [90°/θ°]s glass/epoxy beams using Hachin failure criterion.

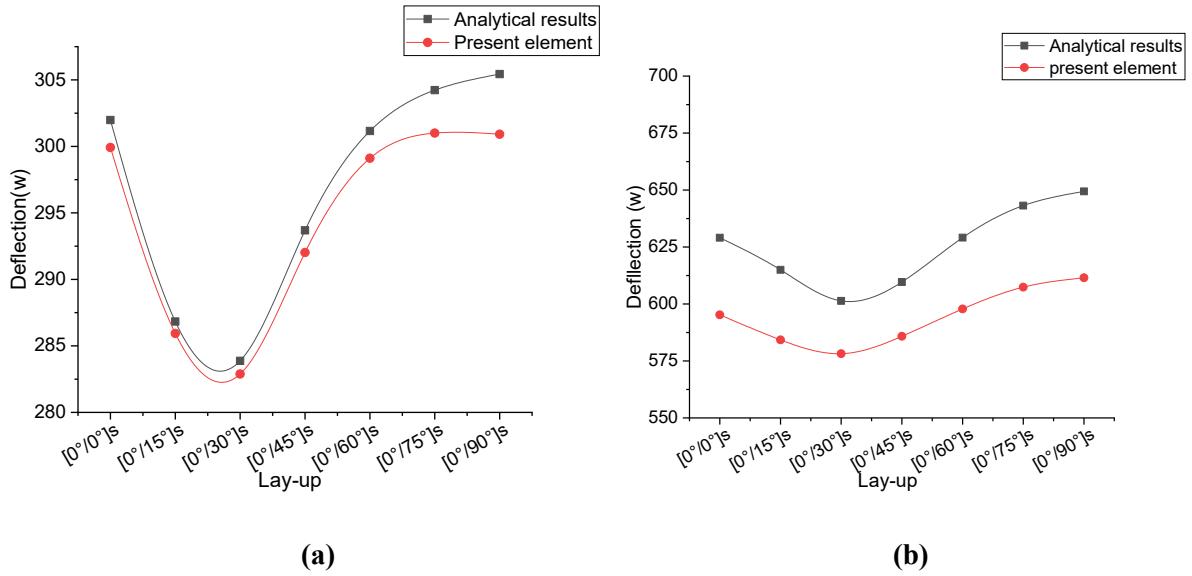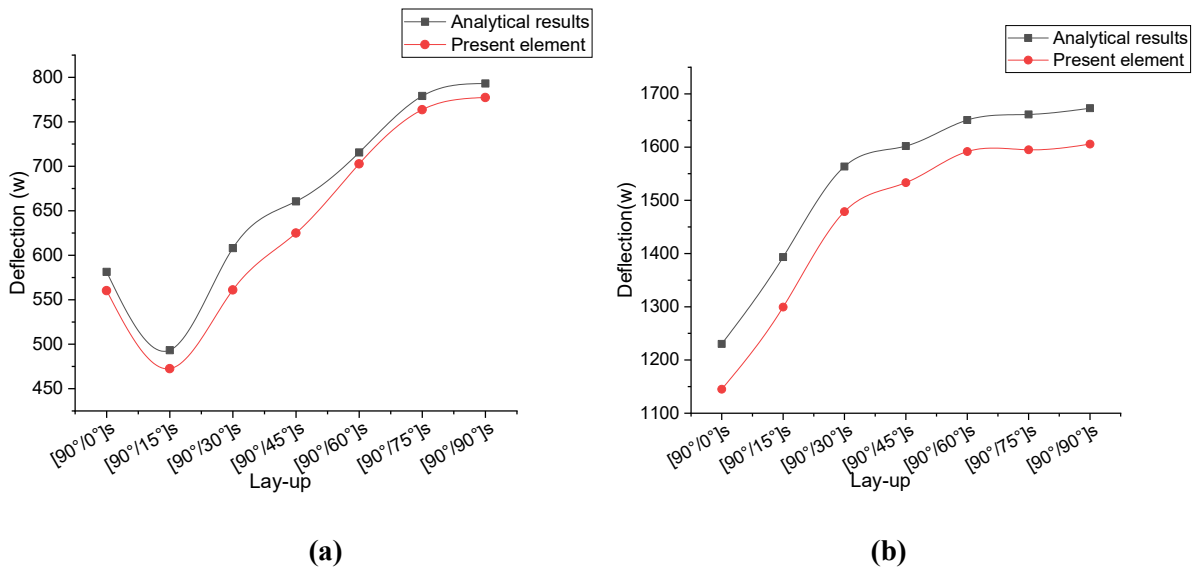From Tables 4.17 and 4.18, it is observed that the clamped beam with layers [0°/0°]s has the highest FPF load. One can see also from Table 4.17 that, by increasing the fiber orientation angle, the failure load decreases until it reaches its minimum value for [0°/45°]s beams then it increases to reach a local maximum value for [0°/90°]s. In addition to the previous observations, one can see from Table 4.18 and Fig.4.9 that, if the fiber orientation angles are ranging between 0° and 45°, the failure load is completely affected. The augmentation of fiber orientation angle decreases the values of FPF load to reach its minimum value for [90°/60°]s. However, when the angle values are 60°, 75°, and 90°, the strength of the beams is not affected too much and they are quite close. Thus, whatever the boundary condition is, the increase in the fiber orientation angle reduces the flexural stiffness of the beam and therefore decreases the failure strength.

Table 4.19 and Fig 4.10 demonstrates that when increasing the fiber orientation angle, the deflection (w) of failure load decreases until it reaches its minimum value of [0°/30°]s beams, then it increases to reach a local maximum value of [0°/90°]. One can also see that the beam with layers [0°/90°]s has the highest deflection value (w) of the FPF load, in both cases of boundary condition (clamped and simply).

We notice in Table 4.20 and Fig 4.11 for a clamped supported beam that the value of deflection decreases with an increase in the fiber orientation until it reaches [0°/15°] and then increases until it reaches its maximum value when the fiber orientation [0°/90°]. In the case of a simply supported beam, the deflection value of FPF increases as the fiber orientation increases until it reaches its maximum value when the fiber orientation is [0°/90°].

In addition to the previous observations, one can see from Tables 4.17 and 4.18 and Figs 4.10 and 4.11 that the deflection of FPF obtained by the present element is very close to the analytical results because the value of FPF was also close.

4.4.2.3. *Progressive damage analysis: (Failure index)*

One of the main purposes of progressive damage analysis of laminated beams is to evaluate the macroscopic damage initiation and propagation using the finite element method. As an example of modeling damage growth, the damage initiation and growth in [0°/90°]s glass/epoxy laminated beams are studied using the present element and Tsai-Wu criteria. The considered beam is clamped from one side and simply supported from the other (CS), and it is subjected to a concentrated load at the mid-span of the beam. As the first step for progressive damage
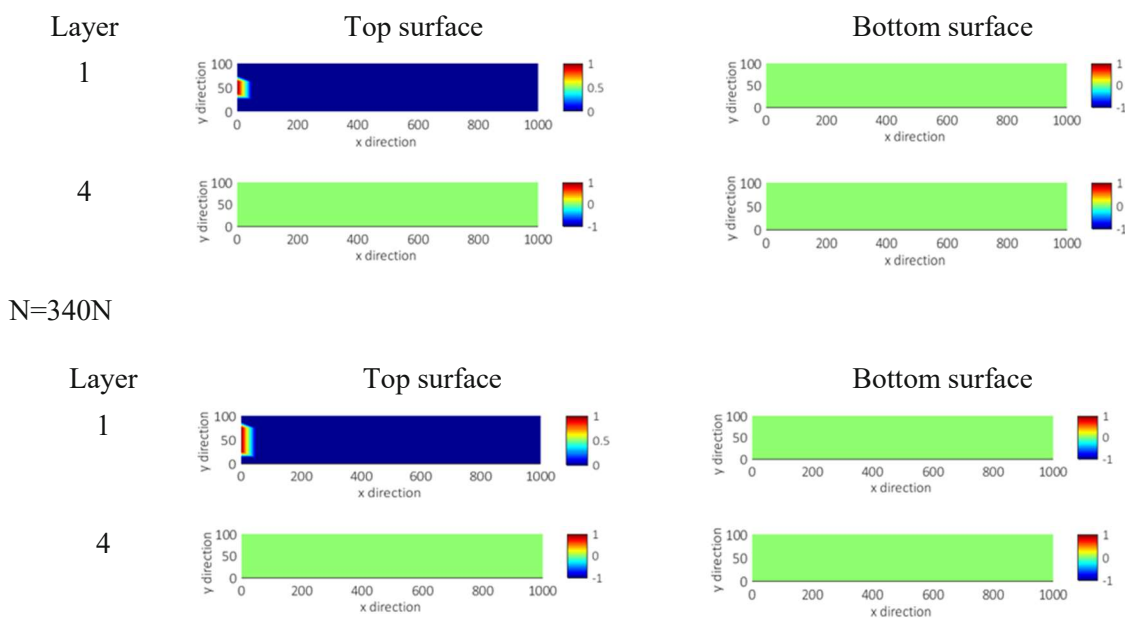
analysis, The initial failure load, commonly known as the first ply failure load (FPF), should be determined as the first step in a progressive damage analysis. Based on the previous examples, the FPF load of this beam is 330N (see Table 4.16).

After the first ply failure, it can be assumed that the material properties of the failed elements are not modified, and the laminated beam is reanalyzed at the current load.

The load is applied incrementally in steps (step-by-step), and the damage growth in each surface of the laminated composite beam is determined using this iterative process. The distributions of damage to the laminated beam are shown in Table 4.21. From the figures, it is observed that:

- The damage starts at the clamped side of the beam, where the stresses are significantly higher.
- The damage starts at the top surface of the first ply.
- Since the laminate beam is symmetric, one can suppose that the damage occurs symmetrically   along the thickness. However, it is not the case considering this example.
- By increasing the applied load, one can see the damage propagation at the top surface of the first ply. The damage starts from the clamped side, and it propagates.
- When the applied load reaches 340 N, the damage occurs at the bottom surface of the last layer, and then it propagates by increasing the applied load.

Table 4. 20: The failure strength distribution for beams $[0/90]_s$ with (CS) boundary condition with N=330N
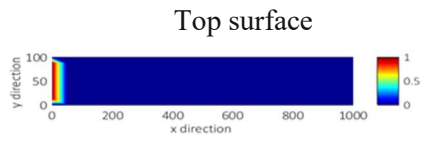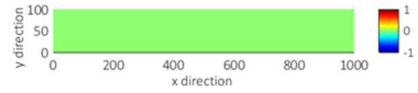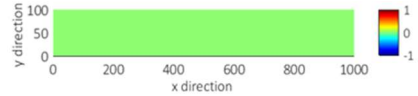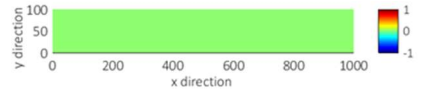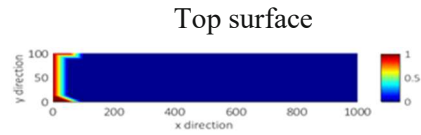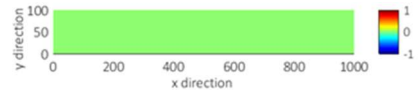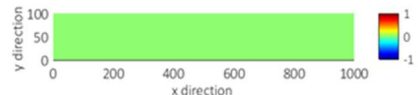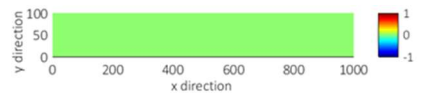
Layer	Top surface	Bottom surface
1		
4		

N=340N

Layer	Top surface	Bottom surface
1		
4		

N=360N

N=380N

N=400N

N=420N

N=440N

N=460N

N=480N

N=500N
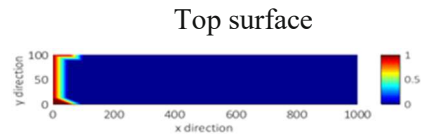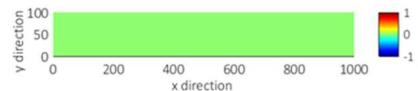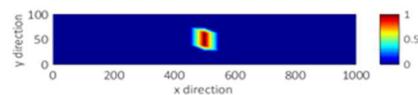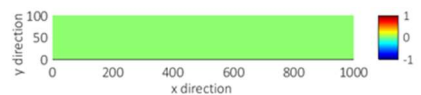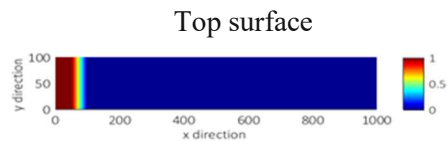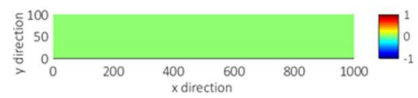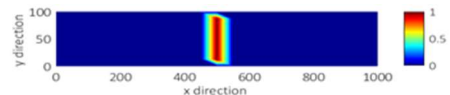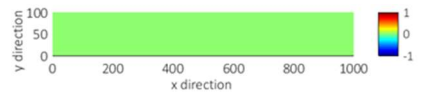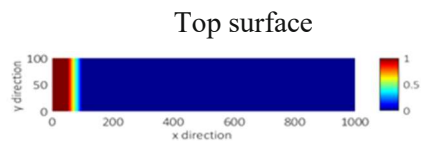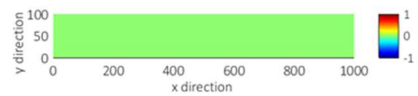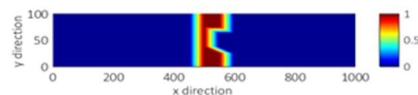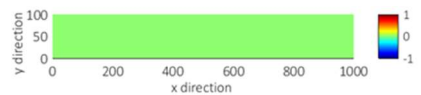
N=520N
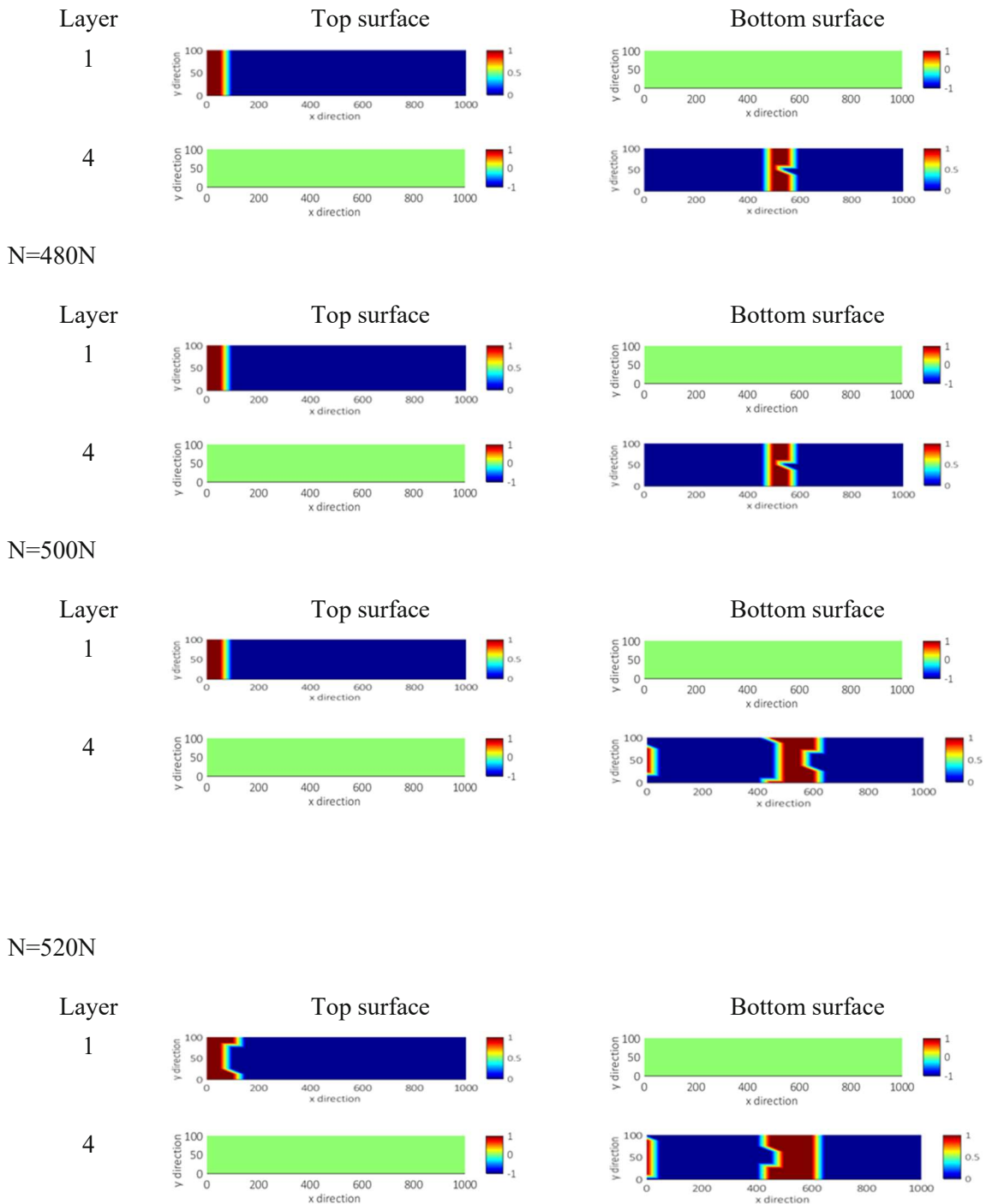
4.4.3. **Laminated beams subjected to hygrothermal load :**

This section examines several numerical and analytical tests to examine the impact of different parameters on the first ply failure and damage location using various failure criteria after evaluating the performance of the present element for the analysis of cross-laminated beams that have been proved.

4.4.3.1. **Effect of type loading and fiber orientation on the FPF strength:**

Assume a symmetric laminated composite beam [0/θ]s with four layers, subjected to in-plane normal N_x and N_y loading. The laminated beams are made of glass/epoxy, and their corresponding geometrical and material characteristics are given in Table 4.15. The effect of fiber orientation angle on the first ply failure is studied and presented in Tables 4.22 and 4.23 using different failure criteria (Tsai-We, Tsai-Hill, and Hashin criteria). The numerical and analytical results are obtained with different fiber orientations and different failure criteria.
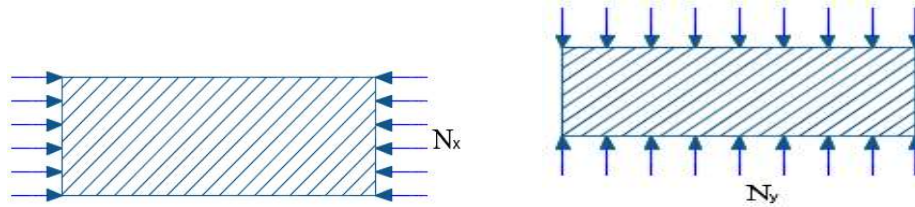
Fig 4. 12: Laminated composite beams with in-plane compressive loading N_x and N_y

Table 4. 21: FPF loads (N) of glass/epoxy beams with fiber orientation [0°/θ°]s subjected to compressive plane normal (N_x) using different failure criterion

	N_x					
	Tsai-We		**Tsai-Hill**		**Hachin**	
	Present element	**Analytical**	**Present element**	**Analytical**	**Present element**	**Analytical**
[0°/0°]s	2002	2002	2002	2002	2002	2002
[0°/15°]s	1344	1344	1388	1388	1394	1485
[0°/30°]s	1114.5	1115	1150	1150	1159	1188
[0°/45°]s	1073	1073	1089	1089	1092	1098
[0°/60°]s	1086	1086	1073	1073	1070	1070
[0°/75°]s	1117.5	1118	1072	1072	1065	1066
[0°/90°]s	1134.5	1135	1073	1073	1066	1066
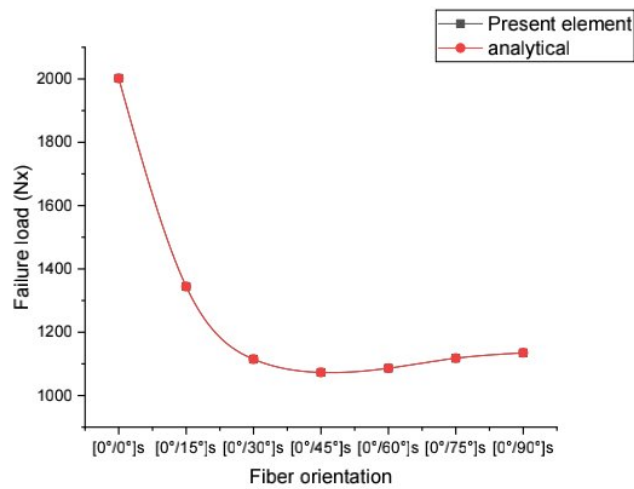
Fig 4. 13: FPF loads (N) of glass/epoxy beams with fiber orientation $[0°/θ°]_s$ subjected to compressive plane normal (N_x) using Tsai-we criteria

Table 4. 22: FPF loads of glass/epoxy beams with fiber orientation $[0°/θ°]_s$ subjected to compressive plane normal (N_y) using different failure criterion

	N_y					
	Tsai-We		Tsai-Hill		Hachin	
	Present element	Analytical	Present element	Analytical	Present element	Analytical
$[0°/0°]_s$	481	481	481	481	481	481
$[0°/15°]_s$	479	479	479	480	476	471
$[0°/30°]_s$	499.5	500	492.5	493	492.5	480
$[0°/45°]_s$	564.5	565	533.5	534	546	525
$[0°/60°]_s$	689.5	690	629	630	686.5	655.5
$[0°/75°]_s$	911.5	912	842.5	843	851	1137
$[0°/90°]_s$	1134.5	1135	1072.5	1073	1065.5	1066

All the results of presented in Tables 4.22 and 4.23 are illustrated in Fig 4.14.
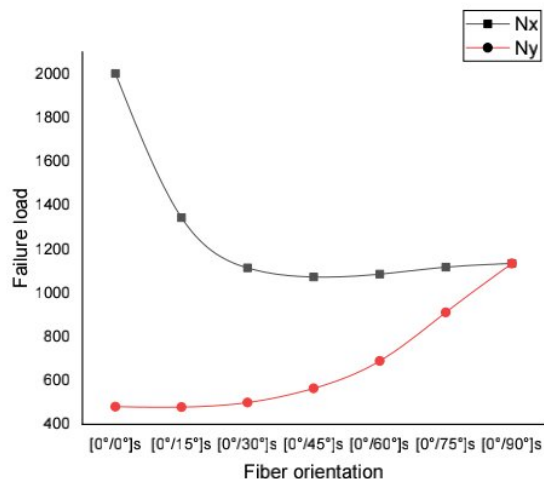
Fig 4. 14: FPF loads (N) of glass/epoxy beams with fiber orientation $[0°/\theta°]_s$ subjected to in-plane load N_x and N_y

Through Table 4.22, when the beam is subjected to a compressive plane normal load in direction x, it should be noted that the first-ply failure decreases as the angle of fiber orientation decreases and it reaches a quasi-stable value at 45°, then, it increases when the angle is equal $[0°/75°]$. This behavior is observed using various failure criteria. In contrast, when the beam is subjected to a compressive plane normal load in direction y (see Table 4.23), it can be seen that the first-ply failure increases as the angle of fiber orientation increases, except when the angle is $[0°/15°]$, in which the value of the failure load is the smallest. In addition to this, it can be noted that the results obtained by the current element are very close to the analytical results (see Fig 4.13).

On the other hand, it is observed in Table 4.22 that the maximum failure load is equal to 2002 and obtained at $\theta = 0°$ for plates subjected to N_x load using different failure cretiria, whereas for plates subjected to N_y load (see table 4.23), the FPF is equal to 1135 at $\theta = 90°$ and obtained by using Tsai-We cretiria. The failure strength is affected by the change in fiber orientation and direction of the load (x or y).

4.4.3.2. Symmetric angle ply composite subjected to uniform temperature and moisture:

The influence of temperature and moisture was examined on a composite beam with varied fiber orientation angles ranging from $[0°/15°]_s$ to $[0°/90°]_s$, through which the maximum temperature carried by the beam was estimated until the first failure of the plate for different

angles of the fiber, and the same example computed the maximum humidity for the first failure. The mechanical properties used in this investigation are presented in Table 4.15. The results of the FPF temperature and moisture are shown in Table 4.24 and Fig 4.15.

Table 4. 23: FPF temperature (T) and moisture (C) of glass/epoxy beams with fiber orientation $[0°/θ°]_s$ using different failure criterion

	T				C			
	Tsai-We		**Tsai-Hill**		**Tsai-We**		**Tsai-Hill**	
	Analytical	**Present element**	**Analytical**	**Present element**	**Analytical**	**Present element**	**Analytical**	**Present element**
$[0°/15°]_s$	3850	3849	3750	3748	0.354	0.354	0.345	0.3444
$[0°/30°]_s$	1950	1949	1879	1878	0.18	0.1791	0.173	0.1726
$[0°/45°]_s$	1308	1308.25	1269	1268.25	0.1203	0.1203	0.117	0.1166
$[0°/60°]_s$	995	994	989	989	0.092	0.0913	0.091	0.0909
$[0°/75°]_s$	834	834.25	859	858.25	0.077	0.0766	0.079	0.0790
$[0°/90°]_s$	783.5	783	821	820.5	0.072	0.072	0.0755	0.07542
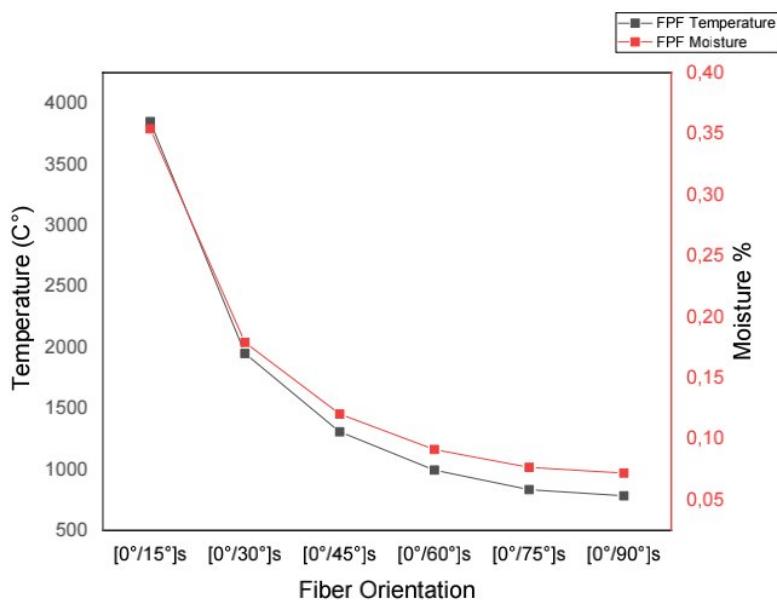
Fig 4. 15: First failure temperature and moisture of glass/epoxy beams with different fiber orientation

Table 4.24 shows the largest analytical and numerical values of temperature and moisture that lead to the first-ply failure of beams with different fiber orientations and various failure criteria.

The results show that the temperature and humidity that lead to the first-ply failure of laminate are higher at a $θ = 15°$ fiber orientation angle, where the temperature value reaches 3850 °C and the humidity is up to 35.4%. The temperature and moisture then decrease with the increase

in fiber orientation. This indicates that the laminate has good resistance to temperature but is sensitive to moisture. can also be concluded that the resistance of the laminate to heat and humidity changes with the change of the fiber orientation, as shown in Fig 4.15. For example, when the angle is 90° the temperature is 783.5 °C, it decreases by approximately 80%. when the direction of the fiber was 15°.

4.4.3.3. Symmetric angle ply composite subjected to thermo-mechanical loading condition

In Algeria during the summer, the temperature in some regions of the south, including the city of Biskra, reaches 55 °C. For this reason, we studied the effect of this degree on the plates when they are exposed to loads.

In this investigation a symmetric laminated beam with four layers subjected to in-plane loading (N_x and N_y) and uniformed temperature T = 55° are considered , we kept the same geometrical and mechanical properties of the previous beams, changing only the fiber orientation, which ranging to $[0°/θ°]_s$. The results obtained numerically and analytically of first-ply failure loads N_x and N_y subjected to uniform temperature are tabulated in Tables 4.25 and 4.26 for two types of loads and various failure cretiria. In addition, both tables show the location of the damage of the FPF.

Table 4. 24: FPF load N_x and damage location of glass/epoxy beams with fiber orientation $[0°/θ°]_s$ subjected to uniform temperature T=55° using different failure criterion

| | N_x | | | | | | |
| | Tsai-We | | Tsai-Hill | | Hachin | | |
	Present element	Analytical	Present element	Analytical	Present element	Analytical	Local damage
$[0°/0°]_s$	2002	2002	2002	2002	2002	2002	All layers
$[0°/15°]_s$	1355	1355	1395	1395.5	1403	1485.5	Layer 1,4
$[0°/30°]_s$	1132.75	1133	1161	1161.5	1167	1190	Layer 1,4
$[0°/45°]_s$	1101.25	1101.5	1101.25	1101.5	1101	1104	Layaer 1,4
$[0°/60°]_s$	1128	1129	1086	1086.5	1080.5	1081	Layaer 1,4
$[0°/75°]_s$	1173.25	1174	1087	1087.5	1079	1081	Layaer 1,4
$[0°/90°]_s$	1197	1197.5	1090	1090.5	1082.5	1083.5	Layaer 1,4

Table 4. 25: FPF load N_y and damage location of glass/epoxy beams with fiber orientation $[0°/θ°]_s$ subjected to uniform temperature T=55° using different failure criterion

| | N_y | | | | | | | | |
| | Tsai-We | | | Tsai-Hill | | | Hachin | | |
	Present element	Analytical	Local damage	Present element	Analytical	Local damage	Present element	Analytical	Local damage
$[0°/0°]_s$	480.25	480.5	All layers	480.25	480.5	Layer 2,3	480.25	480.5	All layers
$[0°/15°]_s$	477.25	477.5	Layer 1,4	479.5	480.25	Laye 2.3	476.5	472	Layer 2,3
$[0°/30°]_s$	497.5	498	Layer 1,4	493	495.5	Laye 2.3	496	484	Laye 2.3
$[0°/45°]_s$	560.75	561	Layer 1,4	534.5	539	Laye 2.3	555	530.5	Laye 2.3
$[0°/60°]_s$	702.5	702	Layer 2,3	632	637	Laye 2.3	701.5	661	Laye 2.3
$[0°/75°]_s$	944	945	Layer 2,3	852	855	Layer 2,3	870	1142	All layers
$[0°/90°]_s$	1197	1197.5	Layer 2,3	1090	1090	Laye 2.3	1083	1083	Laye 2.3

According to Table 4.25, it is clear that under a compressive load N_x and a temperature of 55°C, the failure strength value decreases as the fiber orientation angle increases for the Tsai-We criterion, except for fiber orientations of $[0/60]_s$, $[0/75]_s$, and $[0/90]_s$, where the failure load increases again. The minimum value of FPF is equal to 1101.5 MPa at an angle of 45°. For the Tsai-Hill criterion, the first ply failure strength value decreases with increasing fiber direction angle, except when $\theta=75°$ and $\theta= 90°$, where the FPF value increases again, but slightly. The minimum value of failure strength is equal to 1086.5 MPa at a fiber direction angle of $\theta= 60°$. With the Hashin criterion, the failure strength decreases in all fiber directions except when $\theta=90°$, where the FPF increases slightly again. Furthermore, the maximum FPF strength is observed when the fiber direction angle is $\theta=0°$ for various failure criteria and equal to 2002 MPa , which is also the case when the plate is subjected to in-plane loading only. This indicates that temperature does not affect the failure strength when the fiber orientation is $[0/0]_s$, and this is also observed when a force is applied in the y-direction of the plate (N_y), as shown in Table 4.26. In addition, the first damage location is at layers 1 and 4.

The failure strength N_y and damage location of glass/epoxy beams with fiber orientation $[0°/\theta°]_s$ subjected to a uniform temperature T=55°C using different failure criteria are presented in Table 4.26. These results indicate that the failure strength increases with an increase in the fiber orientation angle for all failure criteria. The highest failure strength values in this case are 1197 MPa, 1090 MPa, and 1083 MPa in the Tsai-We, Tsai-Hill, and Hashin criteria, respectively, when the fiber orientation is $[0°/90°]_s$ for various failure criteria. According to several criteria, the minimum value of strength is between 476.5 and 480 MPa at the fiber angle $[0°/15°]_s$. The damage locations are presented in Table 4.26.

However, the failure loads N_x and N_y are the same ($N_x=N_y$) when the fiber orientation is $[0°/90°]_s$ in both cases, whether the beam is subjected to in-plane load only or with temperature.

4.4.3.4. Symmetric angle ply composite subjected to hugro-thermo-mechanical loading condition

After obtaining the failure strength under in-plane load only and at a temperature of T=55°C, we now present the results of a hygrothermal study aimed at determining the failure strength and demonstrating the effect of these parameters. During the summer in Algeria, particularly in certain regions of the south, such as the city of Biskra, temperatures can reach 55°C with a moisture content of 4%. Therefore, we studied the effect of these conditions on the beams when subjected to loads N_x and N_y by using different failure criteria. The obtained results for various loading conditions (N_x and N_y) and various failure criteria are presented in Tables 4.27 and 4.28.

Table 4. 26: FPF load N_x and damage location of glass/epoxy beams with fiber orientation $[0°/θ°]_s$ subjected to hygrothermal load (T=55°C, C=4%) using different failure criterion

	N_x						
	Tsai-We		Tsai-Hill		Hachin		
	Present element	Analytical	Present element	Analytical	Present element	Analytical	Local damage
$[0°/0°]_s$	2002	2002	2002	2002	2002	2002	All layer
$[0°/15°]_s$	1429.5	1430	1450	1450.5	1453	1493	Layer1,4
$[0°/30°]_s$	1248	1248	1217	1218	1212	1213	Layer1,4
$[0°/45°]_s$	1249	1250	1128	1129	1123	1151	Layer1,4
$[0°/60°]_s$	1314.5	1315	1074	1075	1111	1163	Layer1,4
$[0°/75°]_s$	1398	1399	1043	1044	1168	1197	Layer1,4
$[0°/90°]_s$	1439	1440	1035	1036	1215	1215	All layer

Table 4. 27: FPF load N_y and damage location of glass/epoxy beams with fiber orientation $[0°/θ°]_s$ subjected to hygrothermal load (T=55° C, C=4%) using different failure criterion

	N_y						
	Tsai-We		Tsai-Hill		Hachin		
	Present element	Analytical	Present element	Analytical	Present element	Analytical	Local damage
$[0°/0°]_s$	480.5	481	480.25	480.5	480.25	480.5	All layer
$[0°/15°]_s$	467	468	475	475.5	478	478	Layer1,4
$[0°/30°]_s$	467	467	484	484	490	491.5	Layer1,4
$[0°/45°]_s$	498	500	516	516.5	525	526	Layer1,4

[0°/60°]s	571	571	598	598.5	606	607.5	Layer1,4
[0°/75°]s	807	808	789	816	815	816	Layer2,3
[0°/90°]s	1439	1440	1035	1036	1034	1034.75	Layer2,3

An interesting fact about hygrothermal effects on the failure strength of beams can be observed from Tables 4.27 and 4.28. Table 4.27 presents the FPF load N_x and damage location of glass/epoxy beams with fiber orientation $[0°/θ°]_s$ under a hygrothermal load (T = 55°C, C =4%) using different failure criteria. It is clear from the table that the failure strength of N_x decreases with an increase in fiber orientation. However, when the fiber orientation is $[0°/60°]_s$, the failure strength of N_x increases in both the Tsai-We and Hashin failure criteria. In contrast, the failure strength decreases with increasing fiber orientation in the Tsai-Hill criterion. It is also observed that the first and fourth layers are the ones that experience the first failure, irrespective of changes in the fiber orientation angle, except when it is $[0°/0°]_s$ and $[0°/90°]_s$, where failure occurs in all layers.

Table 4.28 presents the first ply failure (FPF) strength N_y and damage location of glass/epoxy beams with a fiber orientation of $[0°/θ°]_s$ under a hygrothermal load (T=55°C, C=4%) using different failure criteria. It shows the effect of temperature and humidity on the failure strength of N_y, where it is observed that the failure strength decreases as the fiber direction increases. However, when the fiber orientation is $[0°/45°]_s$, the failure strength increases again, and this behavior is observed in various failure criteria. The location of failure changes according to the change in fiber orientation. Additionally, the largest failure strength value of N_y ranges from 1034 MPa to 1440 MPa, depending on the applicable failure, and it is observed when the fiber orientation is $[0°/90°]_s$. The smallest failure value is observed when the fiber orientation is $[0°/15°]_s$, ranging from 467 MPa to 478 MPa.

4.4.3.5. Comparison of the FPF load under different loadings :

The comparison of the FPF strength, calculated using the Tsai-Wu criteria for laminated beams with different fiber orientation angles under mechanical loading N_x and N_y, as well as thermo-mechanical and hygro-thermo-mechanical loading conditions, is shown in Figs 4.16 and 4.17.

Through the Fig. 4.16, it can be seen that the hygro-thermo-mechanical loading is greater than the thermo-mechanical loading, which is again greater than mechanical loading for orientation angles. It can also be noted that when the beams are exposed to a compressive load N_x and a temperature of 55°C (Thermo-mechanical load), the value of the failure strength N_x increases

from 0% to 5% regardless of the change in the fiber orientation and in various failure criteria except when the fiber orientation is equal to $[0°/0°]_s$. In this case, the beam is not affected by temperature and moisture, and the failure strength remains the same no matter how much the temperature increases. The largest failure load value, N_x, is in this orientation.

It can also be observed that when the beams are subjected to a hygro-thermal mechanical load, the value of the failure strength N_x increases from 0% to 27% (Tsai-We criteria) regardless of the change in the fiber orientation. From which conclude that the failure strength of the compressive load N_x is affected by temperature and humidity (a positive effect).
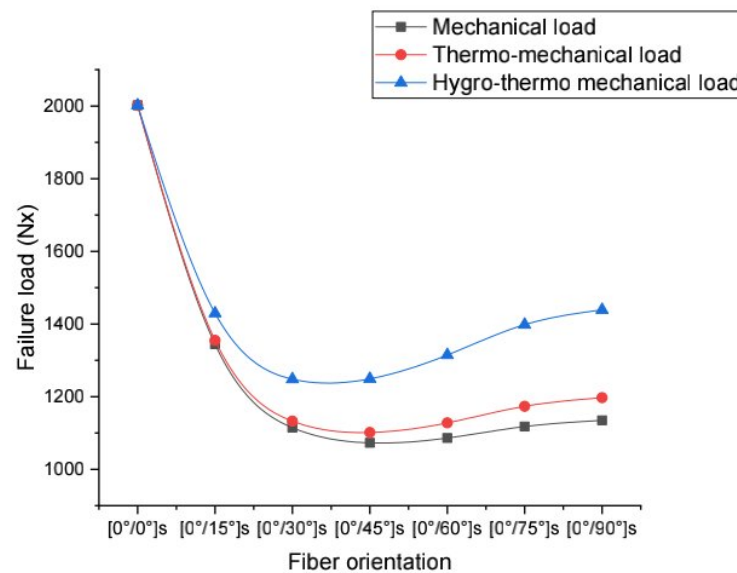
Fig 4. 16: Comparison of the FPF load calculated using Tsai-Wu criteria for laminated beams for different fiber orientation angles under mechanical loading N_x, thermo mechanical loading and Hygro-thermo-mechanical loading
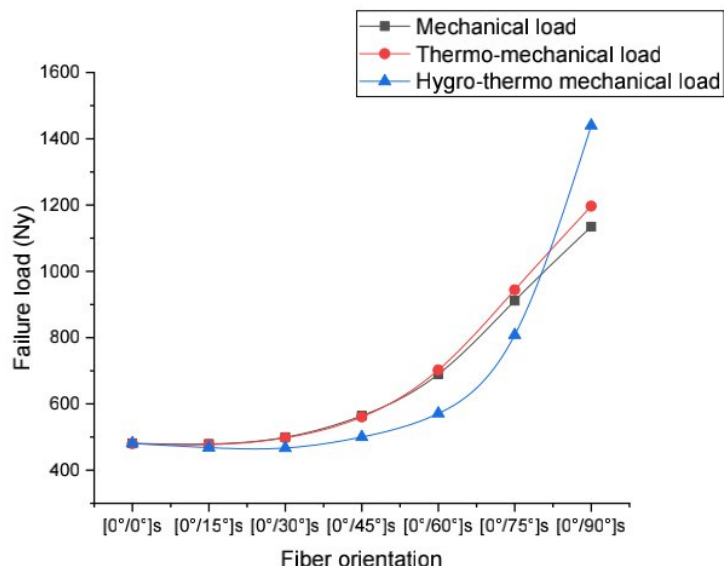
Fig 4. 17: Comparison of the FPF load calculated using Tsai-Wu criteria for laminated beams for different fiber orientation angles under mechanical loading N_y, thermo mechanical loading and Hygro-thermo-mechanical loading

Based on Fig.4.17, it is evident that the hygro-thermo-mechanical loading is lower than both the thermo-mechanical and mechanical loading for various orientation angles, excluding $[0°/90°]_s$ the failure strength of N_y increases when subjected to hygro-thermo-mechanical loading.

It should also be noted that when the beams are under a compressive load N_y and a temperature of 55°C (thermo-mechanical load), the failure load N_y decreases slightly by 0.66% for beams with fiber orientations $[0°/0°]_s$, $[0°/15°]_s$, $[0°/30°]_s$, and $[0°/45°]_s$, and subsequently increases from 1.88% to 5.5% for beams with $[0°/60°]_s$, $[0°/75°]_s$, and $[0°/90°]_s$ fiber orientation angles. Furthermore, under hygro-thermo-mechanical loading, the failure strength of N_y reduces between 0% and 11.4% for various fiber orientation angles except $[0°/90°]_s$. Conversely, for $[0°/90°]_s$ fiber orientation angle, the failure strength of N_y increases by 26.8%.

4.4.3.6. A comparison of several failure criteria based on first-ply failure load

Various failure criteria are compared for a glass/epoxy laminated beam subjected to mechanical load, thermo-mechanical load, and hygro-thermo-mechanical load in two directions (*x* and *y*) based on the FPF load. The first-ply failure load is pridected using three failure criteria: Tsai-We, Tsai-Hill, and Hashin for different fiber orientation angles. The results are plotted and presented in Figs 4.18, 4.19, and 4.20, respectively.

Based on the curves presented in Figs.4.18, 4.19, and 4.20, it can be observed that the beam's behavior remains consistent even when the failure criteria is changed.
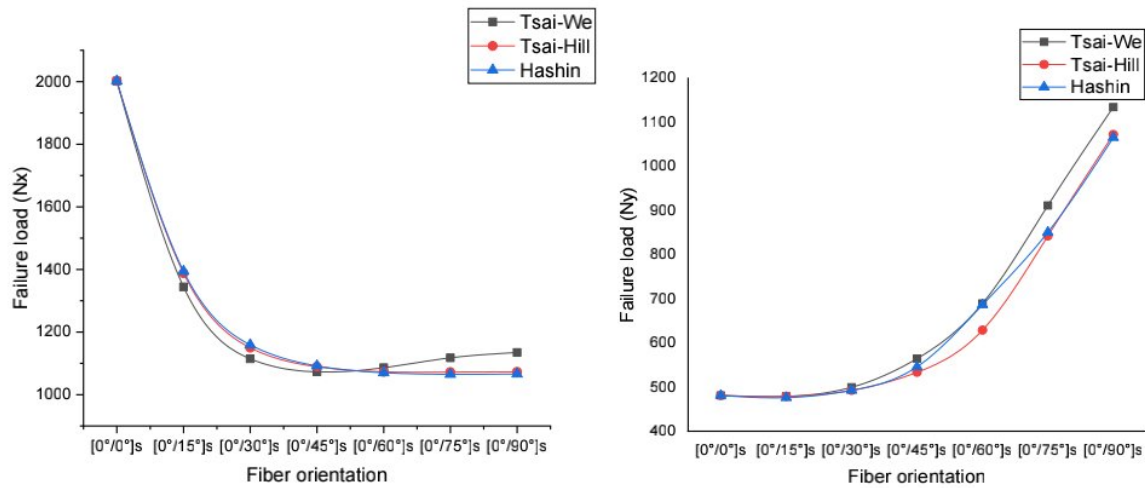
Fig 4. 18: FPF loads (N) of glass/epoxy beams with fiber orientation $[0°/θ°]_s$ subjected to compressive plane normal (N_x, N_y) using different failure criterion
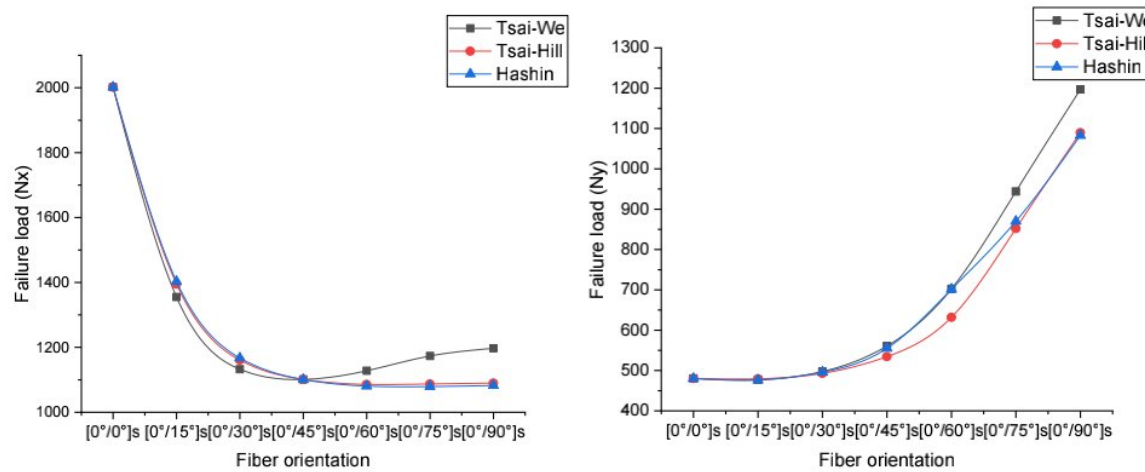
Fig 4. 19: FPF loads (N) of glass/epoxy beams with fiber orientation $[0°/θ°]_s$ subjected to compressive plane normal (N_x, N_y) and temperature T=55°C using different failure criterion
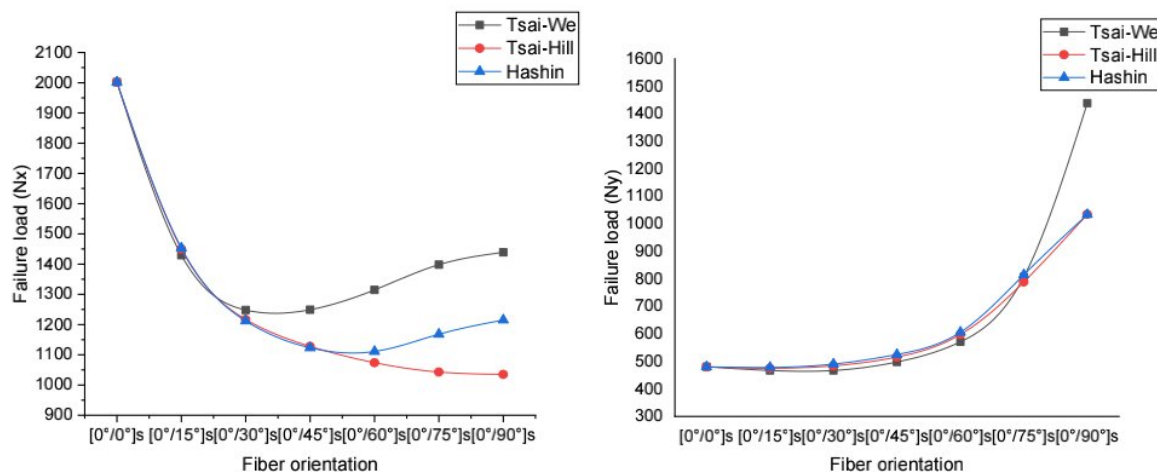
Fig 4. 20: FPF loads (N) of glass/epoxy beams with fiber orientation $[0°/\theta°]_s$ subjected to compressive plane normal (N_x, N_y) and temperature T=55°C and moisture using different failure criterion

4.4.3.7. Failure strength under different environmental conditions:

In order to investigate the effects of the environmental conditions on the failure strengths of different types of loads N_x and N_y (compressive load) for beams with fiber orientation $[0°/75°]_s$, we assume four different environments, each with two seasons: summer and winter.

The FPF load of in-plane loading can be pridected using Tsai-We failure criteria (how the load is affected by environmental conditions). The environmental conditions of each zone are presented in Table 4.29. The FPF load of in-plane loading in two directions (*x* and *y*) obtained by analytical methods for different zones in two seasons: summer and winter, is tabulated in Table 4.30.

Table 4. 28: environmental conditions of each zone

Zone	Summer		Winter	
	T	C	T	C
1	55	0.04	2	0.06
2	30	0.05	-8	0.07
3	37	0.055	-5	0.07
4	42	0.045	0	0.065

Table 4. 29: The first-ply failure strengths N_x and N_y were tested under different environmental conditions during both the summer and the winter.

Zone	N_x		N_y	
	Summer	winter	summer	winter
1	1399	830	808	540
2	1199	371	675	285
3	917	357	562	276
4	1395	585	745	405
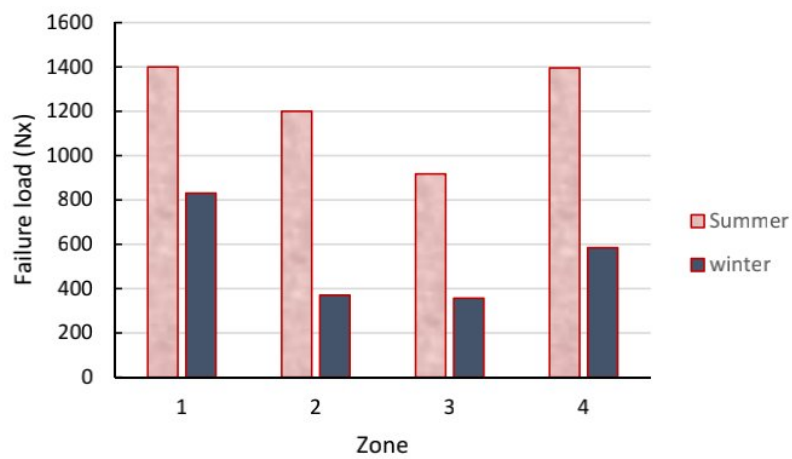
Fig 4. 21: The first-ply failure strengths N_x was tested under different environmental conditions during both the summer and the winter.
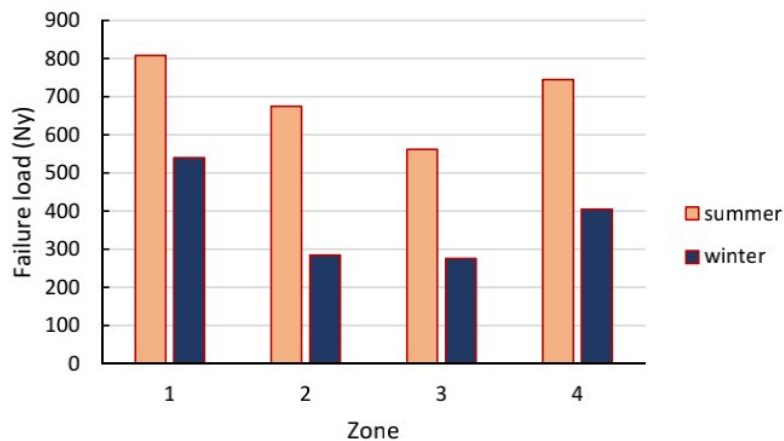
Fig 4. 22: The first-ply failure strengths N_y was tested under different environmental conditions during both the summer and the winter.

Figs 4.21 and 4.22 show the first-ply failure strengths N_x and N_y, which were tested under different environmental conditions (different zones) during both the summer and the winter, respectively. In both cases, it is observed that the FPF load is high during the summer and significantly decreases during the winter. This phenomenon is caused by the higher humidity levels during the winter compared to the summer. This indicates that laminated plates or beams made of glass/epoxy are more affected by moisture than temperature.

4.5. Conclusion

In this study, the first ply failure load (FPF) in a ply laminated composite beam subjected to various types of loading, such as bending loading, in-plane loading, and hygrothermal loading, with various boundary conditions, was investigated. The maximum stress criterion, Tsai-Wu, Tsai-Hill, and Hashin failure criterion are used to pridect the FPF strength and damage location. The numerical and analytical results were obtained. In the first part of this chapter, was the validation of present element. The numerical results obtained by the current element compare favorably with those given by the analytical approach. The numerical results are observed to be very close to the analytical results, showing the accuracy of the current element. Several parameters, such as fiber orientations, stacking sequences, boundary conditions, and the effects of temperature, moisture, and hygrothermal load with different fiber orientations, are considered in order to determine and understand their effects on the strength of these laminated beams. Some broad conclusions may be drawn from the results presented in the previous section.

- The maximum transverse displacement and FPF loads of glass-epoxy laminated beams were compared using various failure criteria, various schemes of loadings, and different boundary conditions. It can be observed that the BC and loading have a remarkable impact on the FPF loads.

- Two different configurations of stacking sequences, $[0°/\theta°]_s$ and $[90°/\theta°]_s$, are considered to know the effect of fiber orientation on FPF load. by using Hashin and Tsai-Wu criterion

- Tsai-Wu criteria are used to investigate the initiation and growth of damage in $[0°/90°]_s$ glass-epoxy laminated beams. The considered beam is clamped from one side and simply supported from the other (CS), and it is subjected to a concentrated load at the mid-span of the beam (Progressive damage analysis) we noticed that the damage starts at the top surface and at the clamped side of the beam.

- The fiber orientation and direction of load (x and y) have a significant impact on the FPF load.

- Temperature and moisture are significantly influenced by the fiber orientation.

- when the angle is 90° the temperature is 783.5 °C, it decreases by approximately 80%. when the direction of the fiber was 15°.

- The hygro-thermo-mechanical loading is greater than the thermo-mechanical loading, which is again greater than mechanical loading for different orientation angles.

- the hygro-thermo-mechanical loading is lower than both the thermo-mechanical and mechanical loading for all orientation angles, excluding $[0°/90°]_s$ the failure strength of N_y increases when subjected to hygro-thermo-mechanical loading.

- When the beam is subjected to a compressive load N_x and a temperature of 55°C, also known as a thermo-mechanical load, the failure strength of the beam increases from 0% to 5%, regardless of changes in fiber orientation and when using different failure criteria except when the fiber orientation is $[0°/0°]_s$.

- When the beams are under a compressive load N_y and a temperature of 55°C (thermo-mechanical load), the failure load N_y decreases slightly by 0.66% for beams with fiber orientations $[0°/0°]_s$, $[0°/15°]_s$, $[0°/30°]_s$, and $[0°/45°]_s$, and subsequently increases from 1.88% to 5.5% for beams with $[0°/60°]_s$, $[0°/75°]_s$, and $[0°/90°]_s$ fiber orientation angles.

- When the beams are subjected to a hygro-thermal mechanical load, the failure strength value N_x of the beams increases by 0% to 27% based on the Tsai-We criteria, regardless of any changes in fiber orientation. This leads to the conclusion that temperature and humidity have a positive effect on the failure strength of the compressive load N_x.

95

- When subjected to hygro-thermo-mechanical loading, the failure strength of N_y decreases between 0% and 11.4% for all fiber orientation angles except for $[0°/90°]_s$. In contrast, for the $[0°/90°]_s$ fiber orientation angle, the failure strength of N_y increases by 26.8%.

Chapter | 5

RESULTS AND DISCUSSION - STRESS

DISTRIBUTION AND FAILURE STRENGTH

OF PERFORATED LAMINATED PLATE

Chapter 5

Results and Discussion - Stress distribution and failure strength of perforated laminated plate

5.1. Introduction :

In this chapter, we have studied the stress distribution around circular holes and determined the failure strength of perforated laminated materials. The chapter is divided into two parts. In the first part, we validated an extended analytical solution by calculating the stress distribution and stress resultants in an infinite plate with an unsymmetrical stacking sequence under arbitrary axial, biaxial, and shear loading at infinity using a general analytical solution (the Greszczuk solution, as mentioned in Chapter 3). The accuracy of the analytical solution is assessed by comparing its findings with the results of finite element models and analytical results obtained using the complex variable approach. This comparison reveals a high level of agreement between these results, demonstrating the validity and accuracy of the present analytical solution. After validation, In the second part of this chapter, we conducted a parametric study on various parameters, such as fiber orientation, stacking sequence, type and load orientation, and hole size. The first-ply failure load (FPF) predicted using the Tsai-Wu failure criterion is also calculated (in order to show the effect of the presence of the circular hole on the FPF loads).

5.2. Results and Discussion:

The main objective of this investigation is to calculate the distribution of stress concentration and the distributions of the forces around a circular hole in unsymmetric, laminated composite plates under an arbitrarily oriented load. Various examples have been studied and compared with some numerical and analytic solutions for accuracy. Therefore, many computer programs have been developed to obtain distributions of stress concentration and stress results around a circular hole. Table 5.1 shows the mechanical characteristics of the various materials employed in this investigation.

Table 5. 1: Material properties of used material

Materials	E_1(Gpa)	E_2 (Gpa)	G_{12} (Gpa)	υ_{12}
Graphit /Epoxy	181	10.3	7.17	0.28
graphite/Bis-Maleimides (BMI)	124	8.46	4.59	0.28
CGYF 70	294	6.4	4.9	0.23

5.2.1. Validation of the analytical results:

In the calculation, a computer program was created to investigate the stress distributions in laminated plates containing circular cutouts using the stress functions given by Eq. (3.55). In this section, several cases of loads $N_y^\infty = 1$, $N_x^\infty = N_y^\infty = 1$, $N_{xy}^\infty = 1$ at infinity are studied by the present analytical solution. To validate the precision of the current solution using the available analytical approach, the results obtained by the current solution are compared with those found by the numerical study (FEM).

The stress and force distribution at edge of a circular cutout in Graphite/Epoxy [0/30/45/90] under different in-plane loading conditions ($N_y^\infty = 1, N_x^\infty = N_y^\infty = 1, N_{xy}^\infty = 1$). The results are shown in Figs 5.1, 5.2, and 5.3

From the curves shown in Fig 5.1, it can be seen that for the plate under uniaxial load, $N_y^\infty = 1$, the stress concentration value is around 3 at 0° and 180° and its value decreases to -1 at 90°. N_x , N_y, and N_{xy} have maximum positive values around 0.6, 3, and 0.8, respectively. In one hand, the greatest negative values of N_x, N_y, and N_{xy} are 1.2, 0.1, and 0.8, respectively.

As for the plate under the biaxial load ($N_x^\infty = N_y^\infty = 1$), the largest value of stress concentration is 2.1 at 0°, 90°, and 180°. The highest values of stress concentration, Nx, and Ny for the plate under biaxial load ($N_x^\infty = N_y^\infty = 1$) are 2.1 at 0°, 90°, and 180 for stress concentration, 90° for Nx, and 0°, 180° for Ny, as shown in Fig 5.2.

On the other hand, the SCF and the stress resultant distribution around a circular opening in a plate under shear load ($N_{xy}^\infty = 1$) are studied and plotted in Fig 5.3

It can be observed that the value of stress concentration is greater when applying shear force and reaches 4 at 135°, whereas its value is 0 at 0° and negative between 0° and 90°.

From the curves shown below, it can be noted that the present solution is utterly identical to the results obtained by FEM, regardless of the nature of the applied force, which indicates the correctness of the current solution.
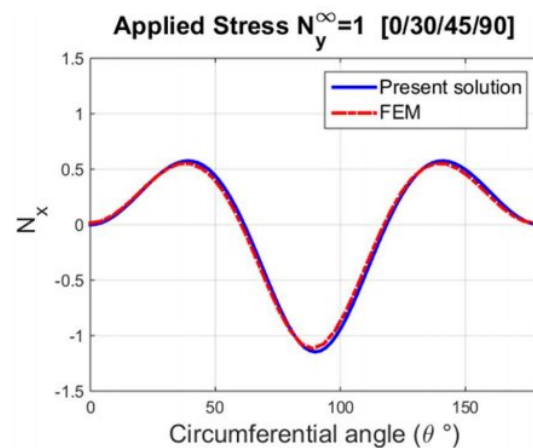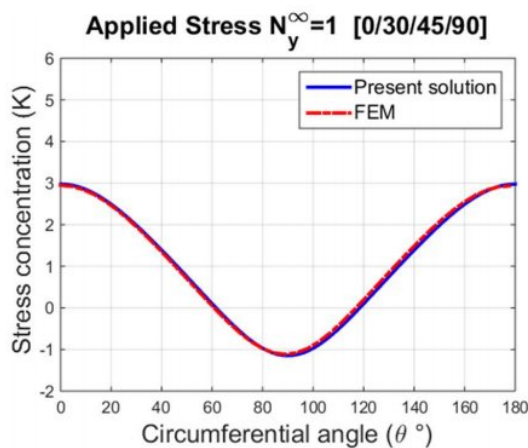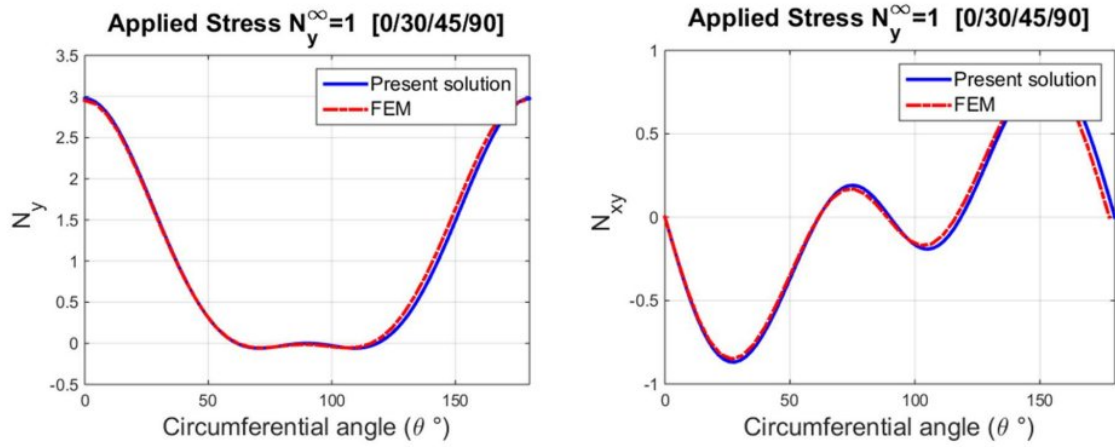
Fig 5. 1: Stress concentration and stress resultants N_x, N_y and N_{xy} obtained by the present solution and the FEM in Graphite Epoxy plates under uniaxial loading $N_y^\infty = 1$.
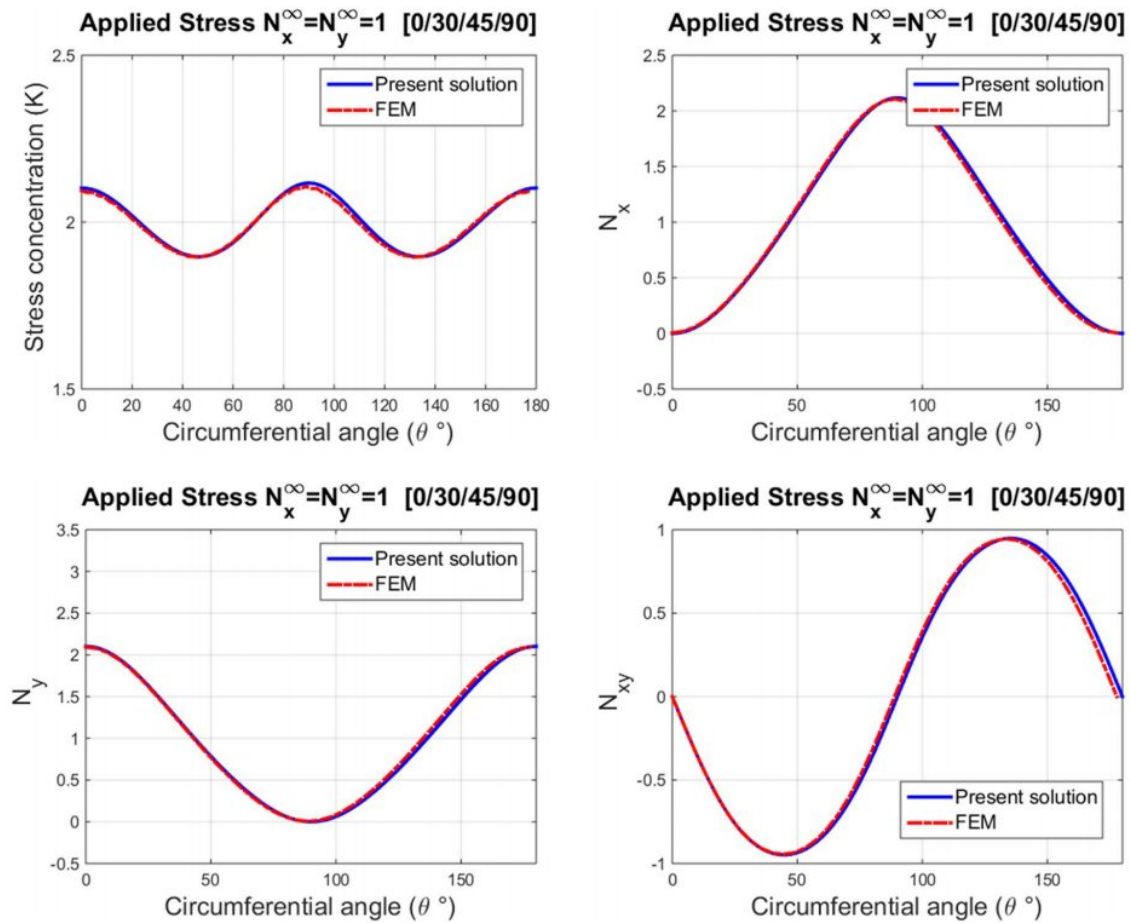
Fig 5. 2: Stress concentration and stress resultants N_x, N_y and N_{xy} obtained by the present solution and the FEM in graphite/epoxy plates under biaxial loading $N_x^\infty = N_y^\infty = 1$
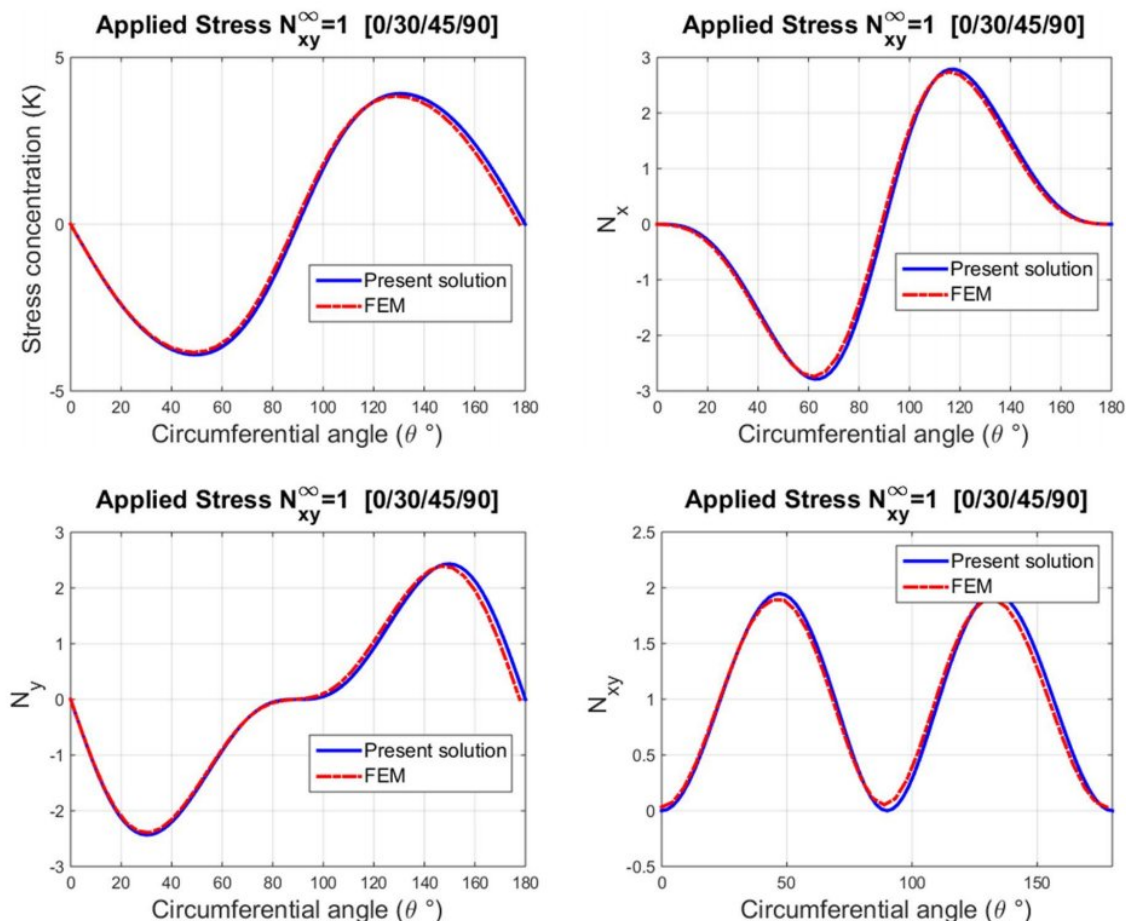
Fig 5. 3: Stress concentration and stress resultants N_x, N_y and N_{xy} obtained by the present solution and the FEM in graphite/epoxy plates under shear loading $N_{xy}^{\infty} = 1$

5.2.2. Parametric study:

After establishing the validity and accuracy of the current analytical solution by contrasting the current results with results obtained by FEM, this section considers a number of tests in order to understand the effect of stacking sequence, load angle, and hole size of different unsymmetrical plates on stress concentration, stress resultants and failure load for different materials.

5.2.2.1 [0 / 90] *Laminated plate :*

In the first example, a graphite /epoxy laminated plate [0 / 90] under uniaxial loading at infinity, $N_y^{\infty} = 1$, was employed to calculate the stress concentration around a circular hole. Fig 5.4

shows the distributions of stress concentration and the stress resultants (N_x, N_y and N_{xy}) on the boundary of the hole. The elastic mechanical characteristics listed in Table 5.1.
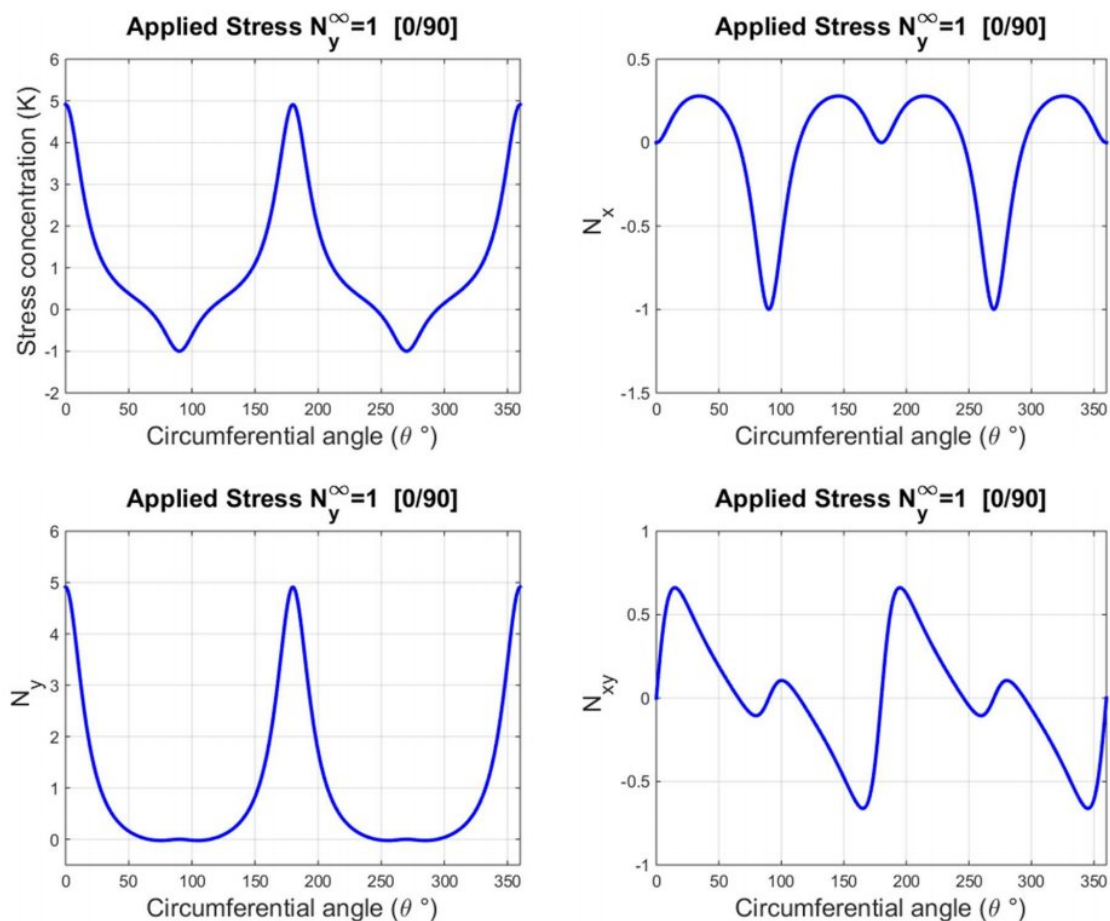
Fig 5. 4: Stress concentration and stress resultants (N_x, N_y and N_{xy}) around circular hole in uniaxial loading at infinity in graphite/epoxy plate [0 / 90]

The distributions of the stress concentration and N_x, N_y, and N_{xy} are symmetric regarding both principal directions x and y. The maximum stress concentration value found with the current solution is 4.91 at 0°, 180°, and 360°. The same results were found by Sharma et al. [82] and Khechai et al. [73].

It should also be noted that the compressive zone is located at 90° and 270°, and the minimum negative value of SCF is equal to 1. The maximum absolute values of N_x, N_y, and N_{xy} are around 1, 4.9 and 0.6, respectively, where the locations of these values are shown in Fig 5.4.

5.2.2.2. $[45/-45]$ *balanced laminated plate:*

The second example is a graphite/BMI laminated plates under equal biaxial loading, $N_x^\infty = N_y^\infty = 1$ were employed. The thickness of each layer is 0.125 mm. The mechanical characteristics of the laminated plate are listed in Table 5.1. The distributions of stresses and the membrane forces around the opening (circular hole) for angle ply $[45/-45]$ are shown in Fig 5.5.
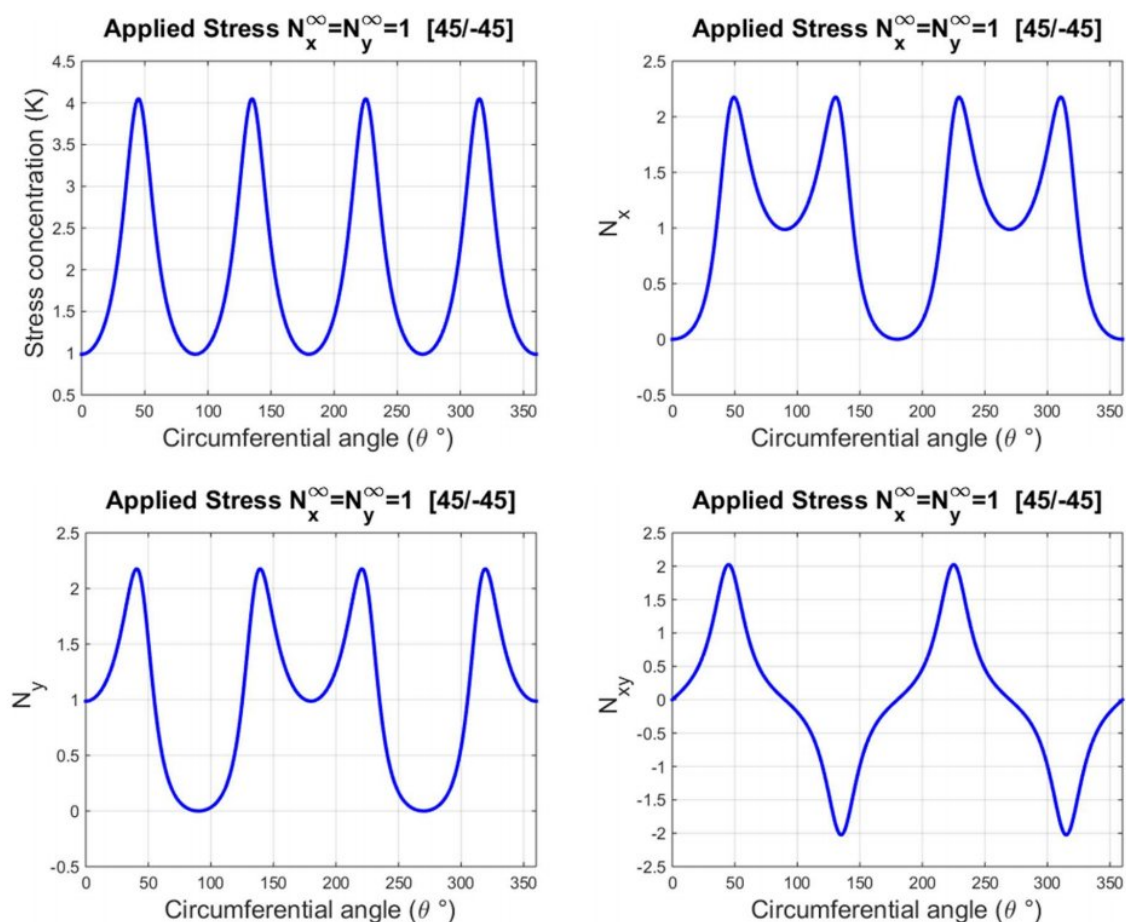
Fig 5. 5: Stress concentration and forces (N_x, N_y and N_{xy}) around a circular hole in biaxial loading at infinity in Graphite /epoxy $[45/-45]$

According to Fig 5.5, the distributions of N_x, N_y and N_{xy} are symmetric about the *x* and *y* axes. The largest stress concentration value for biaxial loading at infinity graphite/epoxy $[45/-45]$ is equal to 4 and is located at 45°, 135°, 225°, and 315°. It is also to be noted that, the greatest values of N_x, N_y and N_{xy} are 2.18, 2.18, and 2.033, respectively, and their positions

are illustrated in Fig 5.5. Almost the same results were found by Chen et al. [102] and Dave et al. [105] .

5.2.2.3. $[0/90/45/-45]$ Laminated plate:

In this example, a remote stress $N_y^\infty = 1$ is applied to the Graphite/BMI laminated plates $[0/90/45/-45]$ with a circular hole. The radius of the cutout is 10 mm. the distributions of the stress concentration and stress resultant around the circular opening are shown in Fig 5.6.
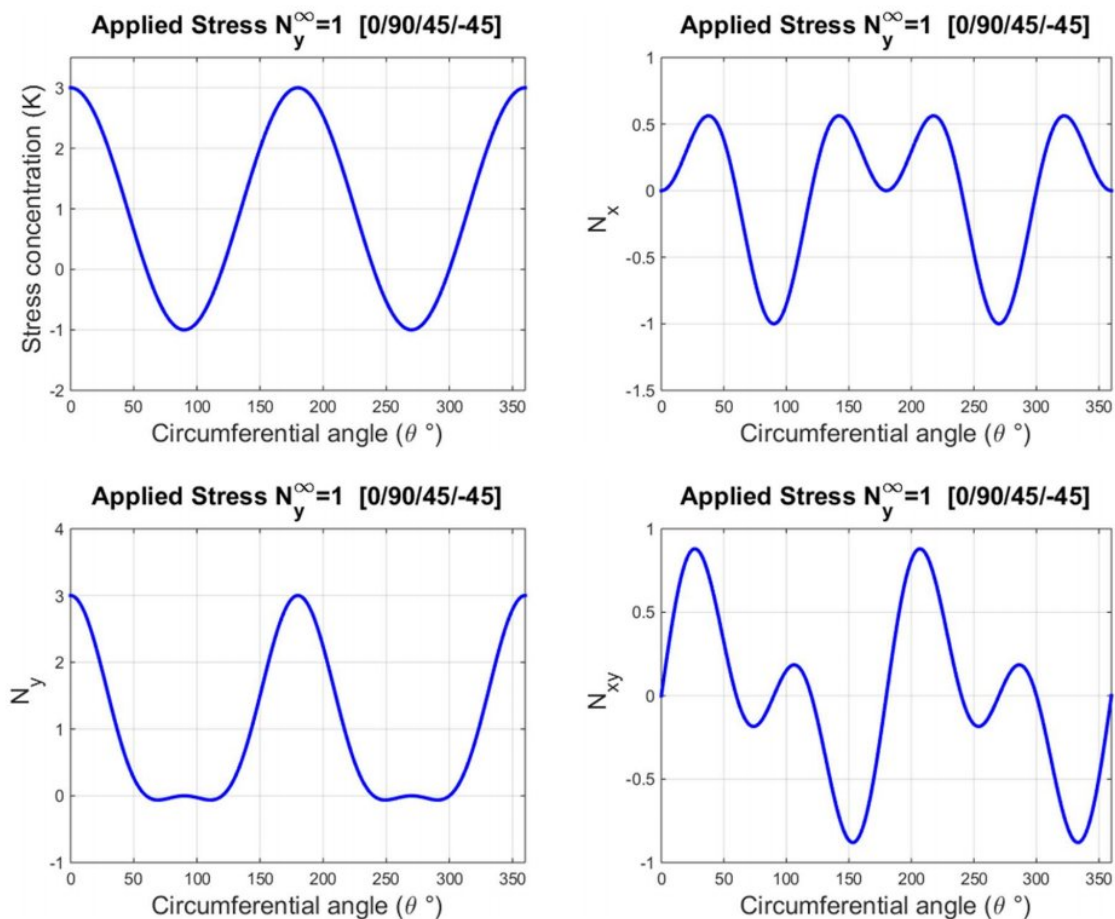
Fig 5. 6: Stress concentration and forces (N_x, N_y and N_{xy}) around a circular hole in uniaxial loading at infinity in graphite /epoxy $[0/90/45/-45]$

The maximum SCF produced is 3 at 0°, 175°, and 360° and decreases until it reaches -1 at 90° and 260° as shown in Fig 5.6. On the other hand, for stress resultants, the greatest values of N_x, N_y, and N_{xy} are 0.5, 3, and 0.8, respectively, and their locations are illustrated in Fig 5.6.

5.2.2.4. Stress and failure load distributions:

One of the main aims for determining the SCF at the boundary of the opening is to predict the plate's failure load. This last was implemented along the hole's edge since free-edge effects are more likely to trigger the failure [73, 86, 118]. The Tsai-Wu failure criteria [119] is employed to calculate the strength of the laminated plate with a circular hole.

The stress distributions and failure strengths for different fiber orientation and load orientation angles in infinite graphite/epoxy plates with a circular cutout under various types of in-plane loading are illustrated in Figs 5.7 and 5.8, respectively. The load angles and the fiber orientation range from 0° to 90° degrees. On the other hand, the distribution of minimum failure load and maximum stress of developed in laminated plates fabricated by other material CGYF 70 that contains a circular hole with various hole sizes and fiber orientations is illustrated in Figs 5.9 and 5.10. The mechanical properties of this material are presented in table 5.1. The fiber angles and opening diameter-to-width ratios are between 0° and 90° and 0.05 and 0.4, respectively. The results for different loading conditions are shown. These distributions will assist designers in determining the optimum stress or strength positions and ideal fiber orientation or load angles.

The strength properties of this material are as follows:

$X_t = 598$, $Y_t = 29.4$, $X_c = 491$, $Y_c = 98.1$, $S = 49.1$

(a)

(b)

(c)

(d)
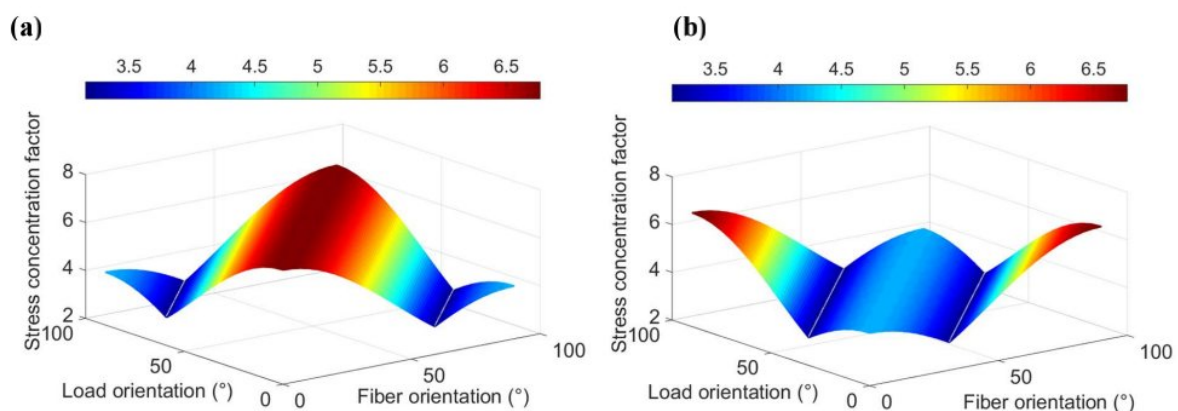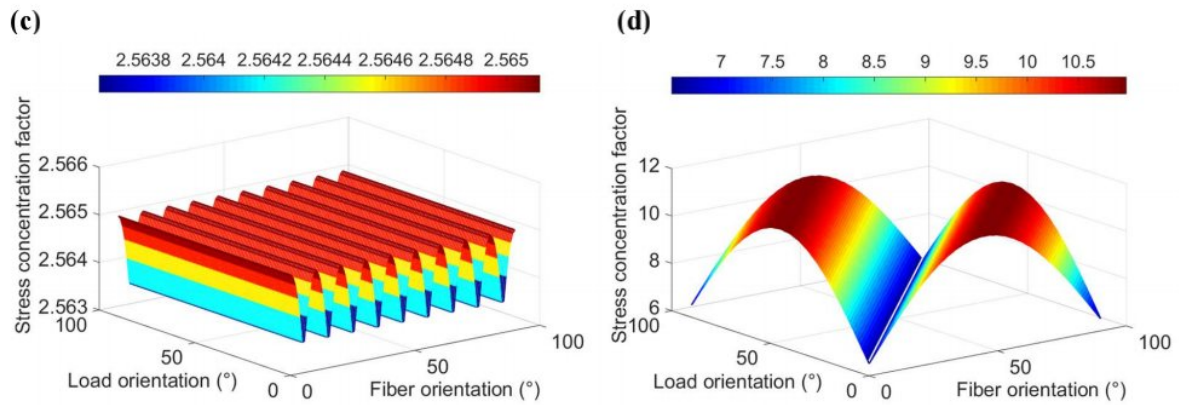
Fig 5. 7: The stress distributions of graphite/epoxy plates for various fiber orientations and load orientation angles with different in plane loading (a): N_x, (b) : N_y, (c) : $N_x = N_y$, and (d) : N_{xy}.

(a)

(b)

(c)

(d)
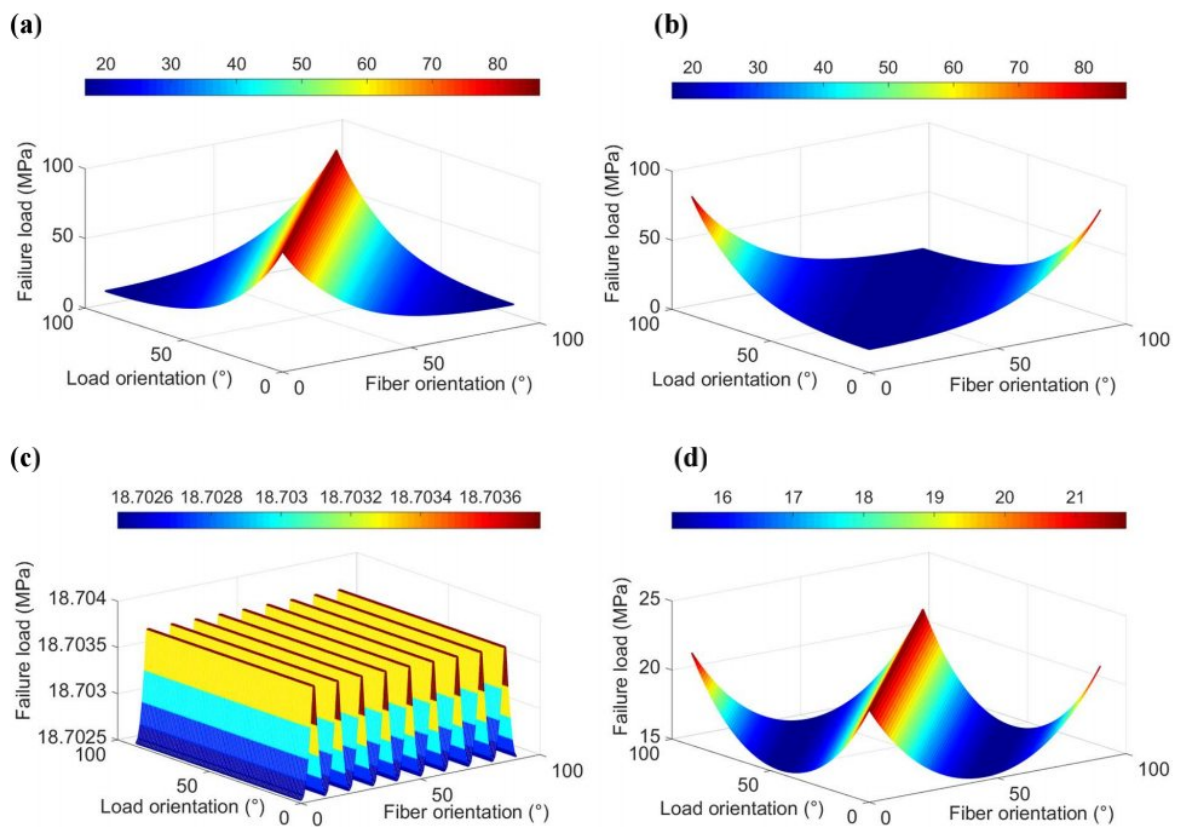
Fig 5. 8: The failure load distribution of graphite/epoxy plates for various fiber orientations and load orientation angles under different in-plane loading (a) : N_x, (b) : N_y, (c) : $N_x = N_y$, and (d) : N_{xy}.

One cans see from the above figures that the minimum stress concentration values for graphite/epoxy plates subjected to uniaxial (x and y), N_x, N_y, equibiaxial, $N_x = N_y$, and shear

106

, N_{xy}, loading are around 6.2, 6.2, 2.563, and 10.5 and the ideal values of the failure load are approximately 90, 90, 18.7036, and 22 MPa, respectively. Under equibiaxial stress, several fiber orientation /load orientation angle combinations offer the best plate positions.
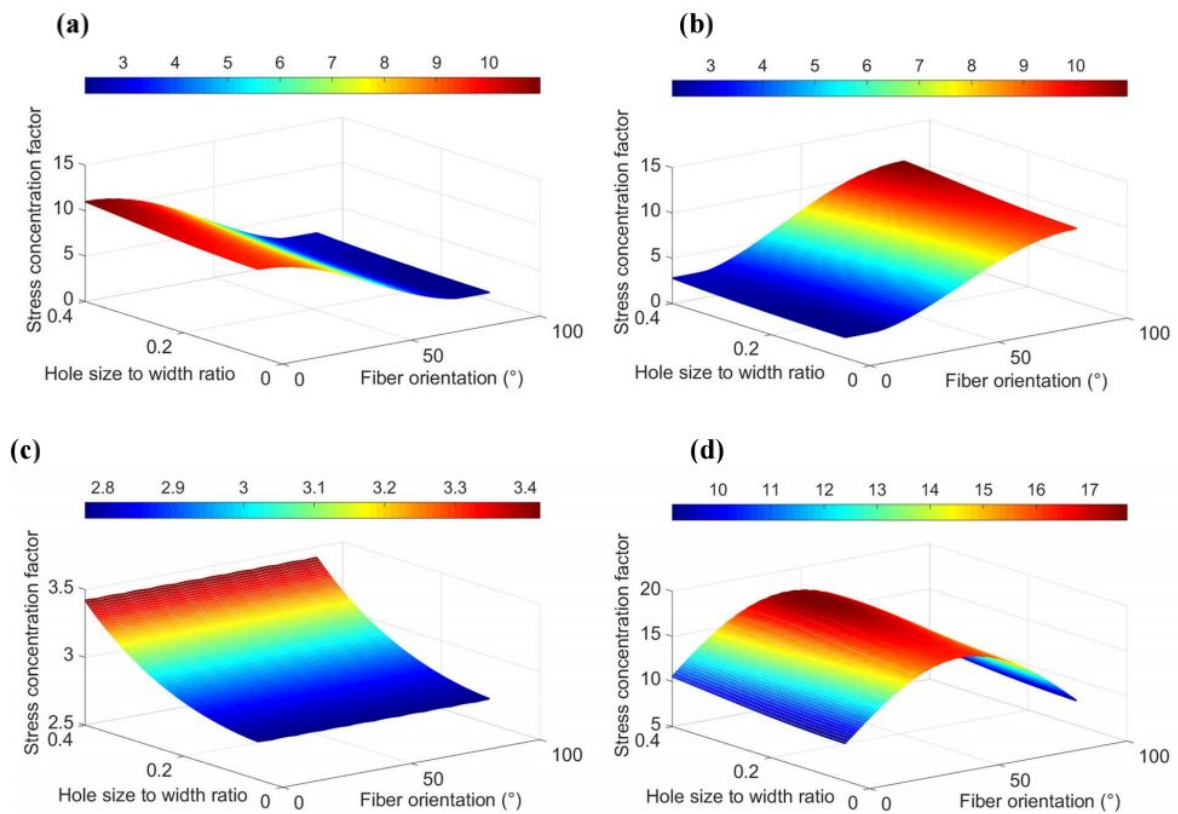
Fig 5. 9: The stress concentration factor distribution in CGYF 70 plates under various in-plane loading conditions (a) : N_x , (b) : N_y , (c) : $N_x = N_y$, and (d) : N_{xy} . ., with various fiber orientation angles and hole sizes to width ratios.
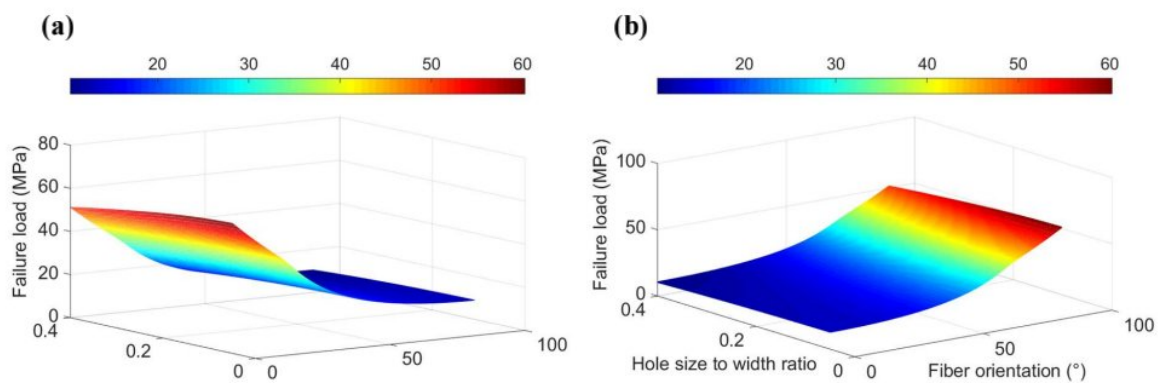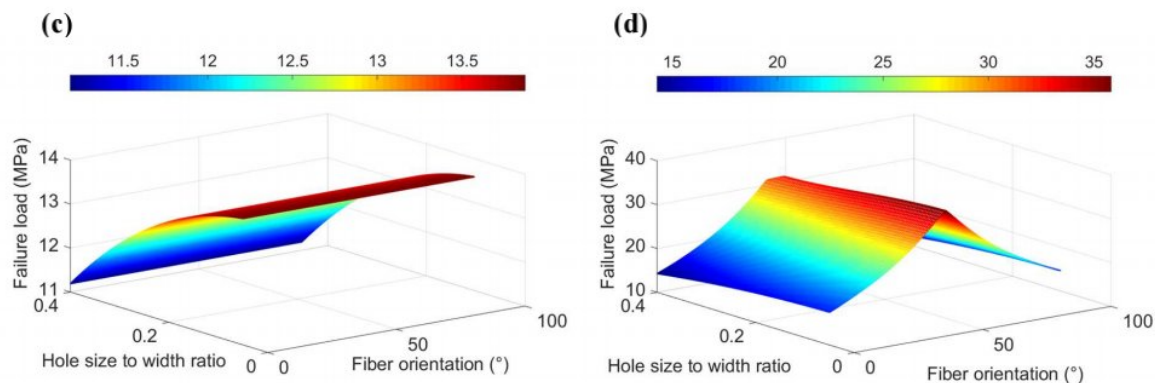
Fig 5. 10: Failure load distribution in CGYF 70 material plates for various fiber orientation angles and hole size to width ratios under different in-plane loading conditions (a): N_x, (b): N_y, (c): $N_x = N_y$ and (d): N_{xy}.

Figs 5.9 and 5.10 illustrate the distribution of maximum stress concentration factor and minimum failure load for various fiber orientation and hole sizes in CGYF 70 material plates with circular holes. Through these figures, it can be noted that the value of the maximum SCF increases and the value of the failure strength decreases with the increase in the hole's size. Several experimental studies [120-122] validate these findings.

For plates subjected to N_x, N_y and N_{xy} loadings, the optimal stress are almost around fiber orientation θ equals 0°, 90°, and (0° or 90°), respectively. The minimum values of SCF for CGYF 70 material plates under N_x, N_y, $N_x = N_y$, and N_{xy} loading conditions are about 2.50, 2.50, 2.6, and 11 respectively.

As for optimum failure load for plates under N_x, N_y and N_{xy}, they are almost around fiber orientation θ equals to 0°, 90°, and 45°, respectively. The optimum strength values for plates under to N_x, N_y, $N_x = N_y$, and N_{xy} loading conditions are roughly 50, 50, 13.5, and 35 MPa, respectively.

On the other hand, the maximum stress concentration values for plates subjected to biaxial loading, $N_x = N_y$, and with a specific hole size remain constant for all fiber orientation angles. The minimum failure load exhibits the same behavior. This shows that the stress concentration and failure strength under biaxial loading are unaffected by the fiber orientation angle.

5.2.2.5. Effect of stacking sequence and type of load on SCF:

In the second part of the present study, the behavior of a transverse isotropic plate and infinite unsymmetrical graphite/epoxy plates with various fiber orientations and a number of layers, including a circular hole, subjected to different loading conditions at infinity was studied. The stress distribution changes depending on location (the angle a ranges from 0° to 180°), as illustrated graphically in Figs 5.11, 5.12, 5.13 and 5.14 For each plate, the varying parameters such as the stacking sequence $[0]$, $[90]$, $[0/90]$, $[0_4/\pm45]$, $[90_4/\pm45]$ and $[0_2/\pm45/90_2]$ or the applied load $N_x^\infty = 1$, $N_y^\infty = 1$, $N_x^\infty = N_y^\infty = 1$ and $N_{xy}^\infty = 1$ are considered.

From Fig 5.11, it is evident that the maximum stress concentration values are around 6 when the plate has an $[0]$ orientation at the critical circumferential angle of 90°, and the value of the SCF decreases until it reaches 2 when the plates are $[90]$ and $[90_4/\pm45]$ at 90° as well. The minimum SCF is 0 at 0° for plate has fiber orientation $[0]$. On another hand, as observed when plate subjected to tension in direction y (see Fig 5.12), the maximum stress is 6.9 found at 0° and 180° for plate $[90]$, and the smaller value is 2.2 at 0° and 180° for plates has a $[0]$ orientation and $[0_4/\pm45]$ as for N_x the maximum positive value is approximately equal to 1 and the maximum negative value is 4.3 at 90° when the plate has $[0]$ orientation , and it decreases as the laminated changes until it is null when the plates $[90]$ and $[90_4/\pm45]$ at 90°. On the contrary to N_y the biggest value of SCF when the plate $[90]$ at 0° and then decrease until completely nil at 90°. For the rest of the plate, it has the same behavior.

The cross ply $[0/90]$ laminated plates has the highest values of SCF that is equal to 3.9 at 0°, 90°, and 180°. As shown in Fig 5.13, when the plate is subjected to an equibiaxial load $N_x^\infty = N_y^\infty = 1$ it has the same value for N_x and N_y. For N_x, it is at 90°, and for N_y, it is at 0° and 180°. As for the shear strength, the largest value in absolute value is 1.
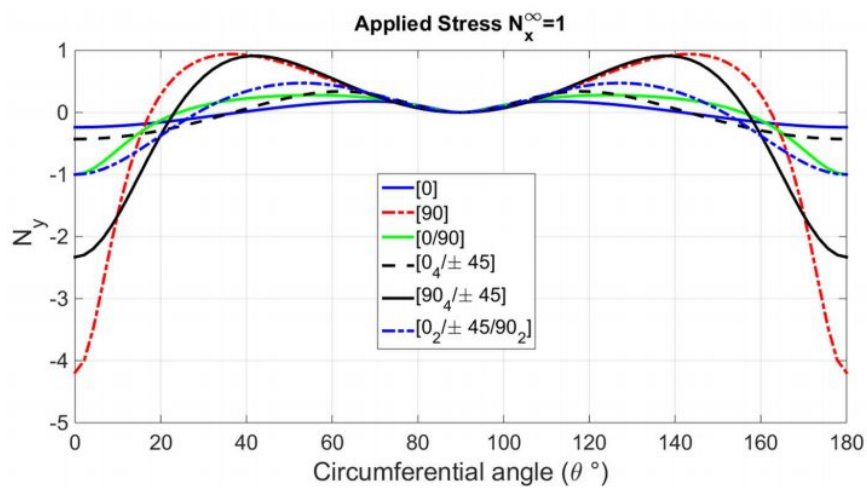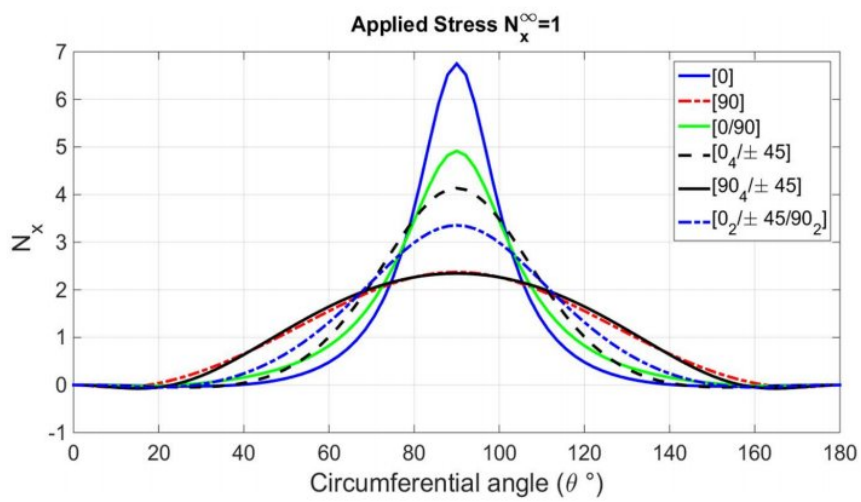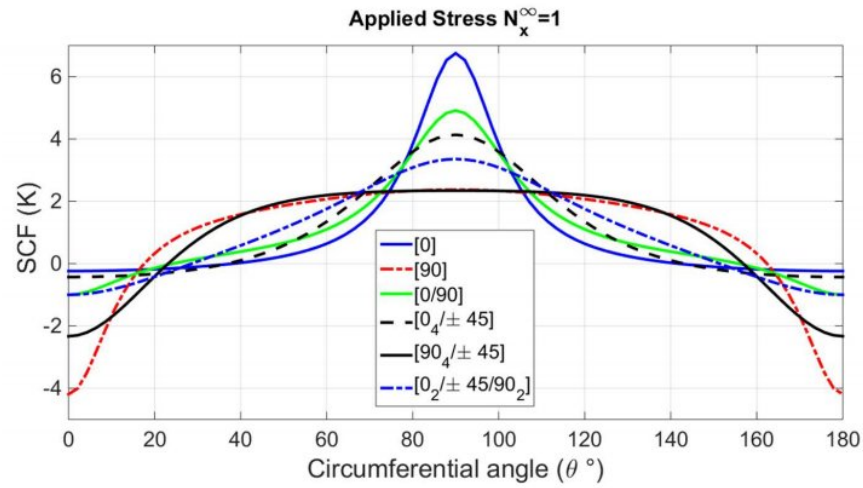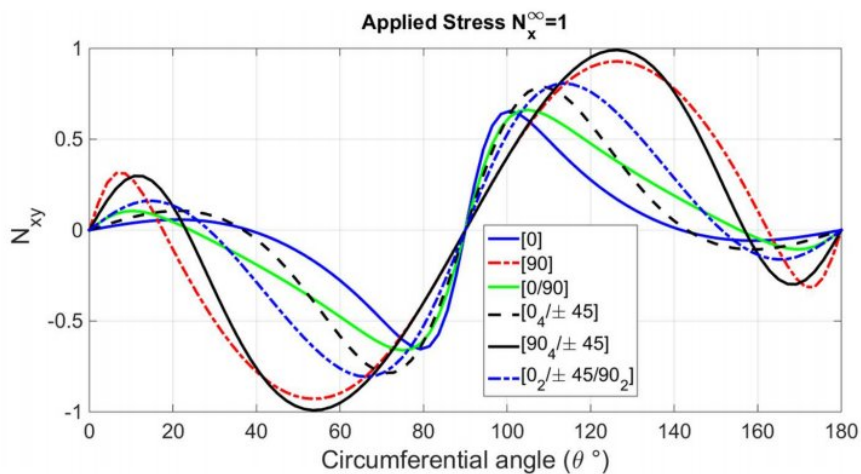
Fig 5. 11: Distributions of SCF and stress resultants (N_x, N_y and N_{xy}) around a circular holes subjected to uniaxial load (x direction)
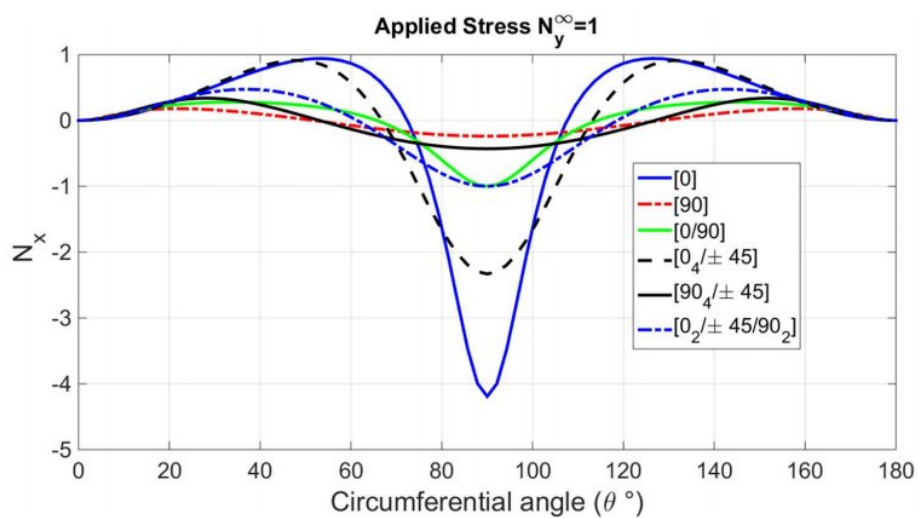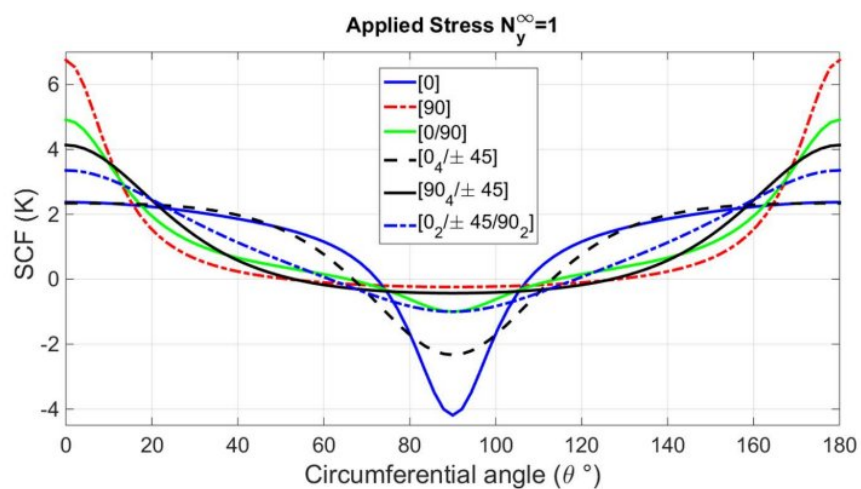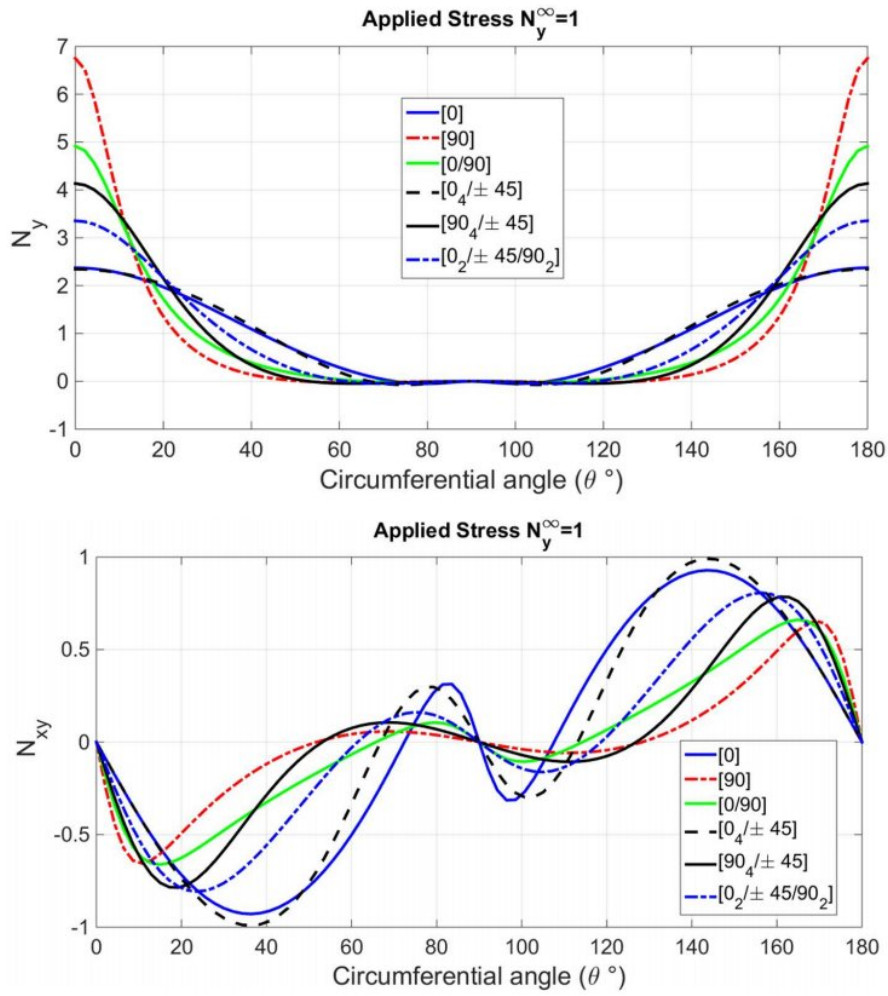
Fig 5. 12: Distributions of SCF and stress resultants (N_x, N_y and N_{xy}) around a circular holes subjected to uniaxial load (y direction)
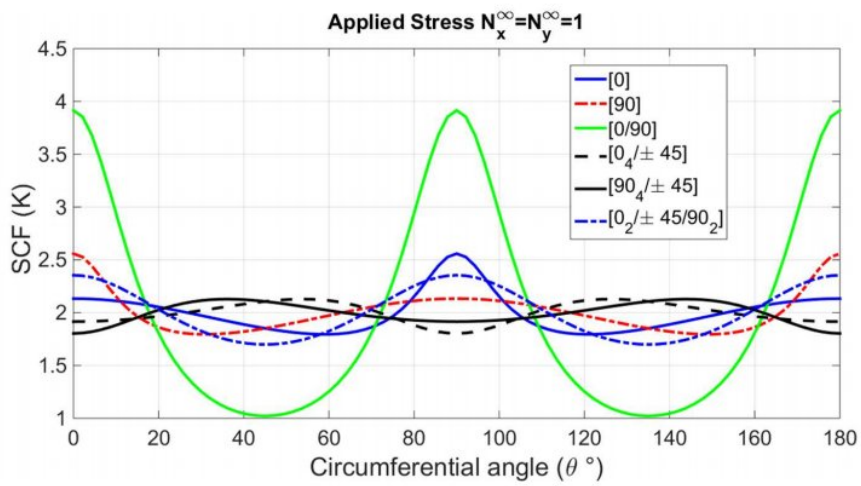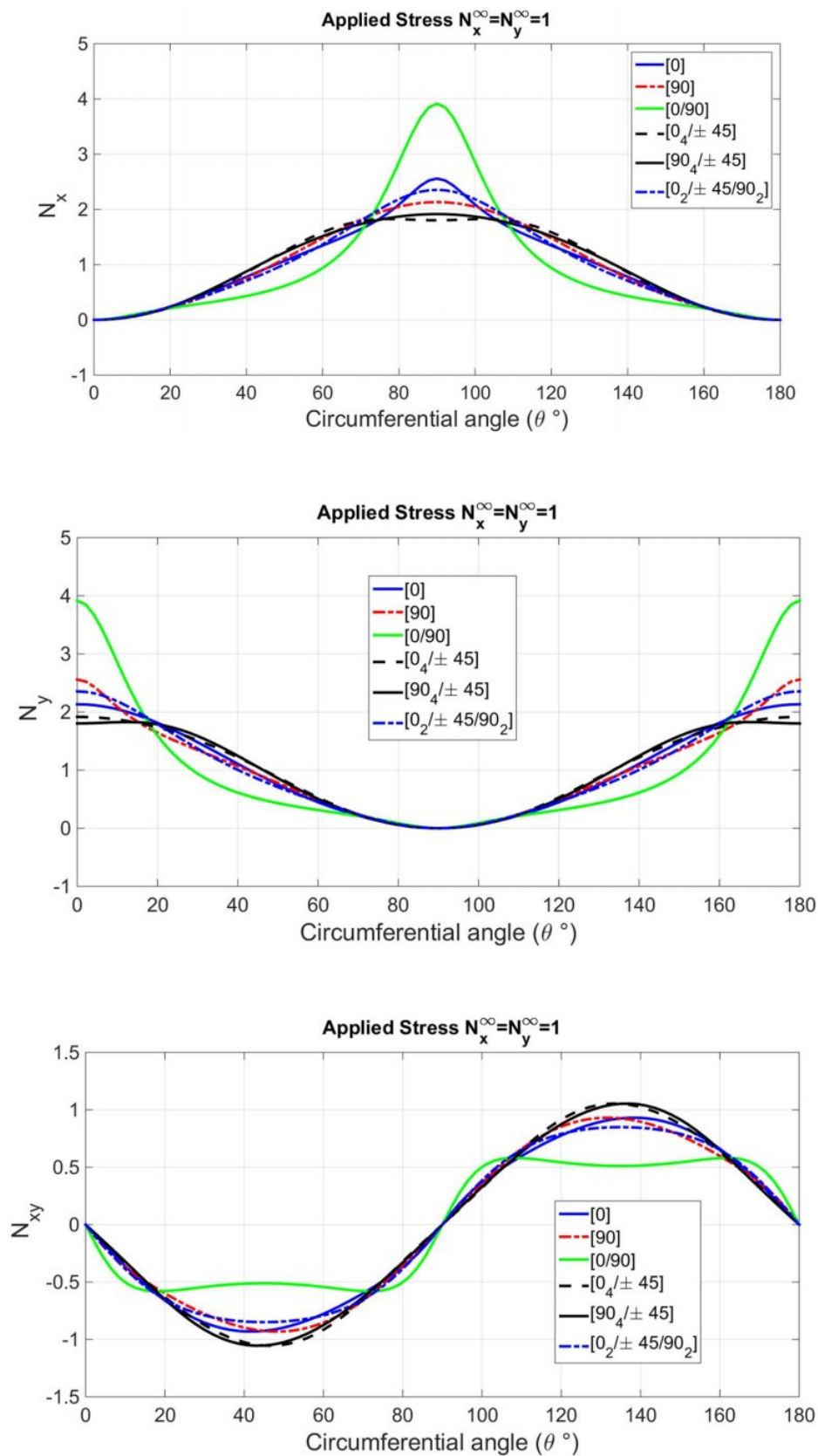
Fig 5. 13: Distributions of SCF and stress resultants (N_x, N_y and N_{xy}) around a circular holes subjected to biaxial load

Applied Stress $N_{xy}^{\infty}=1$

Legend:
- [0]
- [90]
- [0/90]
- $[0_4/\pm 45]$
- $[90_4/\pm 45]$
- $[0_2/\pm 45/90_2]$
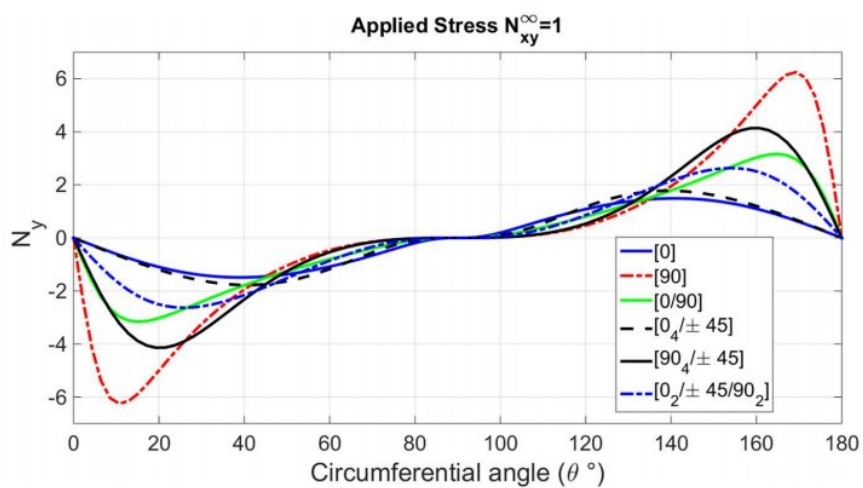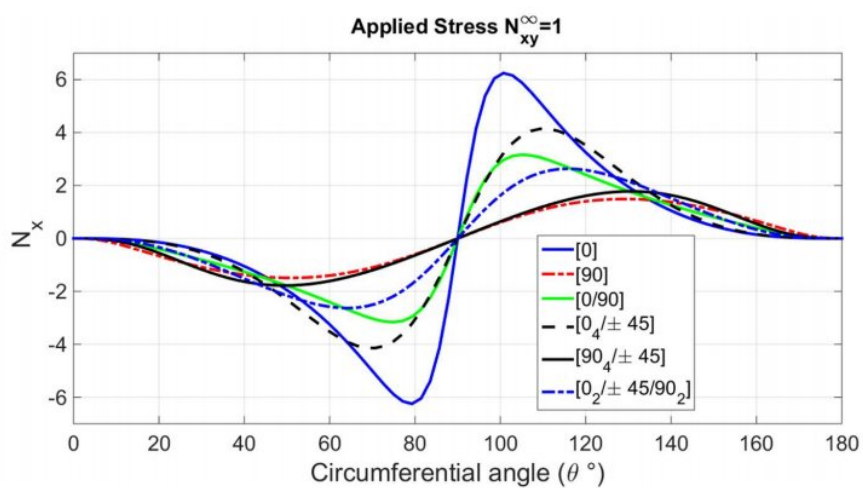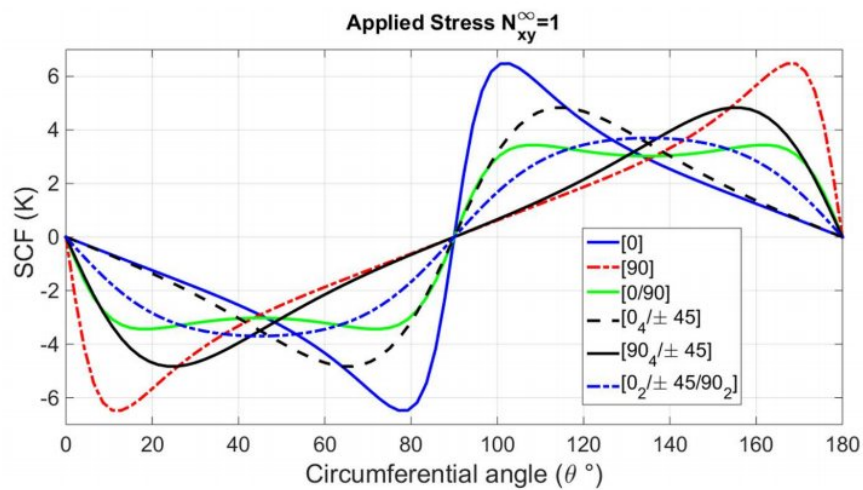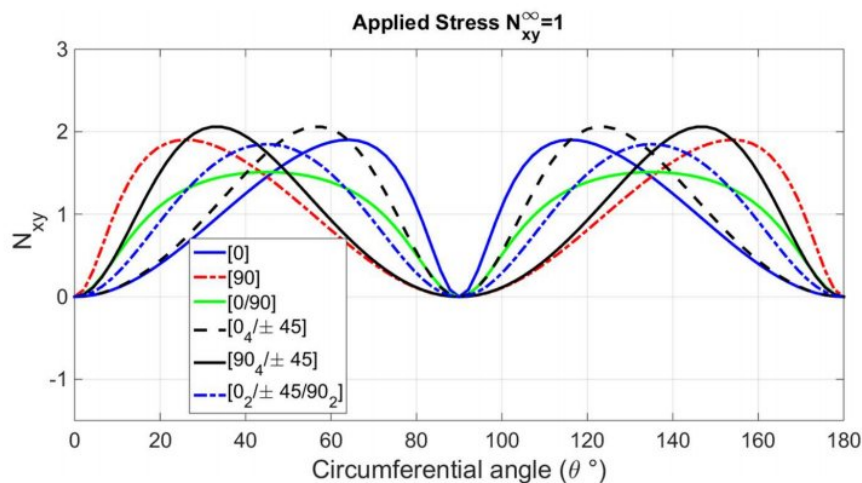
Fig 5. 14: Distribution of SCF and stress resultants (N_x, N_y and N_{xy}) around a circular holes subjected to shear load

For a plate subjected to shear load at infinity $N_{xy}^{\infty} = 1$, the distributions of the stress and stress resultant are plotted in Fig 5.14 using various laminated and stacking sequences. It can be observed that the maximum SCF is equal to 6,2 when the plate has orientations of [0] and [90] , and their locations are shown in the curves.

5.2.3. Conclusion :

In the current sudy, a precise and simple analytical solution has been developed and applied to determine the stress concentration factor (SCF), that occurs in an infinite plate containing a circular cutout with unsymmetrical stacking sequence when loaded with arbitrary in-plane loading at infinity (uniaxial, biaxial, and shear). The current solution was extended based on Greszczuk's solution. The effects of several parameters, including the type of loads, unsymmetrical stacking sequence, number of layers, hole's size, and load angle orientation, on the stress distribution around the opening are considered when discussing typical results obtained using the current solution. On the other hand, the same previous parameters were considered to predict the failure load.

The results of the current solution were successfully compared with results obtained by FEM and some analytical results obtained using the complex variable approach in order to validate the correctness of the solution.

In contrast hand, the following are some important results from this study: for a circular hole

- The location and value of SCF around the circular cutout (along the edge of the hole) are dependent on stacking sequence and fiber orientation for the given material and loading conditions.

- The material characteristics and the loading angle have a significant impact on the stress concentration factor and its location.

- The type of loading has a significant impact on the SCF.

- The value of the failure load changes with the type and direction of the load applied, and it also changes with the change in fiber orientation of the plate and is affected also by hole's size.

Chapter

6

GENERAL CONCLUSION AND SUMMARY

Chapter 6

General Conclusions and Summary

The determination of failure strength and stress concentration in composite laminates under different loading conditions such as bending, arbitrary in-plane loading, and hygrothermal loading (temperature and humidity) is one of the key challenges faced by researchers during the design of structures. Various numerical and analytical methods are used, along with different failure criteria, to address this challenge.

This work focuses on two main objectives : The first objective is to calculate the failure load of laminated composite plates and beams subjected to different loading conditions such as static bending load, in-plane load, and hygrothermal loading in order to determine their failure mechanisms and the first ply failure (FPF) load. To achieve this, a refined rectangular plate element based on classical lamination theory (CLT) is used to calculate in-plane stresses, and several failure criteria, including Tsai-Wu, Tsai-Hill, Hashin, and Maximum Stress criteria, are applied to predict failure mechanisms. These criteria are integrated within the finite element code to predict the different failure damages and responses of laminated beams from initial loading to final failure. The numerical results obtained using the present element are in good agreement with the analytical approaches, demonstrating the accuracy of the present element. The varying parameters such type of load, boundary condition, fiber orientation, stacking sequences, effect of temperature, moisture, and effect of different environmental conditions on the strength of laminated beams.

The second objective is to investigate the effects of presence of opening in composite laminated plate. A precise and simple analytical solution has been developed and applied to determine the stress concentration factor (SCF), that occurs in an infinite plate containing a circular cutout with unsymmetrical stacking sequence when loaded with arbitrary in-plane loading at infinity (uniaxial, biaxial, and shear). The current solution was extended based on Greszczuk's solution. The effective moduli of unsymmetrical laminated plates were expressed using Chen methode. The effects of several parameters, including the type of loads, unsymmetrical stacking sequence, number of layers, hole's size, and load angle orientation, on the stress distribution

around the opening are considered when discussing typical results obtained using the current solution. On the other hand, the same previous parameters were considered to predict the failure load using Tsai-Wu creteria..

The results of the current solution were successfully compared with results obtained by FEM and some analytical results obtained using the complex variable approach in order to validate the correctness of the solution.

The following main remarks can be drawn from the results presented in this work:

- The first ply failure (FPF) loads and maximum transverse displacement of glass-epoxy laminated beams were determined and compared using various failure criteria, different types of loading, and varying boundary conditions. The results indicate that both the boundary conditions and types of loading have a significant impact on the FPF loads.

- When the beam has a fiber orientation of [0°/90°] and is subjected to uniform temperature, the temperature is 783.5 °C, which decreases by approximately 80% compared to when the fiber direction was [0°/15°].

- The hygro-thermo-mechanical loading is greater than the thermo-mechanical loading, which is again greater than the mechanical loading for different orientation angles when the plate is subjected to in-plane loading in direction x.

- Regardless of changes in fiber orientation, the beams exhibit a 0% to 27% increase in failure strength value Nx according to the Tsai-We criteria when subjected to a hygro-thermal mechanical load. This suggests that both temperature and humidity positively impact the failure strength of the compressive load N_x.

- When subjected to hygro-thermo-mechanical loading, the failure strength of N_y decreases between 0% and 11.4% for all fiber orientation angles except for [0/90]. In contrast, for the [0/90] fiber orientation angle, the failure strength of N_y increases by 26.8%.

- The location and value of SCF around the circular cutout (along the edge of the hole) are dependent on stacking sequence and fiber orientation for the given material and loading conditions.

- The type of loading has a significant impact on the SCF.

- The value of the failure load changes with the type and direction of the load applied, and it also changes with the change in fiber orientation of the plate and is affected also by hole's size.

Perspectives :

- The solution can be extended to determine the stress distribution around circular holes in laminated plates, considering hygrothermal loading.

- This solution can be extended to determine the stress distribution in unsymmetric plates with elliptical holes subjected to different loadings.

- Study the effect of a hygrothermal environment on the damage of unsymmetric laminated plates.

Bibliographic references

1. Wang, Y., et al., *Hygrothermal and temperature effects on load-carrying capacity and failure mechanism of open-hole laminates prepared with narrow tape prepreg of GFRP.* Progress in Natural Science: Materials International, 2022.

2. Mára, V., et al., *The effect of long-time moisture exposure and low temperatures on mechanical behavior of open-hole Cfrp laminate.* Polymer Composites, 2021. **42**(7): p. 3603-3618.

3. Hunungare, P., *Numerical analysis of hygrothermal effect on laminated composite plates.* Int. Res. J. Eng. Technol, 2017. **4**(11): p. 1984-1991.

4. Bouzgou, A.A., A. Khechai, and A. Tati, *Stress concentration and deflection in isotropic and orthotropic plates with opening. Finite element study.* Revue des Composites et des matériaux avancés, 2015. **25**.

5. Khechai, A., et al., *A general solution for stress resultants around a circular cutout in laminate plates under different in-plane loadings: analytical and experimental investigations.* Archive of Applied Mechanics, 2018. **88**(7): p. 1187-1208.

6. Ngo, T.-D., *Introduction to composite materials.* Composite and Nanocomposite Materials—From Knowledge to Industrial Applications, 2020.

7. Johnson, T., *History of composites. The evolution of lightweight composite materials.* 2018.

8. Dewhurst, H.A., *The Long-Range Research That Produced Glass Fiber Reinforced Tires.* Research Management, 1970. **13**(3): p. 201-208.

9. Pirkle, M.K., *Effect of Multiple Holes on Stress Concentrations and Damage Initiation in a Quasi-Isotropic Composite Laminate*, 2020.

10. Berthelot, J.-M. and F.F. Ling, *Composite materials: mechanical behavior and structural analysis*. Vol. 435. 1999: Springer.

11. Nechad, H., *Evaluation de l'endommagement et de la rupture de matériaux hétérogènes par ultrasons et émission acoustique: estimation de la durée de vie restante*, 2004, Lyon, INSA.

12. Karpuz, P., *Mechanical characterization of filament wound composite tubes by internal pressure testing*, 2005, Middle East Technical University.

13. Thomas, C., *Étude des mécanismes d'endommagement des composites fibres de carbone/matrice polyamide: application à la réalisation de réservoirs de stockage de gaz sous haute pression de type IV*, 2011, École Nationale Supérieure des Mines de Paris.

14. Gornet, L., *Généralités sur les matériaux composites.* 2008.

15. Lachaud, F., *Delaminage de materiaux composites a fibres de carbone et a matrices organiques: etude numerique et experimentale, suivi par emission acoustique*, 1997, Toulouse 3.

16. REKBI, F.M.L., *Contribution à l'analyse de l'endommagement des matériaux composites*, 2016, Université Mohamed Khider-Biskra.

17. Campbell, F.C., *Structural composite materials*2010: ASM international.

18. Zhang, Y. and C. Yang, *Recent developments in finite element analysis for laminated composite plates.* Composite Structures, 2009. **88**(1): p. 147-157.

19. Keshava Kumar, S., *Review of laminated composite plate theories, with emphasis on variational asymptotic method.* AIAA journal, 2019. **57**(10): p. 4182-4188.

20. Van Paepegem, W. and J. Degrieck, *Modelling strategies for fatigue damage behaviour of fibre-reinforced polymer composites.* environment (eg moisture, toxic agents), 2001. **1**: p. 3.

21.   Reddy, J., *An evaluation of equivalent-single-layer and layerwise theories of composite laminates.* Composite Structures, 1993. **25**(1-4): p. 21-35.

22.   Kirchhoff, G., *Über das Gleichgewicht und die Bewegung einer elastischen Scheibe.* Journal für die reine und angewandte Mathematik (Crelles Journal), 1850. **1850**(40): p. 51-88.

23.   Love, A.E.H., *A treatise on the mathematical theory of elasticity*2013: Cambridge university press.

24.   Love, A., *Mathematical Theory of Elasticity (; Cambridge, Eng.: Cam*, 1934, bridge University Press.

25.   Teotia, M. and R. Soni, *Applications of finite element modelling in failure analysis of laminated glass composites: A review.* Engineering Failure Analysis, 2018. **94**: p. 412-437.

26.   Reddy, J.N., *Mechanics of laminated composite plates and shells: theory and analysis*2003: CRC press.

27.   Ghugal, Y. and R. Shimpi, *A review of refined shear deformation theories of isotropic and anisotropic laminated plates.* Journal of reinforced plastics and composites, 2002. **21**(9): p. 775-813.

28.   Roufaeil, O.L. and T. Tran-Cong, *Finite strip elements for laminated composite plates with transverse shear strain discontinuities.* Composite Structures, 2002. **56**(3): p. 249-258.

29.   Khandan, R., et al., *The development of laminated composite plate theories: a review.* Journal of Materials Science, 2012. **47**: p. 5901-5910.

30.   Reissner, E., *The effect of transverse shear deformation on the bending of elastic plates.* 1945.

31.   Reissner, E., *Reflections on the theory of elastic plates.* 1985.

32.   Reissner, E., *A consistent treatment of transverse shear deformations in laminated anisotropic plates.* AIAA journal, 1972. **10**(5): p. 716-718.

33.   Murty, A.K. and S. Vellaichamy, *On higher order shear deformation theory of laminated composite panels.* Composite Structures, 1987. **8**(4): p. 247-270.

34.   Lo, K., R. Christensen, and E. Wu, *A high-order theory of plate deformation—Part 1: Homogeneous plates.* 1977.

35.   Berthelot, J., *Matériaux composites, comportement et analyse des structures*1992: Masson, Paris.

36.   Tsai, S.W. and E.M. Wu, *A general theory of strength for anisotropic materials.* Journal of Composite Materials, 1971. **5**(1): p. 58-80.

37.   Hill, R., *A theory of the yielding and plastic flow of anisotropic metals.* Proceedings of the Royal Society of London. Series A. Mathematical and Physical Sciences, 1948. **193**(1033): p. 281-297.

38.   Hoffman, O., *The brittle strength of orthotropic materials.* Journal of Composite Materials, 1967. **1**(2): p. 200-206.

39.   Jones, R.M., *Mechanics of composite materials*2018: CRC press.

40.   Yeh, H.-L., *Quadric surfaces criterion for composite materials.* Journal of reinforced plastics and composites, 2003. **22**(6): p. 517-532.

41.   Yeh, H.-L. and H.-Y. Yeh, *The modified quadric surfaces criterion for composite materials.* Journal of reinforced plastics and composites, 2002. **21**(3): p. 279-289.

42.   Hashin, Z., *Fatigue failure criteria for unidirectional fiber composites.* 1981.

43.   Norris, C., *Strength of orthotropic materials subjected to combined stresses.* 1962.

44.   Hart-Smith, L., *Predictions of the original and truncated maximum-strain failure models for certain fibrous composite laminates.* Composites Science and Technology, 1998. **58**(7): p. 1151-1178.

45.   Sun, C.-T., *COMPARATIVE EVALUATION OF FAILURE ANALYSIS METHODS FOR COMPOSITE LAMINATES*, 1996.

46.   Davila, C.G., P.P. Camanho, and C.A. Rose, *Failure criteria for FRP laminates.* Journal of Composite Materials, 2005. **39**(4): p. 323-345.

47.   Puck, A., J. Kopp, and M. Knops, *Guidelines for the determination of the parameters in Puck's action plane strength criterion.* Composites Science and Technology, 2002. **62**(3): p. 371-378.

48.   Catalanotti, G., P. Camanho, and A. Marques, *Three-dimensional failure criteria for fiber-reinforced laminates.* Composite Structures, 2013. **95**: p. 63-79.

49.   Gutkin, R. and S. Pinho, *Review on failure of laminated composites: Experimental perspective and modelling.* 2016.

50.   Hill, R., *The mathematical theory of plasticity*. Vol. 11. 1998: Oxford university press.

51.   Azzi, V. and S.W. Tsai, *Anisotropic strength of composites.* Experimental mechanics, 1965. **5**(9): p. 283-288.

52.   Kim, Y., J.F. Davalos, and E.J. Barbero, *Progressive failure analysis of laminated composite beams.* Journal of Composite Materials, 1996. **30**(5): p. 536-560.

53.   Lezgy-Nazargah, M. and Z. Meshkani, *An efficient partial mixed finite element model for static and free vibration analyses of FGM plates rested on two-parameter elastic foundations.* Struct Eng Mech, 2018. **66**(5): p. 665-676.

54.   Lezgy-Nazargah, M., *A high-performance parametrized mixed finite element model for bending and vibration analyses of thick plates.* Acta Mechanica, 2016. **227**(12): p. 3429-3450.

55.   Lezgy-Nazargah, M. and S. Salahshuran, *A new mixed-field theory for bending and vibration analysis of multi-layered composite plate.* Archives of Civil and Mechanical Engineering, 2018. **18**(3): p. 818-832.

56.   Irhirane, E.H., et al., *Matrix and fibre stiffness degradation of a quasi-isotrope graphite epoxy laminate under flexural bending test.* Journal of reinforced plastics and composites, 2009. **28**(2): p. 201-223.

57.   Moncada, A.M., et al., *Micromechanics-based progressive failure analysis of composite laminates using different constituent failure theories.* Journal of reinforced plastics and composites, 2012. **31**(21): p. 1467-1487.

58.   Hasan, Z. and A. Muliana, *Failure and deformation analyses of smart laminated composites.* Mechanics of composite materials, 2012. **48**(4): p. 391-404.

59.   Daniel, I.M., *Constitutive behavior and failure criteria for composites under static and dynamic loading.* Meccanica, 2015. **50**(2): p. 429-442.

60.   Lezgy-Nazargah, M., *Assessment of refined high-order global–local theory for progressive failure analysis of laminated composite beams.* Acta Mechanica, 2017. **228**(5): p. 1923-1940.

61.   Wu, C. and T. Tauchert, *Thermoelastic analysis of laminated plates. I: Symmetric specially orthotropic laminates.* Journal of Thermal Stresses, 1980. **3**(2): p. 247-259.

62.   Wu, C. and T. Tauchert, *Thermoelastic analysts of laminated plates. 2: Antisymmetric cross-ply and angle-ply laminates.* Journal of Thermal Stresses, 1980. **3**(3): p. 365-378.

63.   Reddy, J. and Y. Hsu, *Effects of shear deformation and anisotropy on the thermal bending of layered composite plates.* Journal of Thermal Stresses, 1980. **3**(4): p. 475-493.

64.   Ram, K.S. and P. Sinha, *Hygrothermal effects on the bending characteristics of laminated composite plates.* Computers & structures, 1991. **40**(4): p. 1009-1015.

65.   Chen, L.-W. and L.-Y. Chen, *Thermal deformation and stress analysis of composite laminated plates by finite element method.* Computers & structures, 1990. **35**(1): p. 41-49.

66.   Ray, C. and M. Dey, *Failure analysis of laminated composite plates under linearly varying temperature.* Journal of reinforced plastics and composites, 2009. **28**(1): p. 99-107.

67.   Zhang, J., et al., *A progressive failure analysis model for composite structures in hygrothermal environments.* Composite Structures, 2015. **133**: p. 331-342.

68.   Choudhury, A., S. Mondal, and S. Sarkar, *Failure analysis of laminated composite plate under hygro-thermo mechanical load and optimisation.* International Journal of Applied Mechanics and Engineering, 2019. **24**(3): p. 509-526.

69.   Soden, P., A. Kaddour, and M. Hinton, *Recommendations for designers and researchers resulting from the world-wide failure exercise*, in *Failure criteria in fibre-reinforced-polymer composites*2004, Elsevier. p. 1223-1251.

70.   Hinton, M., A. Kaddour, and P. Soden, *Evaluation of failure prediction in composite laminates: background to 'part B' of the exercise.* Composites Science and Technology, 2002. **62**(12-13): p. 1481-1488.

71.   Li, S., *The maximum stress failure criterion and the maximum strain failure criterion: their unification and rationalization.* Journal of Composites Science, 2020. **4**(4): p. 157.

72.   Camanho, P.P., *Failure criteria for fibre-reinforced polymer composites.* Secção de Mecânica Aplicada, Departamento de Engenharia Mecânica e Gestão Industrial, Faculdade de Engenharia da Universidade do Porto, 2002.

73.   Khechai, A. and P. Mohite, *Optimum design of perforated symmetric laminates using evolutionary algorithm.* Journal of Composite Materials, 2019. **53**(23): p. 3281-3305.

74.   Lamé, G., *Théorie mathématique de l'élasticité des corps solides*1866.

75.   Airy, G.B., *IV. On the strains in the interior of beams.* Philosophical transactions of the Royal Society of London, 1863(153): p. 49-79.

76.   Muskhelishvili, N.I., *Some basic problems of the mathematical theory of elasticity.* Vol. 15. 1953: Noordhoff Groningen.

77.   Howland, R., *On the stresses in the neighbourhood of a circular hole in a strip under tension.* Philosophical Transactions of the Royal Society of London. Series A, Containing Papers of a Mathematical or Physical Character, 1930. **229**(670-680): p. 49-86.

78.   Lekhnitskii, S.G., *Anisotropic plates*, 1968, Foreign Technology Div Wright-Patterson Afb Oh.

79.   Savin, G.N., *Stress concentration around holes.* 1961.

80.   Theocaris, P. and L. Petrou, *Stress distributions and intensities at corners of equilateral triangular holes.* International Journal of Fracture, 1986. **31**: p. 271-289.

81.   Theocaris, P. and L. Petrou, *The order of singularities and the stress intensity factors near corners of regular polygonal holes.* International journal of engineering science, 1987. **25**(7): p. 821-832.

82.   Sharma, D.S., *Stress distribution around circular/elliptical/triangular holes in infinite composite plate.* Engineering Letters, 2012. **20**(1): p. 1.

83.   Sharma, D.S., N.P. Patel, and R.R. Trivedi, *Optimum design of laminates containing an elliptical hole.* International Journal of Mechanical Sciences, 2014. **85**: p. 76-87.

84.   Ukadgaonker, V. and D.K. Rao, *A general solution for stresses around holes in symmetric laminates under inplane loading.* Composite Structures, 2000. **49**(3): p. 339-354.

85.   Green, A. and W. Zerna, *Theoretical Elasticity Oxford University Press.* New York, 1954.

86.   Greszczuk, L. *for Orthotropic and Anisotropic Plates with Circular Openings.* in *Composite Materials: Testing and Design: a Conference.* 1972. ASTM International.

87.   Ukadgaonker, V. and V. Kakhandki, *Stress analysis for an orthotropic plate with an irregular shaped hole for different in-plane loading conditions—Part 1.* Composite Structures, 2005. **70**(3): p. 255-274.

88.   Rezaeepazhand, J. and M. Jafari, *Stress analysis of perforated composite plates.* Composite Structures, 2005. **71**(3-4): p. 463-468.

89.   Toralkar, S., et al., *Stress Concentration of Laminated Composite Plate Containing Circular Hole.* J Adv Sci Technol, 2016. **12**(25): p. 470-477.

90.   Rybicki, E.F. and D.W. Schmueser, *Effect of stacking sequence and lay-up angle on free edge stresses around a hole in a laminated plate under tension.* Journal of Composite Materials, 1978. **12**(3): p. 300-313.

91.   Rezaeepazhand, J. and M. Jafari. *Stress analysis of composite plates with non-circular cutout.* in *Key Engineering Materials*. 2008. Trans Tech Publ.

92.   Rezaeepazhand, J. and M. Jafari, *Stress analysis of composite plates with a quasi-square cutout subjected to uniaxial tension.* Journal of reinforced plastics and composites, 2010. **29**(13): p. 2015-2026.

93.   Lekhniṫskiĭ, S.G., *Theory of elasticity of an anisotropic elastic body* 1963: Holden-day.

94.   Khechai, A., A. Tati, and A. Guettala, *Finite element analysis of stress concentrations and failure criteria in composite plates with circular holes.* Frontiers of Mechanical Engineering, 2014. **9**(3): p. 281-294.

95.   Ukadgaonker, V. and D. Rao, *Stress distribution around triangular holes in anisotropic plates.* Composite Structures, 1999. **45**(3): p. 171-183.

96.   Daoust, J. and S. Hoa, *An analytical solution for anisotropic plates containing triangular holes.* Composite Structures, 1991. **19**(2): p. 107-130.

97.   Gao, X.-L., *A general solution of an infinite elastic plate with an elliptic hole under biaxial loading.* International Journal of Pressure Vessels and Piping, 1996. **67**(1): p. 95-104.

98.   Simha, K. and S. Mohapatra, *Stress concentration around irregular holes using complex variable method.* Sadhana, 1998. **23**(4): p. 393-412.

99.   Magar, A. and A. Lal, *Stress analysis of infinite laminated composite plate with elliptical cutout under different in plane loadings in hygrothermal environment.* Curved and Layered Structures, 2021. **8**(1): p. 1-12.

100.   Dharmin, P., P. Khushbu, and J. Chetan, *A review on stress analysis of an infinite plate with cut-outs.* International Journal of Scientific and Research Publications, 2012. **2**(11): p. 1-7.

101.   Nagpal, S., N. Jain, and S. Sanyal, *Stress concentration and its mitigation techniques in flat plate with singularities-A critical review.* Engineering Journal, 2012. **16**(1): p. 1-16.

102.   Chen, P. and Z. Shen, *Stress resultants and moments around holes in unsymmetrical composite laminates subjected to remote uniform loading.* Mechanics Research Communications, 2003. **30**(1): p. 79-86.

103.   Chen, P. and Z. Shen, *Extension of Lekhnitskii's complex potential approach to unsymmetric composite laminates.* Mechanics Research Communications, 2001. **28**(4): p. 423-428.

104.   Puhui, C. and S. Zhen, *Green's functions for an unsymmetric laminated plate with an elliptic hole.* Mechanics Research Communications, 2001. **28**(5): p. 519-524.

105.   Dave, J.M., D.S. Sharma, and M.M. Chauhan, *Stress analysis of an unsymmetric composite plate with variance of oval-shaped cutout.* Mathematics and Mechanics of Solids, 2017. **22**(4): p. 692-707.

106.   Louhghalam, A., et al., *Analysis of stress concentrations in plates with rectangular openings by a combined conformal mapping–finite element approach.* International Journal of Solids and Structures, 2011. **48**(13): p. 1991-2004.

107.   Talib, A.A., et al., *Influence of cut-out hole on multi-layer Kevlar-29/epoxy composite laminated plates.* Materials & design, 2013. **43**: p. 89-98.

108.   Chen, H.C., *Special finite elements including stress concentration effects of a hole.* Finite elements in analysis and design, 1993. **13**(4): p. 249-258.

109.   Piltner, R., *Special finite elements with holes and internal cracks.* International journal for numerical methods in engineering, 1985. **21**(8): p. 1471-1485.

110.   Wang, H. and Q.-H. Qin, *A new special element for stress concentration analysis of a plate with elliptical holes.* Acta Mechanica, 2012. **223**: p. 1323-1340.

111.   Tan, S.C., *Finite-width correction factors for anisotropic plate containing a central opening.* Journal of Composite Materials, 1988. **22**(11): p. 1080-1097.

112.   Ounis, H., A. Tati, and A. Benchabane, *Thermal buckling behavior of laminated composite plates: a finite-element study.* Frontiers of Mechanical Engineering, 2014. **9**(1): p. 41-49.

113.   Arslan, H.M., M.Y. Kaltakci, and H.R. Yerli, *EFFECT OF CIRCULAR HOLES ON CROSS-PLY LAMINATED COMPOSITE PLATES.* Arabian Journal for Science & Engineering (Springer Science & Business Media BV), 2009. **34**.

114.   Khechai, A., et al., *A general analytical solution of stresses around circular holes in functionally graded plates under various in-plane loading conditions.* Acta Mechanica, 2022: p. 1-21.

115.   Chen, D. and W. Chan. *Use of composite effective moduli for lumping layers in finite element analysis.* in *37th Structure, Structural Dynamics and Materials Conference.* 1996.

116.   Reddy, J.N., *A simple higher-order theory for laminated composite plates.* 1984.

117.   Pandya, B. and T. Kant, *Flexural analysis of laminated composites using refined higher-order C° plate bending elements.* Computer Methods in Applied Mechanics and Engineering, 1988. **66**(2): p. 173-198.

118.   Kaltakci, M.Y., *Stress concentrations and failure criteria in anisotropic plates with circular holes subjected to tension or compression.* Computers & structures, 1996. **61**(1): p. 67-78.

119.   Tsai, S.W. and H.T. Hahn, *Introduction to composite materials (Vol. 1)*, 1980, CRC Press, Lancaster.

120.   Liu, G. and K. Tang, *Study on stress concentration in notched cross-ply laminates under tensile loading.* Journal of Composite Materials, 2016. **50**(3): p. 283-296.

121.   Hwan, C.-L., et al., *Strength prediction of woven hybrid composite laminates each with a center hole.* Journal of Composite Materials, 2014. **48**(13): p. 1637-1644.

122.   Mohamed Makki, M. and B. Chokri, *Experimental, analytical, and finite element study of stress concentration factors for composite materials.* Journal of Composite Materials, 2017. **51**(11): p. 1583-1594.

Annex

3.2.1 In membrane:

$$u(x,y) = \alpha_1 + \alpha_2 x + \alpha_3 y + \alpha_4 xy$$

$$v(x,y) = \alpha_5 + \alpha_6 x + \alpha_7 y + \alpha_8 xy \tag{1}$$

These equations can be written in matrix form:

$$\begin{Bmatrix} u(x,y) \\ v(x,y) \end{Bmatrix} = \begin{bmatrix} 1 & x & y & xy & 0 & 0 & 0 & 0 \\ 0 & 0 & 0 & 0 & 1 & x & y & xy \end{bmatrix} \begin{Bmatrix} \alpha_1 \\ \alpha_2 \\ \alpha_3 \\ \alpha_4 \\ \alpha_5 \\ \alpha_6 \\ \alpha_7 \\ \alpha_8 \end{Bmatrix} \tag{2}$$

Node 1 : (x=0, y=0) $\rightarrow$ $\begin{Bmatrix} u_1 \\ v_1 \end{Bmatrix} = \begin{bmatrix} 1 & 0 & 0 & 0 & 0 & 0 & 0 & 0 \\ 0 & 0 & 0 & 0 & 1 & 0 & 0 & 0 \end{bmatrix} \{\alpha_i\}, \, i = 1,8$

Node 2 : (x=a, y=0) $\rightarrow$ $\begin{Bmatrix} u_2 \\ v_2 \end{Bmatrix} = \begin{bmatrix} 1 & a & 0 & 0 & 0 & 0 & 0 & 0 \\ 0 & 0 & 0 & 0 & 1 & a & 0 & 0 \end{bmatrix} \{\alpha_i\}, \, i = 1,8$

Node 3 : (x=a, y=b) $\rightarrow$ $\begin{Bmatrix} u_3 \\ v_3 \end{Bmatrix} = \begin{bmatrix} 1 & a & b & ab & 0 & 0 & 0 & 0 \\ 0 & 0 & 0 & 0 & 1 & a & b & ab \end{bmatrix} \{\alpha_i\}, \, i = 1,8$

Node 4 : (x=0, y=b) $\rightarrow$ $\begin{Bmatrix} u_4 \\ v_4 \end{Bmatrix} = \begin{bmatrix} 1 & 0 & b & 0 & 0 & 0 & 0 & 0 \\ 0 & 0 & 0 & 0 & 1 & 0 & b & 0 \end{bmatrix} \{\alpha_i\}, \, i = 1,8$

$$\{\delta_m^e\}_{8\times1} = [X]_{8\times8} \{\alpha_i\}_{8\times1} , \text{ So} \Longrightarrow \{\alpha_i\}_{8\times1} = [X]_{8\times8}^{-1} \{\delta_m^e\}_{8\times1} \quad \text{With } \{\delta_m^e\} = \begin{Bmatrix} u_1 \\ v_1 \\ u_2 \\ v_2 \\ u_3 \\ v_3 \\ u_4 \\ v_4 \end{Bmatrix}$$

$$\begin{Bmatrix} u(x,y) \\ v(x,y) \end{Bmatrix} = \begin{bmatrix} 1 & x & y & xy & 0 & 0 & 0 & 0 \\ 0 & 0 & 0 & 0 & 1 & x & y & xy \end{bmatrix} [X]^{-1} \{\delta_m^e\}$$

The presented element is a combination of a membrane element and a rectangular plate element with a high degree of accuracy. The membrane displacement of the developed element, through the element, can be expressed in terms of the interpolation functions as

$$\begin{Bmatrix} u(x,y) \\ v(x,y) \end{Bmatrix} = \begin{bmatrix} -\dfrac{x}{a}-\dfrac{y}{b}+\dfrac{xy}{ab}+1 & 0 & \dfrac{x}{a}-\dfrac{xy}{ab} & 0 & \dfrac{xy}{ab} & 0 & \dfrac{y}{b}-\dfrac{xy}{ab} & 0 \\ 0 & -\dfrac{x}{a}-\dfrac{y}{b}+\dfrac{xy}{ab}+1 & 0 & \dfrac{x}{a}-\dfrac{xy}{ab} & 0 & \dfrac{xy}{ab} & 0 & \dfrac{y}{b}-\dfrac{xy}{ab} \end{bmatrix} \{\delta_m^e\}$$

(3)

Where $\{\delta_m^e\}$ is the membrane displacement vector of the element. The Eq. (3) can be written as

$$\begin{Bmatrix} u(x,y) \\ v(x,y) \end{Bmatrix} = \begin{bmatrix} N_1^m & 0 & N_2^m & 0 & N_3^m & 0 & N_4^m & 0 \\ 0 & N_1^m & 0 & N_2^m & 0 & N_3^m & 0 & N_4^m \end{bmatrix} \{\delta_m^e\}$$

(4)

The interpolation functions can be used to express the membrane strain-displacement relation as

$$\{\varepsilon(x,y)\} = [B_m]\{\delta_m^e\}$$

(5)

$$[B_m] = \begin{bmatrix} -\dfrac{1}{a}+\dfrac{y}{ab} & 0 & \dfrac{1}{a}-\dfrac{y}{ab} & 0 & \dfrac{y}{ab} & 0 & -\dfrac{y}{ab} & 0 \\ 0 & -\dfrac{1}{b}+\dfrac{x}{ab} & 0 & -\dfrac{x}{ab} & 0 & \dfrac{x}{ab} & 0 & \dfrac{1}{b}-\dfrac{x}{ab} \\ -\dfrac{1}{b}+\dfrac{x}{ab} & -\dfrac{1}{a}+\dfrac{y}{ab} & -\dfrac{x}{ab} & \dfrac{1}{a}-\dfrac{y}{ab} & \dfrac{x}{ab} & \dfrac{y}{ab} & \dfrac{1}{b}-\dfrac{x}{ab} & -\dfrac{y}{ab} \end{bmatrix}$$

$$[B_m] = \begin{bmatrix} \dfrac{\partial N_1^m}{\partial x} & 0 & \dfrac{\partial N_2^m}{\partial x} & 0 & \dfrac{\partial N_3^m}{\partial x} & 0 & \dfrac{\partial N_4^m}{\partial x} & 0 \\ 0 & \dfrac{\partial N_1^m}{\partial y} & 0 & \dfrac{\partial N_2^m}{\partial y} & 0 & \dfrac{\partial N_3^m}{\partial y} & 0 & \dfrac{\partial N_4^m}{\partial y} \\ \dfrac{\partial N_1^m}{\partial y} & \dfrac{\partial N_1^m}{\partial x} & \dfrac{\partial N_2^m}{\partial y} & \dfrac{\partial N_2^m}{\partial x} & \dfrac{\partial N_3^m}{\partial y} & \dfrac{\partial N_3^m}{\partial x} & \dfrac{\partial N_4^m}{\partial y} & \dfrac{\partial N_4^m}{\partial x} \end{bmatrix}$$

(6)

3.2.2 In bending

The transverse displacement w of the element is expressed as

$$w(x,y) = \begin{bmatrix} \alpha_1 + \alpha_2 x + \alpha_3 y + \alpha_4 x^2 + \alpha_5 xy + \alpha_6 y^2 + \alpha_7 x^3 + \alpha_8 x^2 y + \alpha_9 xy^2 + \alpha_{10} y^3 + \alpha_{11} x^3 y + \\ \alpha_{12} x^2 y^2 + \alpha_{13} xy^3 + \alpha_{14} x^3 y^2 + \alpha_{15} x^2 y^3 + \alpha_{16} x^3 y^3 \end{bmatrix}$$

(7)

The displacement function of the plate element, given by Eq. (7), can be written in a vector form as

$$w(x, y) = \{P(x, y)\}\{\alpha\}^T$$

(8)

$$\{P(x, y)\} = \{1 \quad x \quad y \quad x^2 \quad xy \quad y^2 \quad x^3 \quad x^2 y \quad xy^2 \quad y^3 \quad x^3 y \quad x^2 y^2 \quad xy^3 \quad x^3 y^2 \quad x^2 y^3 \quad x^3 y^3\}$$

With $w(x, y)$ is the displacement function of the plate element and $\{\alpha\}^T$ is the constant parameters vector. As the plate element requires four degrees of freedom per node,

$$\delta_f^e = \left\{ w_i, \theta_{xi} = \frac{\partial w_i}{\partial x}, \theta_{yi} = \frac{\partial w_i}{\partial y}, \theta_{xyi} = \frac{\partial^2 w_i}{\partial x \partial y} \right\}_{i=1,4}$$

$$\begin{Bmatrix} w(x,y) \\ \dfrac{\partial w(x,y)}{\partial x} \\ \dfrac{\partial w(x,y)}{\partial y} \\ \dfrac{\partial^2 w(x,y)}{\partial x \partial y} \end{Bmatrix} =$$

$$\begin{bmatrix} 1 & x & y & x^2 & xy & y^2 & x^3 & x^2 y & xy^2 & y^3 & x^3 y & x^2 y^2 & xy^3 & x^3 y^2 & x^2 y^3 & x^3 y^3 \\ 0 & 1 & 0 & 2x & y & 0 & 3x^2 & 2xy & y^2 & 0 & 3x^2 y & 2xy^2 & y^3 & 3x^2 y^2 & 2xy^3 & 3x^2 y^3 \\ 0 & 0 & 1 & 0 & x & 2y & 0 & x^2 & 2xy & 3y^2 & x^3 & 2x^2 y & 3xy^2 & 2x^3 y & 3x^2 y^2 & 3x^3 y^2 \\ 0 & 0 & 0 & 0 & 1 & 0 & 0 & 2x & 2y & 0 & 3x^2 & 4xy & 3y^2 & 6x^2 y & 6xy^2 & 9x^2 y^2 \end{bmatrix} \{\alpha_i\}$$

Node 1 : (x=0, y=0) $\begin{Bmatrix} w_1 \\ \dfrac{\partial w_1}{\partial x} \\ \dfrac{\partial w_1}{\partial y} \\ \dfrac{\partial^2 w_1}{\partial x \partial y} \end{Bmatrix} = \begin{bmatrix} 1 & 0 & 0 & 0 & 0 & 0 & 0 & 0 & 0 & 0 & 0 & 0 & 0 & 0 & 0 & 0 \\ 0 & 1 & 0 & 0 & 0 & 0 & 0 & 0 & 0 & 0 & 0 & 0 & 0 & 0 & 0 & 0 \\ 0 & 0 & 1 & 0 & 0 & 0 & 0 & 0 & 0 & 0 & 0 & 0 & 0 & 0 & 0 & 0 \\ 0 & 0 & 0 & 0 & 1 & 0 & 0 & 0 & 0 & 0 & 0 & 0 & 0 & 0 & 0 & 0 \end{bmatrix} \{\alpha_i\}, \; i = 1,16$

Node 2: $(x=a, y=0)$ $\rightarrow$ $\begin{Bmatrix} w_2 \\ \dfrac{\partial w_2}{\partial x} \\ \dfrac{\partial w_2}{\partial y} \\ \dfrac{\partial^2 w_2}{\partial x \partial y} \end{Bmatrix} = \begin{bmatrix} 1 & a & 0 & a^2 & 0 & 0 & a^3 & 0 & 0 & 0 & 0 & 0 & 0 & 0 & 0 & 0 \\ 0 & 1 & 0 & 2a & 0 & 0 & 3a^2 & 0 & 0 & 0 & 0 & 0 & 0 & 0 & 0 & 0 \\ 0 & 0 & 1 & 0 & a & 0 & 0 & a^2 & 0 & 0 & a^3 & 0 & 0 & 0 & 0 & 0 \\ 0 & 0 & 0 & 0 & 1 & 0 & 0 & 2a & 0 & 0 & 3a^2 & 0 & 0 & 0 & 0 & 0 \end{bmatrix} \{\alpha_i\}, i=1,16$

Node 3: $(x=a, y=b)$ $\rightarrow$

$\begin{Bmatrix} w_3 \\ \dfrac{\partial w_3}{\partial x} \\ \dfrac{\partial w_3}{\partial y} \\ \dfrac{\partial^2 w_3}{\partial x \partial y} \end{Bmatrix} =$

$\begin{bmatrix} 1 & a & b & a^2 & ab & b^2 & a^3 & a^2 b & ab^2 & b^3 & a^3 b & a^2 b^2 & ab^3 & a^3 b^2 & a^2 b^3 & a^3 b^3 \\ 0 & 1 & 0 & 2a & b & 0 & 3a^2 & 2ab & b^2 & 0 & 3a^2 b & 2ab^2 & b^3 & 3a^2 b^2 & 2ab^3 & 3a^2 b^3 \\ 0 & 0 & 1 & 0 & a & 2b & 0 & a^2 & 2ab & 3b^2 & a^3 & 2a^2 b & 3ab^2 & 2a^3 b & 3a^2 b^2 & 3a^3 b^2 \\ 0 & 0 & 0 & 0 & 1 & 0 & 0 & 2a & 2b & 0 & 3a^2 & 4ab & 3b^2 & 6a^2 b & 6ab^2 & 9a^2 b^2 \end{bmatrix} \{\alpha_i\}$

Node 4: $(x=0, y=b)$ $\rightarrow$

$\begin{Bmatrix} w_4 \\ \dfrac{\partial w_4}{\partial x} \\ \dfrac{\partial w_4}{\partial y} \\ \dfrac{\partial^2 w_4}{\partial x \partial y} \end{Bmatrix} = \begin{bmatrix} 1 & 0 & b & 0 & 0 & b^2 & 0 & 0 & 0 & b^3 & 0 & 0 & 0 & 0 & 0 & 0 \\ 0 & 1 & 0 & 0 & b & 0 & 0 & 0 & b^2 & 0 & 0 & 0 & b^3 & 0 & 0 & 0 \\ 0 & 0 & 1 & 0 & 0 & 2b & 0 & 0 & 0 & 3b^2 & 0 & 0 & 0 & 0 & 0 & 0 \\ 0 & 0 & 0 & 0 & 1 & 0 & 0 & 0 & 2b & 0 & 0 & 0 & 3b^2 & 0 & 0 & 0 \end{bmatrix} \{\alpha_i\}, i=1,16$

The plate displacements through the element can be expressed in terms of the nodal displacements as

$$\{\delta_f^e\}_{16\times1} = [X]_{16\times16} \{\alpha_i\}_{16\times1}, \quad \text{So} \Longrightarrow \quad \{\alpha_i\}_{16\times1} = [X]_{16\times16}^{-1} \{\delta_f^e\}_{16\times1} \tag{9}$$

$$w(x,y) = \{P(x,y)\}_{1\times16} [X]_{16\times16}^{-1} \{\delta_f^e\}_{16\times1} \tag{10}$$

So

$$w(x,y) = \begin{bmatrix} N_1^f & N_2^f & N_3^f & N_4^f & \cdots & \cdots & N_{13}^f & N_{14}^f & N_{15}^f & N_{16}^f \end{bmatrix} \{\delta_f^e\} \tag{11}$$

Where the interpolation functions of the plate element are written as

$$w^*_1(x,y)=(1-3\frac{x^2}{a^2}+2\frac{x^3}{a^3})(1-3\frac{y^2}{b^2}+2\frac{y^3}{b^3})w_1+(-x(\frac{x}{a}-1)^2)(1-3\frac{y^2}{b^2}+2\frac{y^3}{b^3})\theta_{x1}+(1-3\frac{x^2}{a^2}+2\frac{x^3}{a^3})y(\frac{y}{b}-1)^2\theta_{y1}+$$

$$(-x(\frac{x}{a}-1)^2)y(\frac{y}{b}-1)^2\theta_{xy1}$$

$$w^*_2(x,y)=(3\frac{x^2}{a^2}-2\frac{x^3}{a^3})(1-3\frac{y^2}{b^2}+2\frac{y^3}{b^3})w_2+(-x(\frac{x^2}{a^2}-\frac{x}{a}))(1-3\frac{y^2}{b^2}+2\frac{y^3}{b^3})\theta_{x2}+(3\frac{x^2}{a^2}-2\frac{x^3}{a^3})y(\frac{y}{b}-1)^2\theta_{y2}+$$

$$(-x(\frac{x^2}{a^2}-\frac{x}{a}))y(\frac{y}{b}-1)^2\theta_{xy2}$$

$$w^*_3(x,y)=(3\frac{x^2}{a^2}-2\frac{x^3}{a^3})(3\frac{y^2}{b^2}-2\frac{y^3}{b^3})w_3+(-x(\frac{x^2}{a^2}-\frac{x}{a}))(3\frac{y^2}{b^2}-2\frac{y^3}{b^3})\theta_{x3}+(3\frac{x^2}{a^2}-2\frac{x^3}{a^3})y(\frac{y^2}{b^2}-\frac{y}{b})\theta_{y3}+$$

$$(-x(\frac{x^2}{a^2}-\frac{x}{a}))y(\frac{y^2}{b^2}-\frac{y}{b})\theta_{xy3}$$

$$w^*_4(x,y)=(1-3\frac{x^2}{a^2}+2\frac{x^3}{a^3})(3\frac{y^2}{b^2}-2\frac{y^3}{b^3})w_4+(-x(\frac{x}{a}-1)^2)(3\frac{y^2}{b^2}-2\frac{y^3}{b^3})\theta_{x4}+(1-3\frac{x^2}{a^2}+2\frac{x^3}{a^3})y(\frac{y^2}{b^2}-\frac{y}{b})\theta_{y4}+$$

$$(-x(\frac{x}{a}-1)^2)y(\frac{y^2}{b^2}-\frac{y}{b})\theta_{xy4} \tag{12}$$

The present element is based on the CLT, so the in-plane and out-of-plane displacements are given using eq. (14). On the other hand, based on the strain-displacement relation, the curvatures k can be given as

$$\{k(x,y)\}=-\begin{Bmatrix}\dfrac{\partial^2 w}{\partial x^2}\\[4pt]\dfrac{\partial^2 w}{\partial y^2}\\[4pt]2\dfrac{\partial^2 w}{\partial x\partial y}\end{Bmatrix}=-\begin{bmatrix}\dfrac{\partial^2}{\partial x^2}\\[4pt]\dfrac{\partial^2}{\partial y^2}\\[4pt]2\dfrac{\partial^2}{\partial x\partial y}\end{bmatrix}\{P(x,y)\}[X]^{-1}\{\delta^e_f\}=-\begin{bmatrix}\dfrac{\partial^2\{P(x,y)\}}{\partial x^2}\\[4pt]\dfrac{\partial^2\{P(x,y)\}}{\partial y^2}\\[4pt]2\dfrac{\partial^2\{P(x,y)\}}{\partial x\partial y}\end{bmatrix}[X]^{-1}\{\delta^e_f\}$$

$$\{k(x,y)\}=[Q]_{3\times16}[X]^{-1}_{16\times16}\{\delta^e_f\}_{16\times1}=[B_f]_{3\times16}\{\delta^e_f\} \tag{13}$$